

**FABRICATION AND CHARACTERIZATION OF STEEL-MAGNESIUM
LAMINATED METAL COMPOSITES**

by

HANQING CHE

B.E., Xi'an Jiaotong University, 2008

A THESIS SUBMITTED IN PARTIAL FULFILLMENT OF
THE REQUIREMENTS FOR THE DEGREE OF

MASTER OF APPLIED SCIENCE

in

THE FACULTY OF GRADUATE STUDIES

(Materials Engineering)

THE UNIVERSITY OF BRITISH COLUMBIA

(Vancouver)

February 2012

© Hanqing Che, 2012

Abstract

In this study, interstitial-free steel and commercial purity magnesium sheets were used to fabricate steel-magnesium laminated metal composites by roll bonding at 300°C. It was found that the steel and magnesium can achieve reasonable bonding after a 47% rolling reduction when the volume fraction of the laminate is 10-15% magnesium. The microstructure of the laminated composites was observed with scanning electron microscope. It was found that a continuous interface between the IF steel and the magnesium was produced during the roll bonding process. There was no evidence of intermetallic formation at the interface.

A seven layer steel-magnesium laminate was fabricated by accumulative roll bonding at 300°C with an overall reduction of 77 percent. Through-width cracks were found in the surface steel layers after the one cycle accumulative roll bonding process. The longitudinal cross-sectional microstructure of the laminate revealed that multi-localizations and even fracture occurred in steel layers inside the laminate.

The mechanical properties, including tensile behavior, micro-hardness and bending behavior, of the laminated composites were assessed. The tensile property of the laminated composites was compared with those of monolithic steel and magnesium with equivalent deformation amount deformed under the same conditions. It was found that the UTS of the laminated composites obeyed the simple rule of mixtures. The fracture surfaces of the laminated composites were examined with SEM and compared with those of the monolithic IF steel and magnesium rolled under the same conditions. It was found that the fracture

modes of each component were different in the laminated composites compared to the monolithic materials.

Three-point bending test was conducted and it was observed that no debonding at the interface occurred for moderate strains. To investigate the fracture behavior of the laminats in bending, a series of U-shape bending tests were conducted and the bend tips were observed. Localization of the outer steel layer was observed, followed by the formation of a major crack at 45 degree to the maximum tensile stress direction. Shear cracks in the magnesium core were also found in some places adjacent to the major crack, and delamination between the steel and magnesium layers occurred.

Table of Contents

Abstract.....	ii
Table of Contents	iv
List of Tables	vii
List of Figures.....	viii
Acknowledgements	xiii
Chapter 1: Introduction	1
Chapter 2: Literature review	4
2.1. Designing hybrid materials	4
2.1.1. Introduction to hybrid materials.....	4
2.1.2. What could we achieve by designing a hybrid?.....	6
2.1.3. Design of hybrid materials.....	8
2.2. Laminated metal composites.....	10
2.2.1. Tensile behavior at low temperatures	12
2.2.2. Toughening mechanisms	15
2.3. Steel-magnesium hybrid materials.....	17
2.4. Roll bonding.....	22
2.4.1. The roll bonding process.....	22
2.4.2. Parameters affect bonding.....	24
2.5. Summary	27
Chapter 3: Scope and objectives	28
3.1. Scope.....	28
3.2. Objectives	29

Chapter 4: Experimental methodology	30
4.1. Starting materials	30
4.2. Rolling.....	32
4.2.1. Rolling of monolithic materials	32
4.2.2. Roll bonding.....	33
4.2.3. Accumulative roll bonding	34
4.3. Microstructural observation	35
4.4. Mechanical behavior tests.....	36
4.4.1. Room temperature tensile tests	36
4.4.2. Micro-hardness tests	37
4.4.3. Bending tests	37
Chapter 5: Experimental results and discussion	41
5.1. Microstructures of the steel-magnesium laminated composites	41
5.1.1. Microstructures of the roll-bonded laminated composites.....	41
5.1.2. Microstructures of the accumulative roll-bonded laminated composites	45
5.1.3. Rollability and deformation responses of the laminated composites.....	48
5.2. Room temperature tensile behavior	50
5.2.1. Tensile behavior of the monolithic materials.....	50
5.2.2. Tensile behavior of the steel-magnesium composites	53
5.3. Micro-hardness results	67
5.4. Bending behavior of the laminated composites	69
5.4.1. Three-point bending test	69
5.4.2. U-shape bending	70

5.4.3. Evaluation of the bending behavior of the laminates.....	73
Chapter 6: Conclusions and future work	76
6.1. Summary and conclusions	76
6.2. Future work.....	78
References	80

List of Tables

Table 2.1. The details of four possibilities of hybridization (summarized according to ref. [13]).....	7
Table 2.2. Physical properties of iron and magnesium.....	17
Table 4.1. The chemical composition (wt. %) of the commercial purity magnesium sheet...	30
Table 4.2. The chemical composition (wt. %) of the IF steel.....	30

List of Figures

Fig. 1.1. The potential for making lightweight steel-magnesium laminated composites.	2
Fig. 2.1. The idea of the hybrid materials (reprinted from [9] with permission from Elsevier).	5
Fig. 2.2. Four typical families of configurations of hybrid materials (reprinted from [9] with permission from Elsevier, “wt” in the figure is the abbreviation for weight).....	5
Fig. 2.3. An illustration of the various composite geometries that can be obtained by decarburization (reprinted from [12] with permission from John Wiley and Sons).....	6
Fig. 2.4. Possibilities of hybridization (reprinted from [9] with permission from Elsevier). ...	7
Fig. 2.5. The steps in designing a hybrid to meet given design requirements (reprinted from [9] with permission from Elsevier).	8
Fig. 2.6. A schematic E - ρ chart showing guidelines for a light, stiff beam (reprinted from [9] with permission from Elsevier).....	10
Fig. 2.7. Photomicrographs of LMCs of UHCS/Fe- 3Si alloy processed by roll bonding [29] (the top and bottom three are under same magnification, respectively, reprinted from [21] with permission from Elsevier).....	11
Fig. 2.8. Breaking strength of ultrathin layer laminated composites as function of modulated spacing d : laminates are based on layers of Cu alternating with either Ni or Monel layers (reprinted from [5] with permission from <i>International Materials Reviews</i> , Maney Publishing, www.maney.co.uk/journals/imr and www.ingentaconnect.com/content/maney/imr).....	13
Fig. 2.9. Experimental yield strength (a) and tensile elongation to fracture (b) of thick-layer laminated composites containing 50 vol.% of each component, compared with prediction based on the rule of averages (given by the solid line) (reprinted from [22] with permission from <i>International Materials Reviews</i> , Maney Publishing, www.maney.co.uk/journals/imr and www.ingentaconnect.com/content/maney/imr).	14

Fig. 2.10. Toughening mechanisms of LMCs (reprinted from [5] with permission from *International Materials Reviews*, Maney Publishing, www.maney.co.uk/journals/imr and www.ingentaconnect.com/content/maney)..... 16

Fig. 2.11. Schematic of the co-extrusion process: (a) original macroscopic steel-magnesium assembly, and (b) the co-extrusion process used for the fabrication of the steel-magnesium composite wire (reprinted from [3] with permission from both Trans Tech Publications Ltd and the authors)..... 19

Fig. 2.12. Experimental results of the steel-magnesium composite wire: (a) and (b) micrographs illustrating the microstructures of the steel-magnesium composite wire in the cross section (steel is brightly imaged while magnesium is dark) at low and high magnification; (c) tensile test results; and (d) the fracture surface for the wire after annealing (reprinted from [3] with permission from both Trans Tech Publications Ltd and the authors).
..... 20

Fig. 2.13. Optical micrographs of as-cast LMCs with (a) 0.2 mm and (b) 0.1 mm layer thickness (the dark phase is steel and the light phase is magnesium, reprinted from [4] with permission from Springer). 21

Fig. 2.14. SEM photographs showing: (a) fracture surface and (b) fracture profile of a 0.2 mm as-cast LMC in secondary electron mode (the light phase is steel and the dark phase is magnesium, reprinted from [4] with permission from Springer)..... 22

Fig. 2.15. Schematic illustration of the cold roll bonding process (reprinted from [50] with permission from STAM, details at creativecommons.org/licenses/by-nc-sa/3.0). 23

Fig. 2.16. Diagrammatic representation of the accumulative roll bonding process (reprinted from [6] with permission from Elsevier). 24

Fig. 2.17. Bond strength in shear as function of deformation reduction for bonds formed by roll bonding (reprinted from [50] with permission from STAM, details at creativecommons.org/licenses/by-nc-sa/3.0). 25

Fig. 3.1. Design process of the steel-magnesium laminated composite. 28

Fig. 4.1. Microstructures of the as-received magnesium, SEM images at four different magnifications (courtesy of Ghazal Nayyeri).	31
Fig. 4.2. OM images showing the microstructure of the as-received IF steel.	32
Fig. 4.3. Schematic of the roll bonding process.....	34
Fig. 4.4. Schematic of the ARB process.	35
Fig. 4.5. Schematic of the setup for three-point bending tests.....	38
Fig. 4.6. Schematic of bending of a sandwich beam.	39
Fig. 5.1. Thickness measurements for the laminated composites and magnesium layer as function of reduction (the magnitude of right axis is set to be 14% of that at the corresponding point on the left axis).	42
Fig. 5.2. SEM micrographs (in secondary electron mode) of the longitudinal cross-section of the roll-bonded steel-magnesium laminated composites after different passes.....	43
Fig. 5.3. SEM images showing details of the longitudinal interface (a) 70% reduction, (b) 80% reduction and (c) 87% reduction.....	44
Fig. 5.5. SEM photographs (in secondary electron mode) showing the cross-sectional microstructure along (a) rolling direction (SEM images assembly) and (b) transverse direction of the ARBed laminated composites.	46
Fig. 5.4. The schematic flow of the two-step accumulative roll bonding process: step 1 with 67% deformation and an overall reduction of 77% after the two steps.	46
Fig. 5.6. Two different deformation responses of the laminates during rolling.	49
Fig. 5.7. Engineering stress vs. engineering strain curves for IF steel (curves are only plotted to the necking point for the deformed samples).....	51
Fig. 5.8. Engineering stress vs. engineering strain curves for the deformed commercial purity magnesium.	51

Fig. 5.9. Fracture surfaces of (a) IF steel (80% deformation, inset is the macro view of the fractured sample) and (b) magnesium (90% deformation).	53
Fig. 5.10. Engineering stress vs. engineering strain curves for the roll-bonded laminated composites (curves are only plotted to the necking point).	55
Fig. 5.11. UTS vs. deformation amount for steel-magnesium laminated composites and monolithic IF steel and magnesium.	56
Fig. 5.12. Engineering stress vs. engineering strain curves for roll-bonded laminated composites with 80% deformation.....	57
Fig. 5.13. Comparison of the engineering stress-engineering strain curves for laminated composites with 80% deformation and the corresponding component materials.....	59
Fig. 5.14. Comparisons of the macro views of fractured samples of (a) monolithic IF steel with 80% deformation, (b) laminates with 80% deformation, (c) laminates with 92% deformation and (d) laminates with 95% deformation.	60
Fig. 5.15. Longitudinal view of the fracture samples for laminates with (a) 80% deformation, (b) 92% deformation (inset is the BSE image showing the detail of the fracture site), (c) 92% deformation (different sample) and (d) 95% deformation.	61
Fig. 5.16. SEM photographs showing the fracture surfaces of laminate samples with 80% deformation: (a) the macroscopic view of the fracture site; (b) debonding between layers and splitting in the IF steel layer; (c) details of the rectangle area in (b); (d) magnesium layer at the fracture site; (e) details of the rectangle area in (d); and (f) interaction between fractures in IF steel layer and magnesium layer.	63
Fig. 5.17. SEM photographs showing the fracture surfaces of laminate samples with 92% deformation: (a) and (b) the macroscopic views of the fracture sites; (c) tearing of magnesium layer; (d) undebonded interface between IF steel and magnesium; (e) IF steel layer at the fracture site; and (f) magnesium layer at the fracture site.....	64
Fig. 5.18. SEM photographs showing the fracture surfaces of laminate samples with 95% deformation: (a) the macroscopic view of the fracture site; (b) splitting of the IF steel layer at	

the fracture site; (c) “transition” zone of the fracture site; (d) details of the left part in (c) showing undebonded interface; (e) details of the right part in (c) showing the debonding between layers; and (f) details of the magnesium layer in (e).	65
Fig. 5.19. Micro-hardness results: (a) the micro-hardness vs. true strain for monolithic IF steel and (b) comparison between the measured UTS and those calculated based on hardness.	67
Fig. 5.20. The load-deflection curve of the three-point bending test of the 80% deformed laminate.....	69
Fig. 5.21. The microstructure of the bending tip of the three-point bent sample (80% deformed laminate) under two magnifications.	70
Fig. 5.22. Optical images of the bent sample (80% deformed laminates) after U-shape bending experiments: (a) macroscopic images assembly, (b) and (c) the microstructural details of the fracture profiles.	71
Fig. 5.23. Optical microscopic images of the bent samples (80% deformed laminates) to different nominal interior angles: (a) 50 °, (b) 35 °(c) 12 °and (d) 0 °.	72
Fig. 5.24. (a) the equivalent flexural modulus of the laminated composites as function of density and (b) the specific flexural modulus as function of the amount of magnesium (calculations based on a support span of 0.1 m in Eq. 5.4).....	74
Fig. 5.25. The flexural moduli of the monolithic component materials as well as the laminated composites with different amounts of magnesium as function of density.	74

Acknowledgements

I owe particular thanks to my supervisors Dr. Warren Poole and Dr. David Embury. I would like to thank Dr. Warren Poole for giving me such a great opportunity to work here in the nice department and for all his kindly help, guidance, supports and inspirations. I thank Dr. David Embury for the unique idea of this exciting project and also for enlarging my vision of materials science and providing tremendous extremely useful suggestions and comments on my work. It is really a great honor for me to be here and work with the two erudite, respectable professors.

I offer my enduring gratitude to the faculty, staff and my fellow students at the Department of Materials Engineering, who have helped me a lot through my work in this field. These include Chad Sinclair, Debbie Burgess, Ross McLeod, Carl Ng, David Torok, Mary Fletcher, Jacob Kabel, Fateh Fazeli, Jayant Jain, Phil Tomlinson, Beth Sterling, Hamid Azizi-Alizamini, Ghazal Nayyeri and many more.

Last but not least, as the only child in my family, I would like to express my special thanks to my parents, who have supported me year after year, both morally and financially.

Chapter 1: Introduction

The demand for lightweight structures and materials is growing all over the world for a wide range of products, including vehicles, body armor, sports and leisure goods. The application of lightweight structures in transportation industry is of primary interest due to the environmental issues, i.e. fuel consumption and CO₂ emissions. The steel-magnesium composite material is an interesting candidate for lightweight materials because it combines the strength and stiffness of the most used structural material, steel, and the lightweight property of the lowest density structural material, magnesium.

Steel-magnesium composites have a number of attractive advantages. The low density of magnesium (1.8 g/cm³) provides good potential to make lightweight composites. A simple calculation for the density of a steel-magnesium composite as a function of the volume fraction of magnesium is shown in Fig. 1.1. It can be seen that for a composite with 30% magnesium, the density is 23% lower than steel. It is also important to note that the mutual solubility of iron and magnesium is extremely low and no intermetallic phases appear on the equilibrium phase diagram [1], so brittle intermetallic phase, which are usually the “hotbeds” of cracks, are not expected to nucleate and grow during thermo-mechanical treatment of the composite [2, 3]. On the other hand, the steel-magnesium composites may also have some disadvantages. It is challenging to fabricate such composite because the melting temperature of iron is higher than even the boiling temperature of magnesium, therefore, conventional casting techniques are eliminated. In addition, the corrosion of magnesium due to the electrochemical reaction in the composite could be a major problem for the applications of steel-magnesium composites.

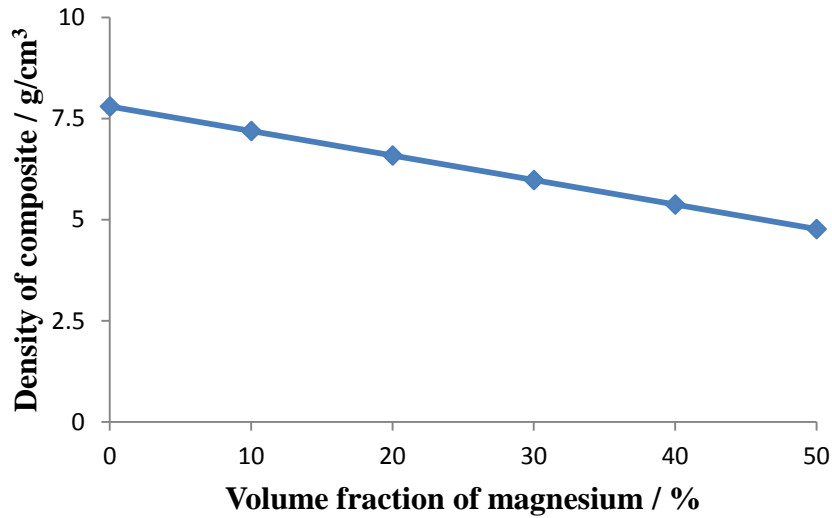


Fig. 1.1. The potential for making lightweight steel-magnesium laminated composites.

For steel-magnesium composite materials, there are recently published explorations of composites in the form of composite wire obtained by repeated co-extrusion [3] and that of laminated metal composites (LMCs) processed by infiltration [4]. The LMCs are a unique form of composite material in which alternating metal or metal containing layers are bonded together with discrete interfaces [5]. There are many techniques to fabricate the LMCs, including deposition techniques, infiltration, adhesive bonding, hot pressing, roll bonding, etc. Among these various techniques, the roll bonding technique used in this work is of particular interest since the process is simple, efficient, and could be applied for large scale production. Roll bonding is a solid phase operation in which the component metal sheets are roll bonded together under pressure and/or heat either sequentially or simultaneously [5]. Recently, Tsuji et al. [6-8] have developed a novel roll bonding technique, the accumulative roll bonding (ARB), in which the normal roll-bonded material is cut into two, stacked and roll-bonded

repeatedly. It is therefore possible to fabricate LMCs with a number of layers by the ARB technique.

The objective of this work is to fabricate the steel-magnesium laminated composites by means of roll bonding and to assess the mechanical properties of the composites in comparison with those of the monolithic component materials. We examine the mechanical responses of the composite, including decohesion between steel and magnesium, during tension and bending. This work also tests the effectiveness of predictions for the tensile strength based on the rule of mixtures. Finally, it is of interest to examine the fracture modes of steel and magnesium with different layer thicknesses in the composites in tension, and to compare those with the fracture modes for monolithic steel and magnesium.

Chapter 2: Literature review

In this chapter, the concept and advantages of the hybrid (composite) materials, as well as the design process of these hybrids will first be reviewed. Then, the room temperature tensile properties of the laminated metal composites will be described. Next, the previously reported results on steel-magnesium composites will be reviewed. Finally, the roll-bonding and accumulative roll bonding processes will be described and the process parameters affecting bonding will be summarized.

2.1. Designing hybrid materials

2.1.1. Introduction to hybrid materials

In contrast to the traditional monolithic materials, hybrid materials, as shown by the central circle in Fig. 2.1 [9], are combinations of two or more materials assembled in such a way as to have attributes not offered by either one alone. As such they combine the properties of two (or more) monolithic materials, or of one material and space. There are a variety of mature designs and competitive products of the hybrid materials in today's market.

There are many types of hybrid materials. According to the length scale of the component materials, there are macrocomposite, mesocomposite and microcomposite [10]. There are also many different hybrid materials categorized by configuration, including particulate and fibrous composites, sandwich structures, lattice structures, segmented structures, and more. These four typical configurations and their potential advantages are shown in Fig. 2.2 [9]. Besides those four typical configurations, many more can be obtained by using advanced processing techniques. For example, a wide variety of geometries can be

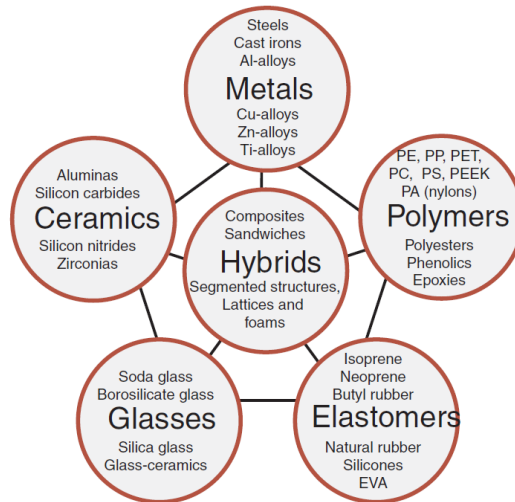


Fig. 2.1. The idea of the hybrid materials (reprinted from [9] with permission from Elsevier).

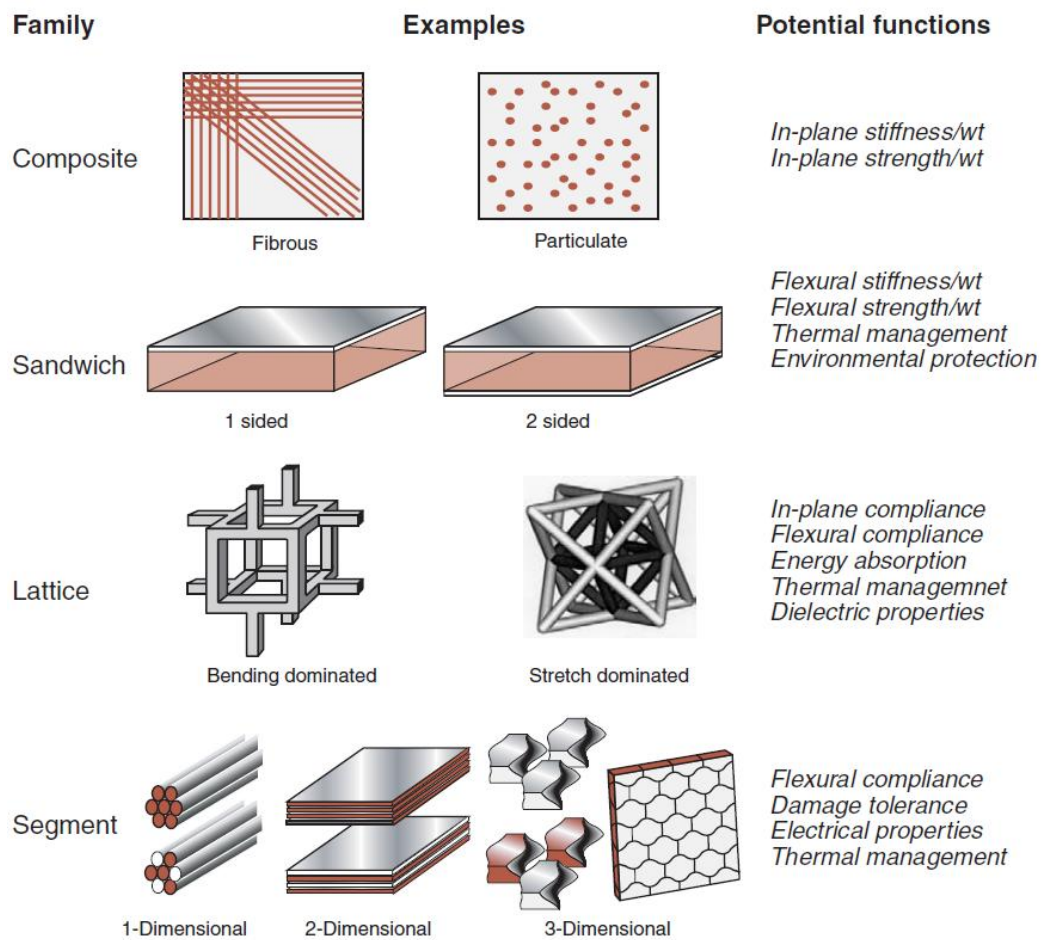


Fig. 2.2. Four typical families of configurations of hybrid materials (reprinted from [9] with permission from Elsevier, “wt” in the figure is the abbreviation for weight).

produced by surface treatments combined with masking or machining operations, as illustrated in Fig. 2.3 [11].

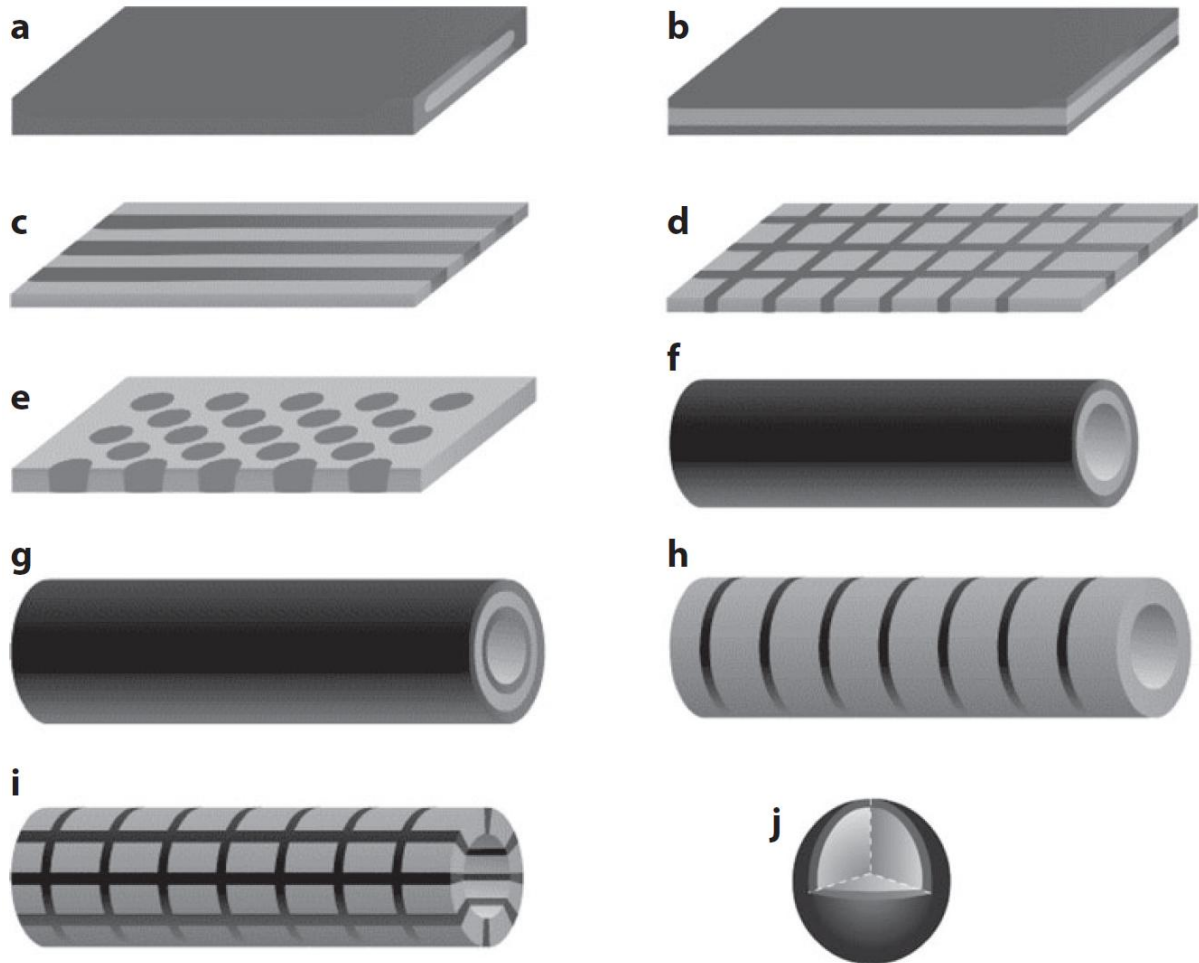


Fig. 2.3. An illustration of the various composite geometries that can be obtained by decarburization (reprinted from [12] with permission from John Wiley and Sons).

2.1.2. What could we achieve by designing a hybrid?

Ashby [9, 13] has summarized some advantages of hybrid material for the four possible scenarios, as shown in Fig 2.4 [9]. In Fig. 2.4, the fields occupied by two materials, M_1 and M_2 , are schematically shown and plotted on a chart with properties P_1 and P_2 as the axes (the

properties are assumed to become better along the positive directions of the axes). With different shapes and different combination methods, one may achieve any one of the scenarios listed in Table 2.1.

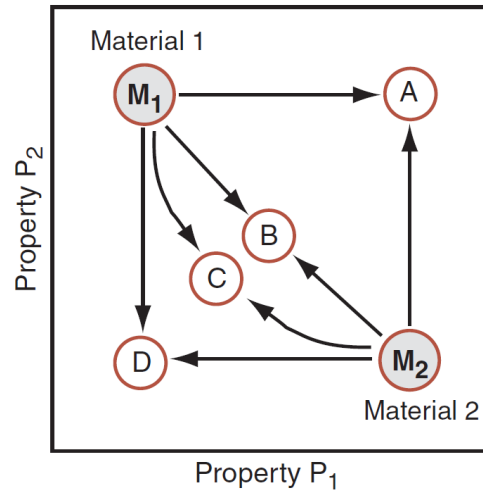


Fig. 2.4. Possibilities of hybridization (reprinted from [9] with permission from Elsevier).

Table 2.1. The details of four possibilities of hybridization (summarized according to ref. [13]).

Points	Scenarios	Descriptions	Examples
A	The best of both	A hybrid with the best properties of both components.	Zinc coated steel, Glazed pottery
B	The rule of mixtures	The best that can be obtained is often the arithmetic average of the properties of the components, weighted by their volume fractions.	Unidirectional fiber composites
C	The weaker link dominates	The hybrid properties fall below those of a rule of mixtures, lying closer to the harmonic than the arithmetic mean of the properties	The stiffness of particulate composites
D	The worst of both	A hybrid with the worst properties of both components.	

It can be seen from Table 2.1 that scenario A is the most desirable case while scenario D is undesirable. In practice, however, “the best of both” is most commonly accomplished

when a bulk property of one material is combined with the surface properties of another, i.e. coating, whereas when bulk properties are combined in a hybrid, as in structural composites, the best that can be obtained is often “the rule of mixtures” scenario.

2.1.3. Design of hybrid materials

A hybrid material is defined as a combination of two or more materials in a predetermined geometry and scale, optimally serving a specific engineering purpose [14]. Based on this definition, Ashby [9, 13] proposed the “A + B + shape + scale” method for designing hybrid materials. The basic idea of this method is illustrated in Fig. 2.5 and explained below.

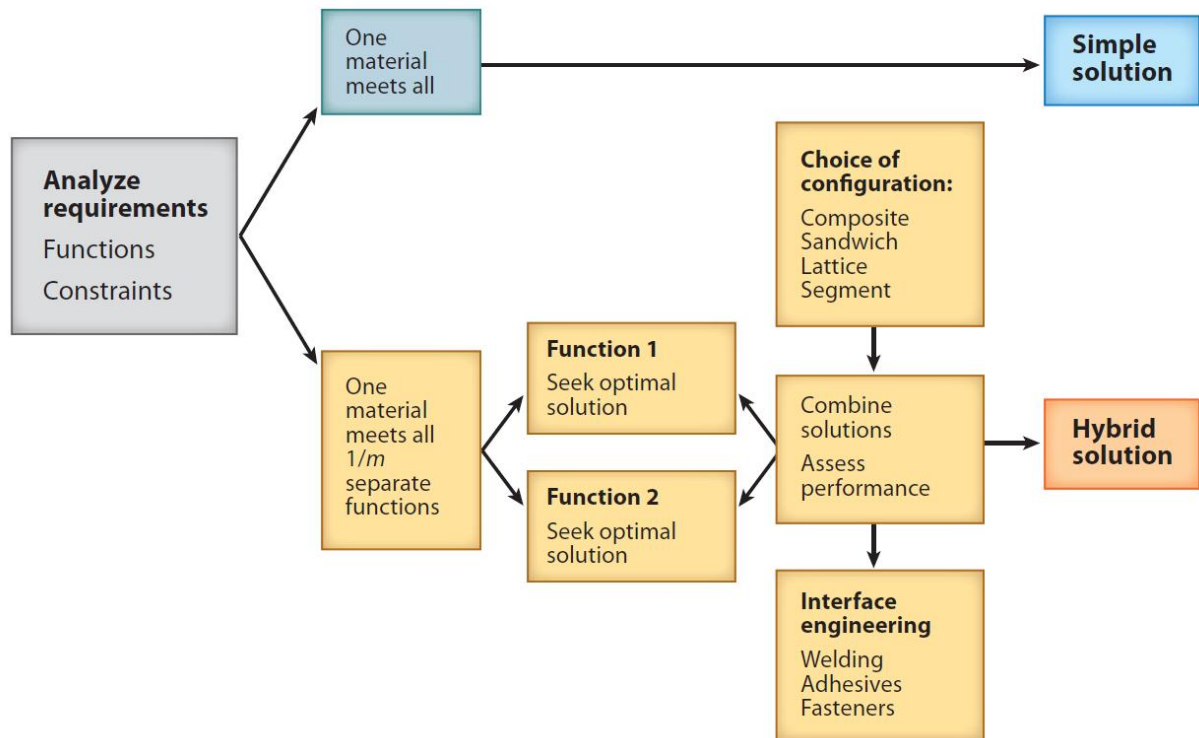


Fig. 2.5. The steps in designing a hybrid to meet given design requirements (reprinted from [9] with permission from Elsevier).

Monolithic materials offer a certain portfolio of properties on which much engineering design is based, and the design requirements isolate a sector of material–property space. In many cases the requirements can be met by a single-material solution; but if the design requirements are exceptionally demanding, no single material may be found that can meet all the requirements. In this case, the way forward is to identify and separate the conflicting requirements, seeking optimal material solutions for each, and then combine them in ways that retain the desirable attributes of both [9].

Ashby has established a systematic multi-objective optimization design [15] and materials selection method [16], in which the most important step is to derive the so-called performance index. A performance index is a property or group of properties which measures the effectiveness of a material in performing a given function [17-20]. For example, the stiffest beam is that with the highest modulus, E , and here E is the performance index. But it can usually be much more complicated. The indices that are often used in mechanical design have been summarized by Ashby [16]. It is expected that the performance index can be maximized during hybrid design to produce properties that are better than those of existing materials.

The performance index can often be shown as a line of equal performance on an Ashby map. One example is illustrated in Fig. 2.6 [9], which plots Young’s modulus vs. density for a wide range of materials. For example, a series of parallel lines with slope equal to $1/2$ on log-log chart, (i.e. constant $E^{1/2}/\rho$) provides a series of lines where the performance of the material is equal. Parallel lines which move to the left and up are materials with superior performance (in this case lighter, stiffer beams).

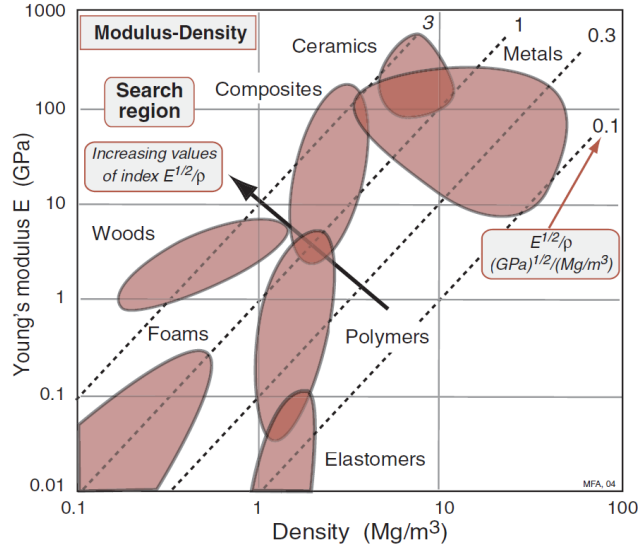


Fig. 2.6. A schematic E - ρ chart showing guidelines for a light, stiff beam (reprinted from [9] with permission from Elsevier).

2.2. Laminated metal composites

Laminated metal composites (LMCs) are a unique form of composite material in which alternating metal or metal containing layers are bonded together with discrete interfaces. Those composites can dramatically improve many properties including fracture toughness, fatigue behavior, impact behavior, wear, corrosion, and damping capacity; or provide enhanced formability or ductility for otherwise brittle materials [5]. The idea of laminating different metals and alloys to form a composite material that exploits the good properties of the constituent materials can be traced back to thousands of years ago in the ancient spears and shields [21]. The modern practical application of LMCs was particularly well examined in the former Soviet Union, where bi-material laminates including steel/steel, Al/steel, Cu/steel, and Al/Cu have been manufactured by means of explosive bonding and welding [22], and over 80 combinations of metals have been successfully laminated including some in which multi-layer laminates have been formed.

Modern LMCs can be made by a variety of techniques, e.g. bonding, deposition, and spray forming. The bonding techniques may be classified into several subgroups, such as adhesive bonding [23, 24], infiltration [25], diffusion bonding [26], reaction bonding [27] (especially for Ti-Al and Ni-Al systems), and deformation bonding such as roll bonding [28]. With these bonding techniques, laminated composites with relatively thick layers (typically from 50 to 1000 μm) can be obtained. On the other hand, deposition techniques involve atomic or molecular scale transport of the component materials such as in sputtering, evaporation, chemical or physical vapor deposition (CVD or PVD), spray or electroplating, by means of which the ultrathin layer (from several nm to 1 μm) laminated composites can be produced [5]. The typical SEM photographs of microstructures of the LMCs produced by roll-bonding with different layer thicknesses are shown in Fig. 2.7 [29].

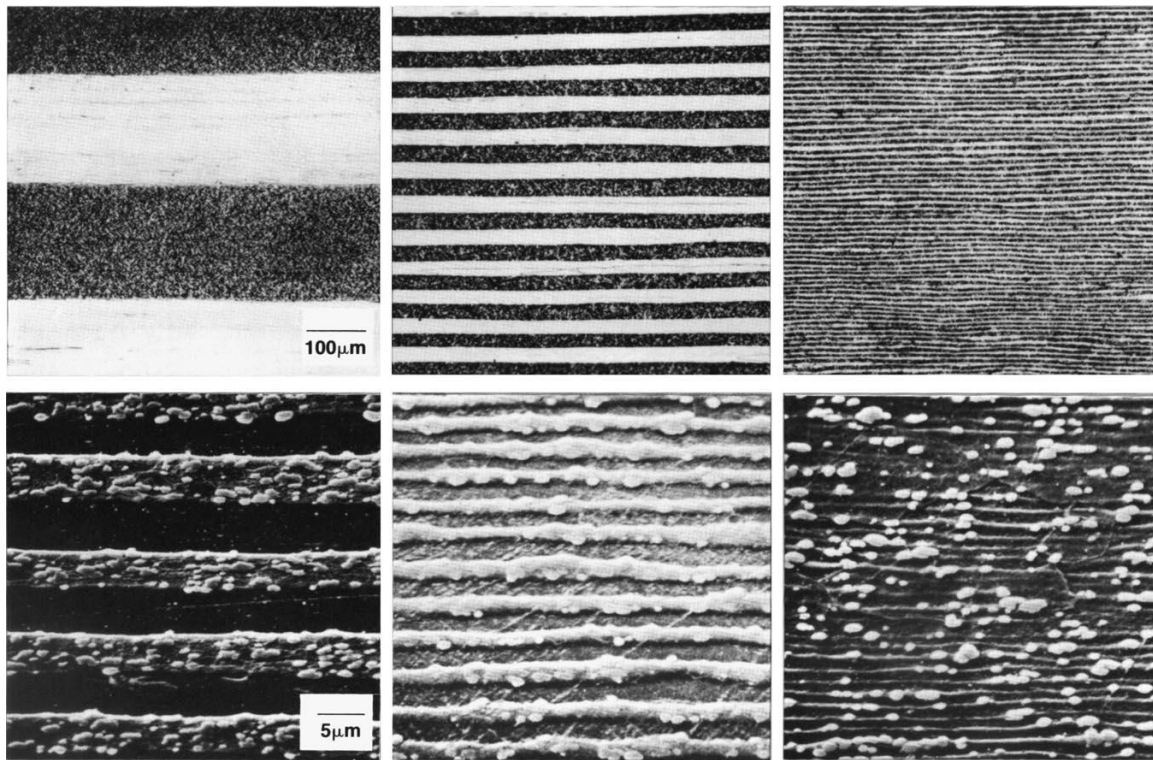


Fig. 2.7. Photomicrographs of LMCs of UHCS/Fe- 3Si alloy processed by roll bonding [29] (the top and bottom three are under same magnification, respectively, reprinted from [21] with permission from Elsevier).

2.2.1. Tensile behavior at low temperatures

LMCs may be categorized roughly into two groups, ultrathin layer LMCs, which have a laminate spacing smaller than several micrometers, and thick layer LMCs, which possess typical layer thicknesses of hundreds of micrometers. The tensile properties of both ultrathin and thick layer LMCs have been studied.

2.2.1.1. Tensile properties of ultrathin layer LMCs

The tensile properties of ultrathin layer LMCs have been studied, but typically only their breaking strength is reported. Lesuer et al. [5] summarized a graph of tensile strength data obtained on such materials processed by electro-deposition or by sputtering, as shown in Fig. 2.8, in which the data are for copper layered with nickel or Monel [5, 30, 31]. The figure shows the breaking strength (essentially equivalent to the ultimate tensile strength) as a function of the reciprocal square root of the multilayer periodicity width. Lesuer et al. [5] pointed out that for each set of data, a Hall-Petch type relation was observed, which means a linear relation was observed over a range of laminate layer spacing, the strength increasing with a decrease in the modulation width. Thus, it can be seen that the laminate spacing is an important variable in controlling the strength of the laminate. It should also be noted that a maximum in strength was observed for two of the individual investigations; and beyond this maximum, the strength decreases with further decreases in modulation width. The reason for the further decrease of strength is, according to the literature [30], that the interface can act a sink for dislocations at fine laminate spacing, thus further decrease of modulation width reduces the dislocation density and contributes to a decrease in strength.

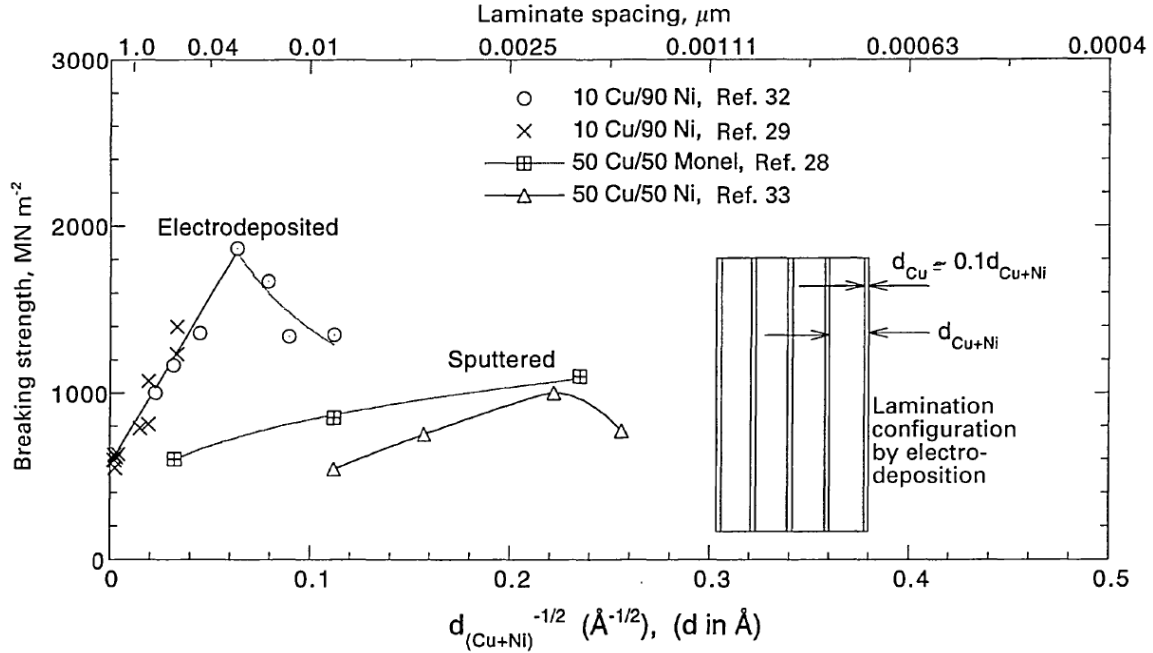


Fig. 2.8. Breaking strength of ultrathin layer laminated composites as function of modulated spacing d : laminates are based on layers of Cu alternating with either Ni or Monel layers (reprinted from [5] with permission from *International Materials Reviews*, Maney Publishing, www.maney.co.uk/journals/imr and www.ingentaconnect.com/content/maney/imr).

2.2.1.2. Tensile properties of thick layer laminated composites

For the thick layer LMCs, the yield strength can be readily predicted by the rule of averages, which has been used for the laminated systems with two components of equal volume fraction. The rule of averages is based on the assumption that both components yield at the same strain, and is described as [5]:

$$\frac{\sigma_y}{(\sigma_y)_A} = 0.5 + 0.5 \times \frac{(\sigma_y)_B}{(\sigma_y)_A} \quad (2.1)$$

where σ_y is the yield strength of the composites, $(\sigma_y)_A$ the yield strength of the strong component, and $(\sigma_y)_B$ the yield strength of the weak component. Lesuer et al. [5] also showed the application of Eq. 2.1 in predicting the normalized strength of the laminate

(normalized by the stronger component) as a function of the yield strength ratio of the component materials, as shown in Fig. 2.9. It can be seen from Fig. 2.9a that for a number of UHCS- or Al- based LMCs [32-36] with a wide range in relative strengths, the experimental results fit well with the line predicted by the rule of averages.

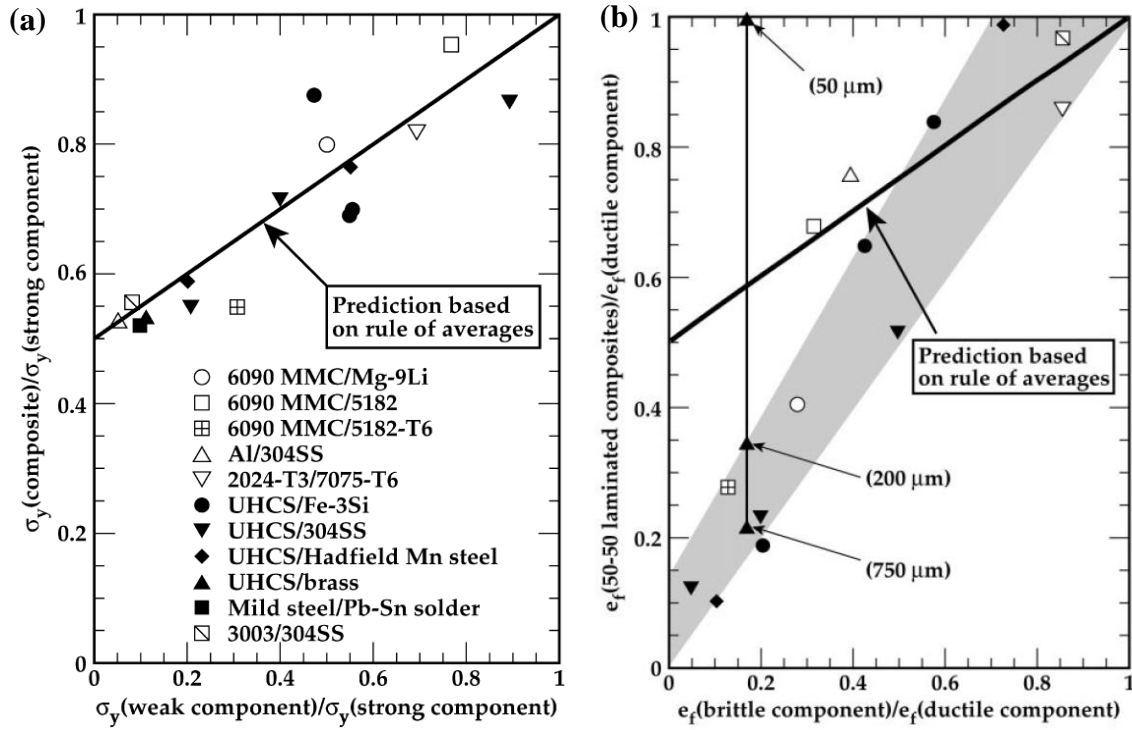


Fig. 2.9. Experimental yield strength (a) and tensile elongation to fracture (b) of thick-layer laminated composites containing 50 vol.% of each component, compared with prediction based on the rule of averages (given by the solid line) (reprinted from [22] with permission from *International Materials Reviews*, Maney Publishing, www.maney.co.uk/journals/imr and www.ingentaconnect.com/content/maney/imr).

In contrast to the yield strength, the tensile ductility cannot be predicted by the rule of averages as can be seen in Fig. 2.9b. The lack of agreement between the rule of averages and the experimental data is attributed to the fact that the tensile ductility of laminates is dependent on many variables, including the susceptibility of the lower ductility layer to cracking, the contribution to cracking from the interlayer region, the ease of delamination,

and the influence of layer thickness [5]. It also should be noted that the tensile ductility of most of laminated composites is lower than that predicted from the rule of averages when the difference between ductility of the two components is large [5].

The most important observation in Fig. 2.9b [5] is that the total elongation to failure results for the UHCS/brass laminate (solid triangles) indicate that the tensile ductility of the laminate can be either less or greater than the prediction from the rule of averages. These results have been interpreted in terms of the effect of layer thickness on the ductility of laminated composites, i.e. when the layer thickness is 750 μm , the tensile ductility is 13%; when the layer thickness is 200 μm , the tensile ductility increases to 21%; and when the layer thickness is 50 μm , the tensile ductility reaches 60% [37]. This trend is attributed to the greater difficulty for delamination as the layer thickness is reduced. Interfacial delamination is suppressed with decreasing layer thickness due to the decrease in residual stresses, which are usually produced by the thermal expansion mismatch between the component materials that occurs during cooling down from the processing temperature [5, 37]. Inhibition of delamination prevents neck formation in the less ductile UHCS layers, which would otherwise create hydrostatic tensile stresses in the neck zone in these layers, leading to crack initiation and the final failure [5].

2.2.2. Toughening mechanisms

An increase in toughness of the material is another area where LMCs possess great potential. Toughening in LMCs can arise from many different sources, including both intrinsic toughening and extrinsic toughening mechanisms [5, 38]. The former one results from the inherent resistance of the microstructure to crack growth and thus is influenced by

the microstructural characteristics such as grain size, particle spacing, particle size, etc; the latter is caused by reducing the local stress intensity at the crack tip and thus the local “driving force” for crack growth, and the distinct layers present in LMCs toughen these materials by various extrinsic mechanisms, which have been summarized by Lesuer et al. [5] in Fig. 2.10. Those toughening mechanisms are also helpful when assessing the tensile fracture and formability of the LMCs.

Mechanism (Testing orientation)	Volume fraction dependence	R-curve behavior possible	
Crack deflection (Crack arrester)	No	...	
Crack blunting (Crack arrester)	No	...	
Crack bridging (Crack arrester)	Yes	Yes	
Stress redistribution (Crack arrester, crack divider)	...	Yes	
Crack front convolution (Crack divider)	Yes	Yes	
Local plane stress deformation (Crack divider)	...	Yes	

Fig. 2.10. Toughening mechanisms of LMCs (reprinted from [5] with permission from *International Materials Reviews*, Maney Publishing, www.maney.co.uk/journals/imr and www.ingentaconnect.com/content/maney).

2.3. Steel-magnesium hybrid materials

Unlike other common systems including Fe/Al, Fe/Cu, Cu/Al, Fe/Ti, Cu/Al etc., the iron/magnesium system is unique because iron and magnesium are immiscible, i.e. the mutual solubility of iron and magnesium is extremely low and they form no intermetallic phases. This is important because brittle intermetallic phases are not expected to form during processing of these hybrids [2, 3]. This is promising since intermetallic phases are often brittle and can be sources for crack nucleation and propagation. On the other hand, the preparation and processing of iron/magnesium hybrid materials is challenging. For example, the preparation of iron-magnesium alloys using conventional casting processes is difficult since the melting temperature of iron is higher than the boiling temperature of magnesium [3]. Besides the melting temperature, other mismatches in properties, such as the large mismatch in the coefficient of thermal expansion (Table 2.2), also contribute to the difficulties of processing iron/magnesium composites.

Table 2.2. Physical properties of iron and magnesium.

Element	Melting temperature (°C)	Lattice structure	Young's modulus (GPa)	Density (g/cm ³)	Thermal expansion coefficient at 20 °C (linear, 10 ⁻⁶ /°C)
Fe	1536	BCC/FCC	200-210	7.86	11.1
Mg	649	HCP	45	1.74	26.0

Since magnesium is considered to be inert when in contact with iron [4, 39] (in the liquid state, magnesium and its alloys are almost universally processed using iron or steel crucibles, pipes, pumps and molds [40]), there have not been many reported results regarding iron/magnesium composites. To the best of the author's knowledge, the first exploration for the possibility of making iron/magnesium composite was made by Viala et al. [41] in 1990s

when they determined the chemical interaction at the interface between mild steel and liquid magnesium. In their experiments, mild steel (E24) pieces and magnesium powder (99.7 wt. % Mg) were cold-pressed together and heated under argon atmosphere at 1000 K for 65 h, then the steel/magnesium interfaces were characterized after cooling down. Their experimental results indicate that the excellent chemical inertness of steel towards liquid magnesium could be altered by the presence of impurities or by the addition of alloying elements to the base metals. It was found by Viala et al. [41] that less than 0.02 wt.% of aluminum or silicon presented in magnesium could react at 1000 K with iron, resulting in the formation of an α - $Fe(Al, Si)$ solid solution. Another quaternary compound, $Fe_2(Al, Mg)C$, was also found to form at the steel/magnesium interface.

Sacerdote-Peronnet et al. [42] studied the local reinforcement of magnesium base castings with mild steel inserts. Bimetallic samples were prepared by dipping E24 mild steel rods into the Mg–Al–Mn–Zn alloys melts held at 650–750°C for 1–5 min, and then the interfaces were observed and the bonding was characterized via push-out tests. No metallurgical bonding was obtained for the case with 30–100s duration at 630–650°C, while partial metallurgical bonding was achieved for 240–360s at 700–730°C. However, when a galvanized E24 steel bar was used, a sound metallurgical bond could easily be obtained at 650°C through the growth of Al–Mn–Zn reaction zones at the interfaces. The schematic of the push-out test setup can be found in [42] and it can be seen clearly from the samples after tests that the galvanized steel has much better bonding with magnesium than the uncoated steel

In addition to these steel-magnesium macrocomposites, mesocomposites and microcomposites of steel-magnesium have also been investigated in both wire and plate

shapes. Bouaziz et al. [3] made steel-magnesium composite wire by repeated co-extrusion. The so-called repeated co-extrusion technique was first developed by Levi [43] to make continuous nanofilamentary Cu-Nb wires [44, 45] or other Cu matrix composites [46]. During the co-extrusion of steel-magnesium wire, as shown in Fig. 2.11 [3], a macroscopic assembly (with an outer diameter of 16 mm) of annealed low carbon steel tubes and annealed magnesium (purity 99.9 %) rods was first made, then it was cold drawn down to a diameter of 1 mm, annealed, reassembled, and redrawn to 1 mm. By making such composite wire, a reduction of about 20 pct in density compared to steel can be achieved. The microstructure of cross-section, tensile test results and fracture surface are shown in Fig. 2.12 [3]. The tensile test results indicate that annealing has strong effects on both the tensile strength and the ductility.

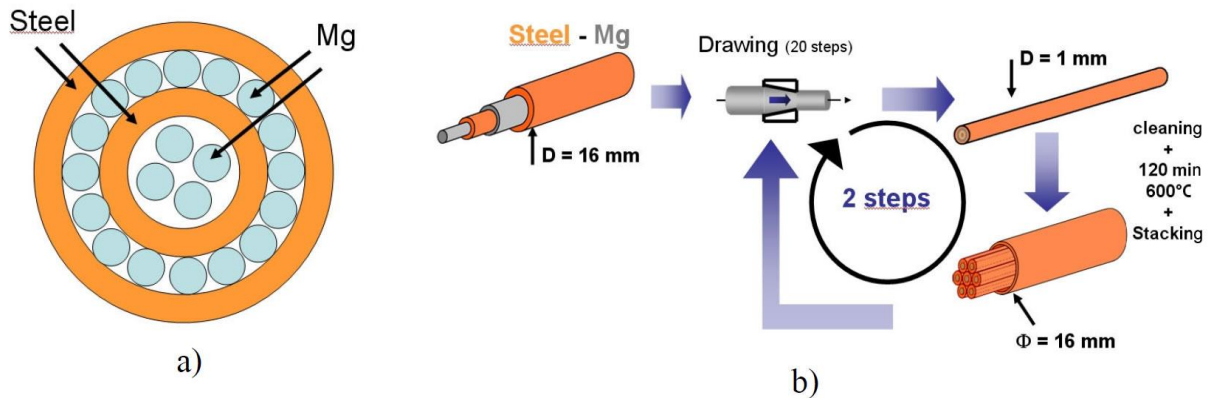


Fig. 2.11. Schematic of the co-extrusion process: (a) original macroscopic steel-magnesium assembly, and (b) the co-extrusion process used for the fabrication of the steel-magnesium composite wire (reprinted from [3] with permission from both Trans Tech Publications Ltd and the authors).

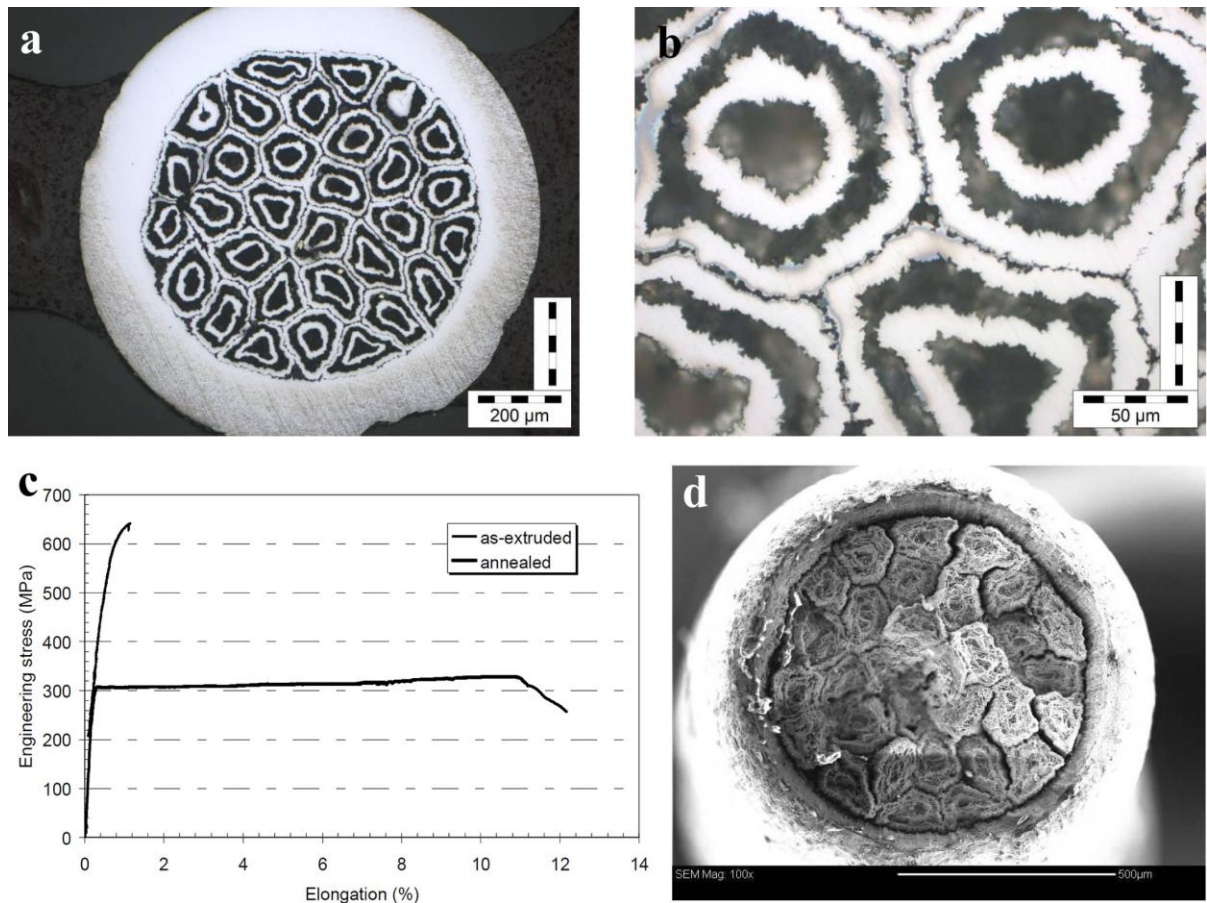


Fig. 2.12. Experimental results of the steel-magnesium composite wire: (a) and (b) micrographs illustrating the microstructures of the steel-magnesium composite wire in the cross section (steel is brightly imaged while magnesium is dark) at low and high magnification; (c) tensile test results; and (d) the fracture surface for the wire after annealing (reprinted from [3] with permission from both Trans Tech Publications Ltd and the authors).

Laminated steel-magnesium composites have been fabricated by Cetin et al. [4] using an infiltration technique. The approach they used consists of stacking low carbon steel sheets with a uniform spacing (0.1 or 0.2 mm) and infiltrating the stack with a liquid ZM21 magnesium alloy in argon atmosphere, and then allowing solidification of the magnesium. The space between layers was the same as the layer thickness so that the volume fraction of magnesium in the composite was 50%. Micrographs (Fig. 2.13) show that there is no gap or obvious intermetallic phase at the interface between the steel and magnesium layers.

However, the manganese in the magnesium alloy was found to migrate to the interface, forming manganese particles, and also diffusing into the steel along a band roughly 1 μm in thickness. The tensile properties were also measured and the results showed the UTS and uniform elongation generally obey the rule of mixture (ROM) predictions based on tensile properties of the individual composite components processed under the same conditions (the measured data were slightly lower than ROM predictions). The examination of the fracture surfaces, as shown in Fig. 2.14, reveals that the steel layers exhibit typical ductile failure [47], i.e. necking, void nucleation, growth, and coalescence; whereas the ZM21 magnesium alloy fails by shear, without necking [4]. A short zone of delamination between the magnesium and steel layers was also found, which probably resulted from the necking of the steel layers. The composites were also rolled by Cetin et al. [4] at 523 K, and it was found that the maximum strains could be reached during warm rolling were on the order of 60 pct, beyond which the laminates tended to debond.

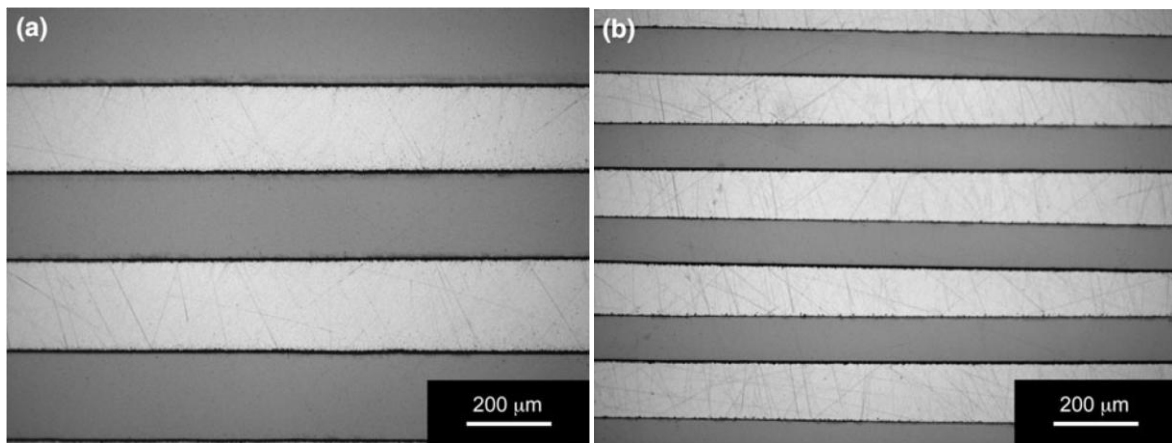


Fig. 2.13. Optical micrographs of as-cast LMCs with (a) 0.2 mm and (b) 0.1 mm layer thickness (the dark phase is steel and the light phase is magnesium, reprinted from [4] with permission from Springer).

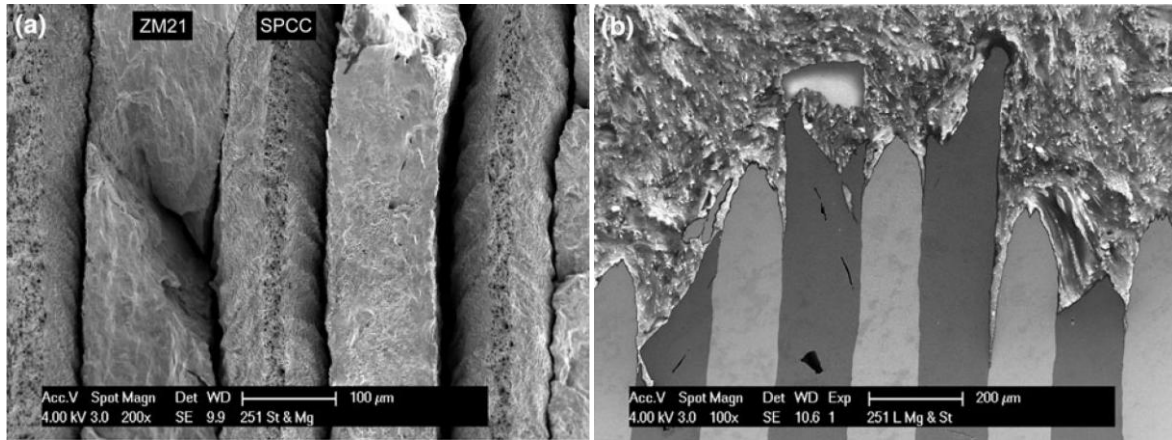


Fig. 2.14. SEM photographs showing: (a) fracture surface and (b) fracture profile of a 0.2 mm as-cast LMC in secondary electron mode (the light phase is steel and the dark phase is magnesium, reprinted from [4] with permission from Springer).

2.4. Roll bonding

Roll bonding, also known as roll welding, is a processing technique in which the component metal sheets are bonded together under pressure and/or heat either sequentially or simultaneously to form a bond between interfaces [5]. This process can be carried out in both cold [48] and hot [49] states (depending on the metal combinations), and sometimes also in the warm state. The cold roll bonding process has been reviewed by Li et al. [50] and the materials which can be cold roll bonded have been summarized by Forster et al. [51].

2.4.1. The roll bonding process

A schematic illustration of the typical cold roll bonding process is presented in Fig. 2.15 [50]. The process involves surface preparation, stacking, rolling, and/or a post heat treatment. During the process, the metal sheets are first surface prepared and stacked together, and then they are rolled with an appropriate amount of deformation to achieve bonding. There are two key points during the process, one is the quality of surface preparation prior to the rolling,

and the other is the amount of deformation in a single pass during rolling. The large amount of deformation can result in the formation of virgin surfaces on the materials being bonded and generate a great amount of heat simultaneously, thus the bonding can be obtained through interfacial mechanical and atomic affinity [50]. After rolling, a heat treatment can enhance the bonding by developing a strong metallurgical bond at the original interfaces between layers [7]. The hot roll bonding and warm roll bonding processes are similar to the cold roll bonding in nature, and the major difference is that there is a step of preheating the metal sheets (in some cases also preheating of the rolls) before rolling for the hot and warm roll bonding processes. The preheating might improve the bonding, but it can also introduce the formation of relatively thick oxide layers on the metals surfaces to be bonded, and this may obstruct the intimate contact between those metal layers and lead to poor bonding.

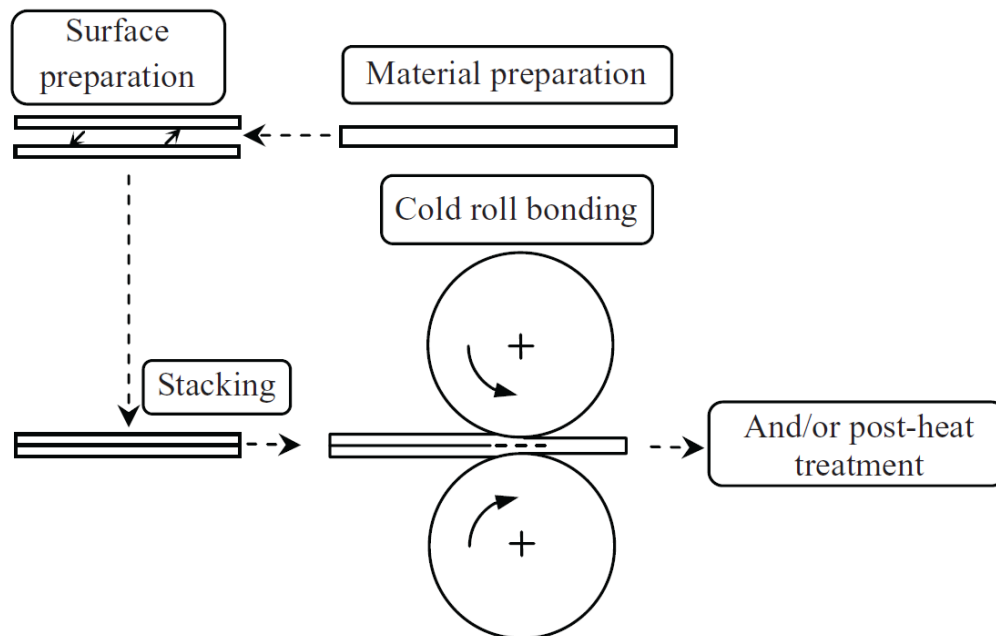


Fig. 2.15. Schematic illustration of the cold roll bonding process (reprinted from [50] with permission from STAM, details at creativecommons.org/licenses/by-nc-sa/3.0).

Recently, Tsuji et al. [6-8] developed a novel roll bonding technique, the accumulative roll bonding (ARB), as shown in Fig. 2.16 [6]. In ARB process, two or more sheets are roll-bonded together in the same way as those in the normal roll bonding process, but the bonded sample is then cut and stacked and roll-bonded again. By repeating the process with 50% reduction in each pass, a large plastic strain accumulation can be obtained. The ARB technique has been successfully used in the fabrication of a variety of composite sheets, including Cu-Zr [52], Al/Ni [53, 54], Al/steel [55], Ti/Ni [56, 57], Cu/Nb [58], etc.

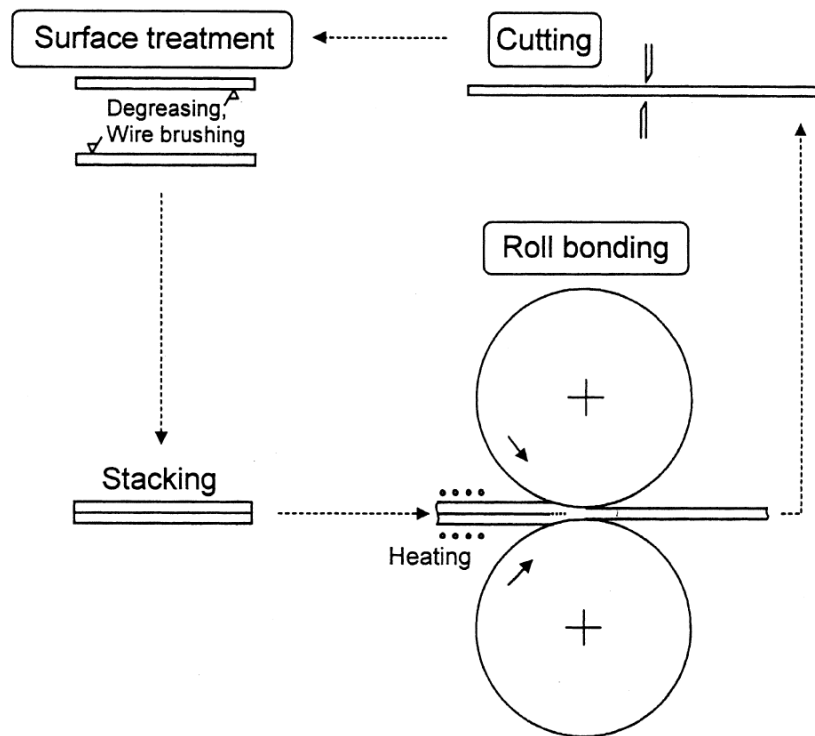


Fig. 2.16. Diagrammatic representation of the accumulative roll bonding process (reprinted from [6] with permission from Elsevier).

2.4.2. Parameters affect bonding

There have been many investigations on the bonding mechanisms and process parameters governing the bonding. The bonding quality can be affected by a number of

factors, including the amount of deformation [59, 60], the temperature of rolling [61, 62], the surface preparation conditions [59-61] and the layer thickness [63].

2.4.2.1. The amount of deformation

It has been found that during the roll bonding process, there is a so called threshold reduction, R_t , which is the minimum percentage reduction that consistently results in bonding emerging from the roll gap [64-66]. It has also been found that there is a relationship between the maximum theoretical bond strength and the percentage reduction [66]. Experimental results have confirmed the relationship between the bond strength and the deformation reduction, as shown in Fig. 2.17 [66, 67] for a variety of materials. The threshold reduction can be clearly seen in Fig. 2.17 since no bond could be obtained below a certain amount of deformation. With deformation larger than R_t , the bond strength increases dramatically with deformation amount in most cases in Fig. 2.17. It should be noted that the threshold reduction only refers to the deformation amount in the very first pass, whereas for multi-pass rolling, the bonding cannot be achieved unless the deformation in the first pass is large enough to initiate bonding [50, 66].

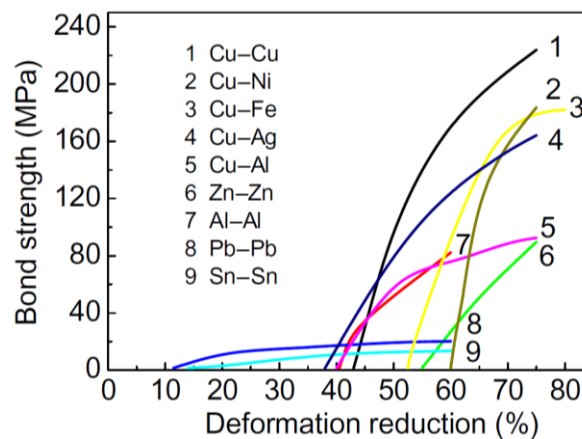


Fig. 2.17. Bond strength in shear as function of deformation reduction for bonds formed by roll bonding (reprinted from [50] with permission from STAM, details at creativecommons.org/licenses/by-nc-sa/3.0).

2.4.2.2. Surface preparation

Since the bonding between layers is facilitated by intimate contact between the virgin surfaces, the surface preparation should be a key parameter governing the bonding during the roll bonding process. In practice, metal surfaces are covered by oxide films and other surface contaminants [64, 68], the existence of which may inhibit bonding. Some researchers have examined the influences of surface contamination by bonding materials together with light loads under high vacuum condition, and it was found that the threshold deformation could decrease dramatically, even down to zero, when the surface is clean [69, 70]. Therefore, it is necessary to remove those oxides, compounds, absorptions, etc. as much as possible from the metal surface before starting roll bonding. Generally, there are two types of surface contaminations, one is the absorbed contaminations, and the other is the oxide layers on the metal surface. For the former one, it is almost impossible to remove all the absorbed contaminations from the metal surface although ultrasonic cleaning in acetone before rolling may be helpful to remove oils, grease and other absorptions. For oxide layers, the oxidation reaction at the fresh metal surface is spontaneous in most cases, so the metal surface is usually coated with an oxide layer (exceptions include gold). The possible solution for the oxide layer is scratch brushing or electropolishing. Previous experimental results have confirmed that the oxide layer is a big obstacle for the roll bonding process, as it was shown that the longer the scratch-brushed samples were exposed to the air, the weaker the bond was observed [66].

2.5. Summary

In summary, the literature review shows that there are large potential benefits of producing laminated metal composite materials. The steel-magnesium system is a system of interest due to the potential to produce laminated composites with significantly lower densities than steel.

Chapter 3: Scope and objectives

3.1. Scope

Although there is currently a large amount of research on high-strength steels, the urgent demand for lightweight materials has not yet been satisfied. Since one monolithic material cannot meet all the requirements for lightweight materials in the automobile industry, it is of interest to examine hybrid material solutions.

The aim of the present work is to develop a new, cost-effective and lightweight material with good formability and other mechanical properties. The details of the design process are illustrated in Fig. 3.1.

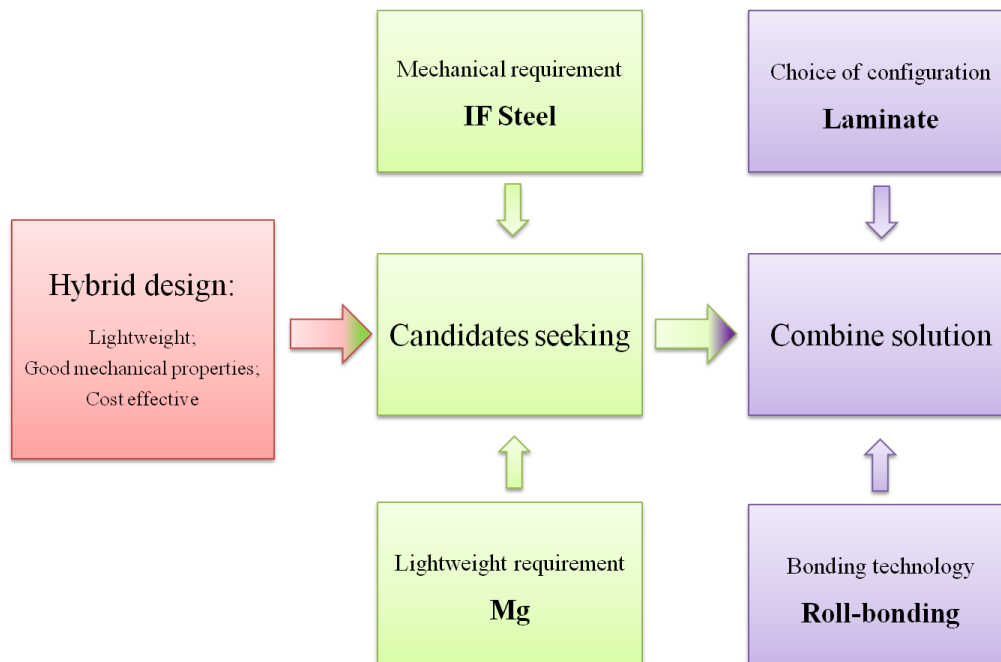


Fig. 3.1. Design process of the steel-magnesium laminated composite.

IF steel and commercial purity magnesium have been used as the two components for the composite. The composite has been produced in the form of laminated metal-metal composites by means of roll bonding. The mechanical behavior of these laminated composite materials with particular emphasis on the deformation and fracture modes of the composite materials in comparison with those of the monolithic component materials will be examined.

3.2. Objectives

The specific objectives of this work include the following:

- 1) Producing a steel-magnesium laminated composite with 10-20% magnesium, i.e. 8-17% reduction in density compared to steel;
- 2) Fabricating the IF steel-magnesium laminated composite with sound bonding by the roll bonding and accumulative roll bonding techniques;
- 3) Evaluating the mechanical responses of the composite materials during tension and bending, including decohesion between steel and magnesium, in comparison with the deformation modes of monolithic steel and magnesium;
- 4) Examining the fracture behaviors of the composite materials during tension and bending, with particular emphasis on the fracture modes of the component materials in the composite in comparison with those of the monolithic steel and magnesium.

Chapter 4: Experimental methodology

In this chapter, a brief description of the starting materials is given, followed by the rolling procedure including rolling of the monolithic materials, roll bonding process and accumulative roll bonding process. Then the microstructure characterization methods are described. Finally, the mechanical behavior tests, including the room temperature tensile tests, micro-hardness tests, three-point bending tests and the U-shape bending test series, are described.

4.1. Starting materials

The starting materials for the fabrication of the steel-magnesium laminated composites were interstitial-free (IF) steel sheet (2 mm in thickness) and commercial purity magnesium sheet (1 or 2 mm in thickness). The chemical compositions for the magnesium and IF steel are listed in Tables 4.1 and 4.2, respectively.

Table 4.1. The chemical composition (wt. %) of the commercial purity magnesium sheet.

	Mg	Al	Mn	Si	Zn
Commercial purity magnesium	bal.	0.06	0.01	0.02	0.01

Table 4.2. The chemical composition (wt. %) of the IF steel.

	Fe	C	S	Mn	Si	Cu	Ni	Nb	Al	Ti	B	N	P	Cr	Zn
I.F. Steel	bal.	0.003	0.012	0.524	0.080	0.024	0.018	0.001	0.049	0.051	0.001	0.002	0.072	0.026	0.001

Samples were cut from the as-received materials and prepared as metallographic samples. For magnesium, the samples were first mechanically ground, polished to 1 μm diamond and then electropolished in 10% nitric acid in ethanol at -20°C . For the IF steel, the samples were metallographically prepared to 1 μm diamond polish and then etched by 2%

nitric acid in ethanol at room temperature. The initial microstructures of the as-received magnesium and IF steel were observed with optical microscope (OM) or a Hitachi S-3000N scanning electron microscope (SEM). These results for magnesium and IF steel are shown in Figs. 4.1 and 4.2, respectively. To quantify the grain size, micrographs from optical microscope were printed out and the grain boundaries were manually traced on a transparent plastic sheet, which was then scanned into computer and analyzed by software. As can be seen in those images, the initial average grain size is approximately 28 μm for magnesium and 23 μm for IF steel. EBSD inversed pole figure suggests that the as-received magnesium is with very strong basal texture (not shown).

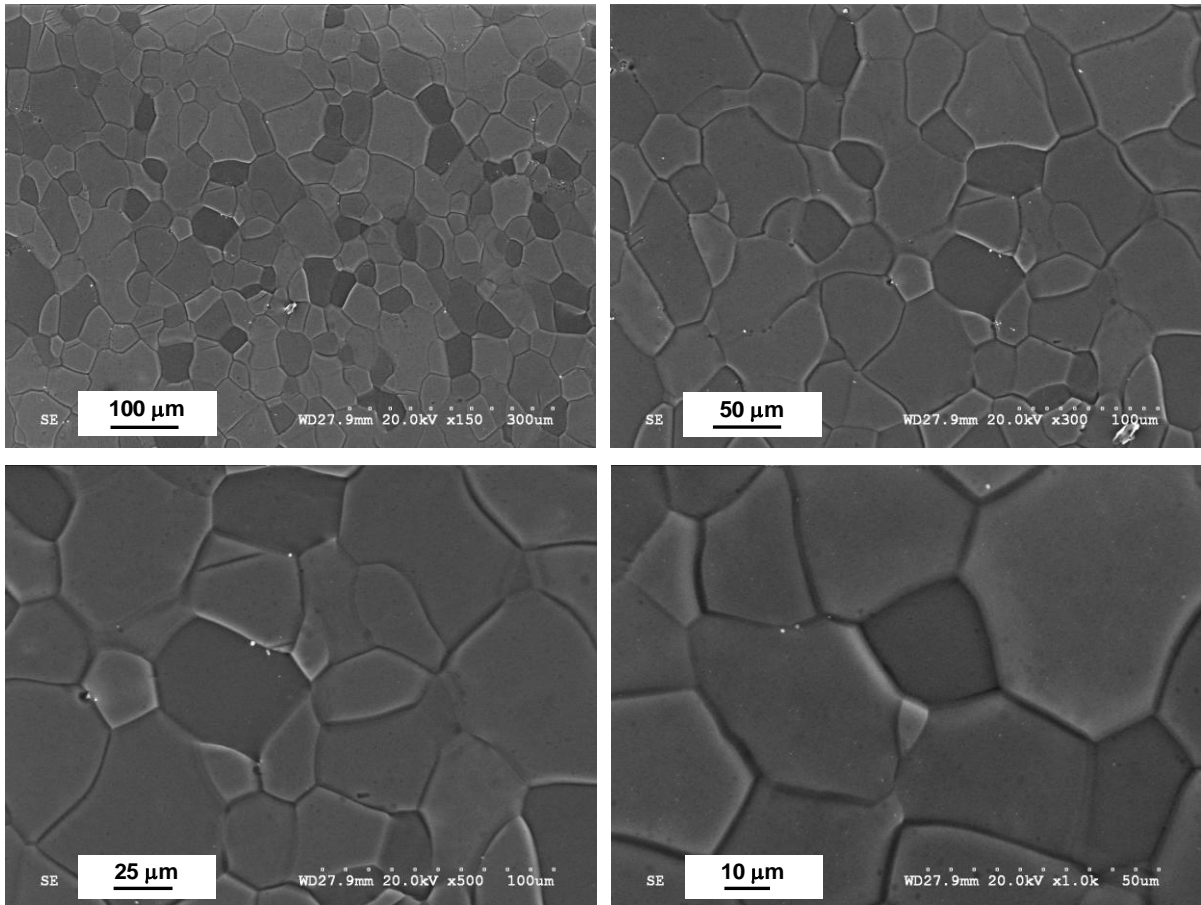


Fig. 4.1. Microstructures of the as-received magnesium, SEM images at four different magnifications (courtesy of Ghazal Nayyeri).

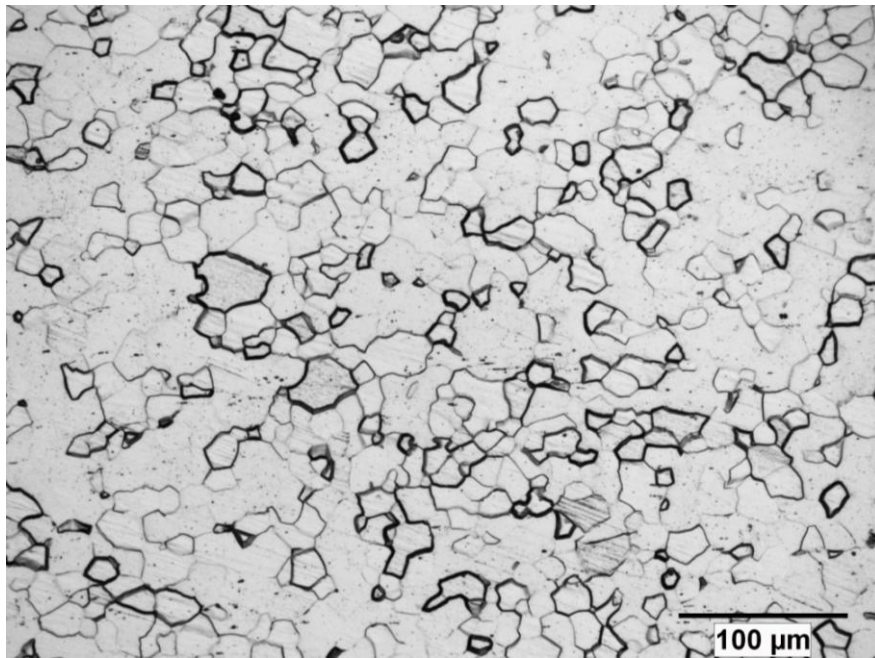


Fig. 4.2. OM images showing the microstructure of the as-received IF steel.

4.2. Rolling

4.2.1. Rolling of monolithic materials

To compare the mechanical properties of the roll-bonded laminates with those of the monolithic materials, monolithic IF steel and 2 mm thick magnesium sheets were rolled at 300°C, (i.e. the same temperature which will be subsequently used for the roll bonding process). These sheets were first heated to 300°C in a preheated box furnace, and then rolled to different thicknesses with total reductions of 30%, 50%, 70%, 80%, 90% and 95%, respectively. The rolling experiments were carried out using a laboratory rolling mill with the rolls at room temperature. The roll diameter was 150 mm and the rotational velocity of the rolls was 14 rpm. Before each pass, the materials were preheated to 300°C, but there was no post heat treatment after rolling for either materials. The largest reduction achievable was 80%

for the IF steel and 90% for the commercial purity magnesium (i.e. the minimum thickness was limited by a combination of the minimum roll gap and the roll separating forces). For larger reductions in the monolithic materials, accumulative roll bonding technique was used. The relevant surface preparation and roll bonding process will be described in Sections 4.2.2 and 4.2.3.

4.2.2. Roll bonding

Samples with dimensions of 100×25 mm were cut from the received IF steel and magnesium sheets and four small holes were drilled at the four corners of each strip. These strips were used for the roll bonding experiments.

The roll bonding process is schematically shown in Fig. 4.3. As shown in Fig. 4.3, before rolling, strips of 2 mm thick IF steel and 1 mm thick magnesium strips were degreased by swabbing with acetone, ground by sandpaper (120 grit) and brushed with steel wire brush (the procedures were similar to these from literatures [8, 50]). Subsequently, the strips were ultrasonically cleaned in acetone for 15 min. Immediately after that, three strips were bundled together at the four corners with steel wires in the sequence of steel/magnesium/steel, and were heated to 300°C in a preheated box furnace equipped with argon inflow. Finally, the unbonded metal combination, was rolled at 300°C using a reduction of about 50% in a single pass with the laboratory rolling mill mentioned above. After the roll bonding pass, some bonded samples were re-heated to 300°C and further rolled to different thicknesses with ~15% reduction per pass for microstructural observation and assessment of mechanical behavior.

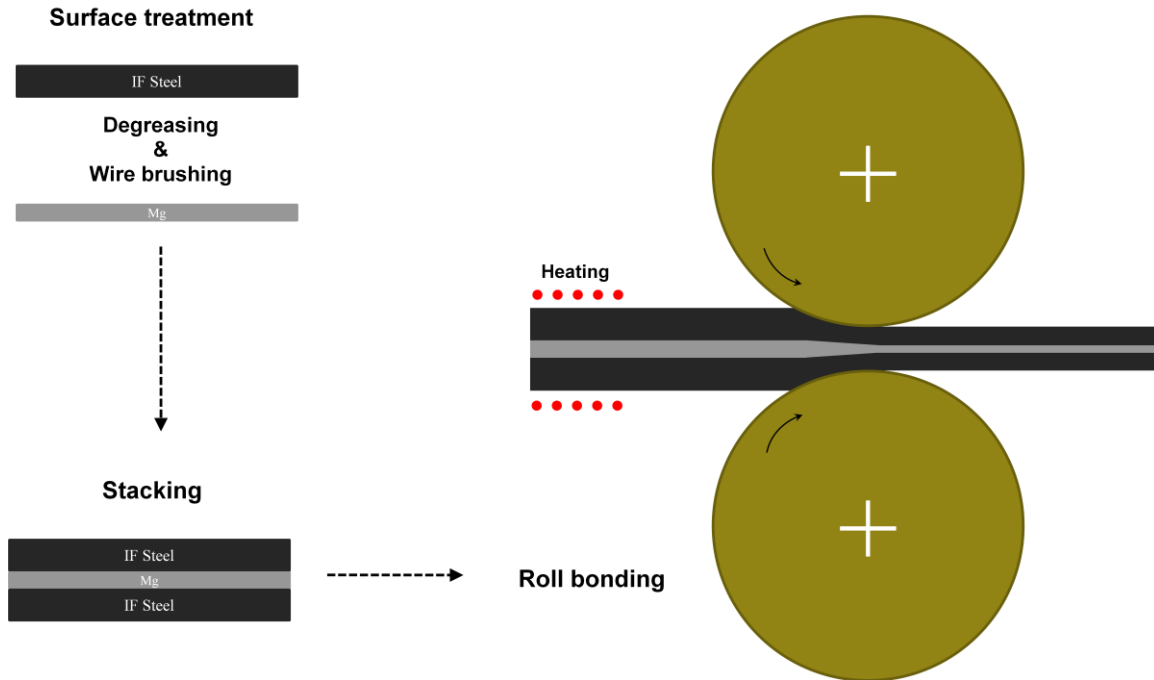


Fig. 4.3. Schematic of the roll bonding process.

4.2.3. Accumulative roll bonding

For ARB experiments, 1 mm thick IF steel was used due to the challenges with the rolling force for a large absolute reduction. The $100 \times 25 \times 2$ mm IF steel strips were cold rolled to 1 mm thick and annealed at 700°C for one hour in a box furnace to recrystallize the samples [71]. Strips with dimensions of 100×25 mm were cut from the recrystallized samples, and four small holes were drilled at the four corners of each strip. The ARB process is illustrated in Fig. 4.4. The roll bonding process was similar to that described in Section 4.2.2. During ARB process, the roll-bonded laminate was further rolled to 1 mm thick and then cut into two halves. Two of those cut laminates along with one 1 mm magnesium strip were surface treated again as described before and stacked together, similar to the steel/magnesium/steel combination, and were then roll-bonded with a reduction of about 50% in a single pass at 300°C .

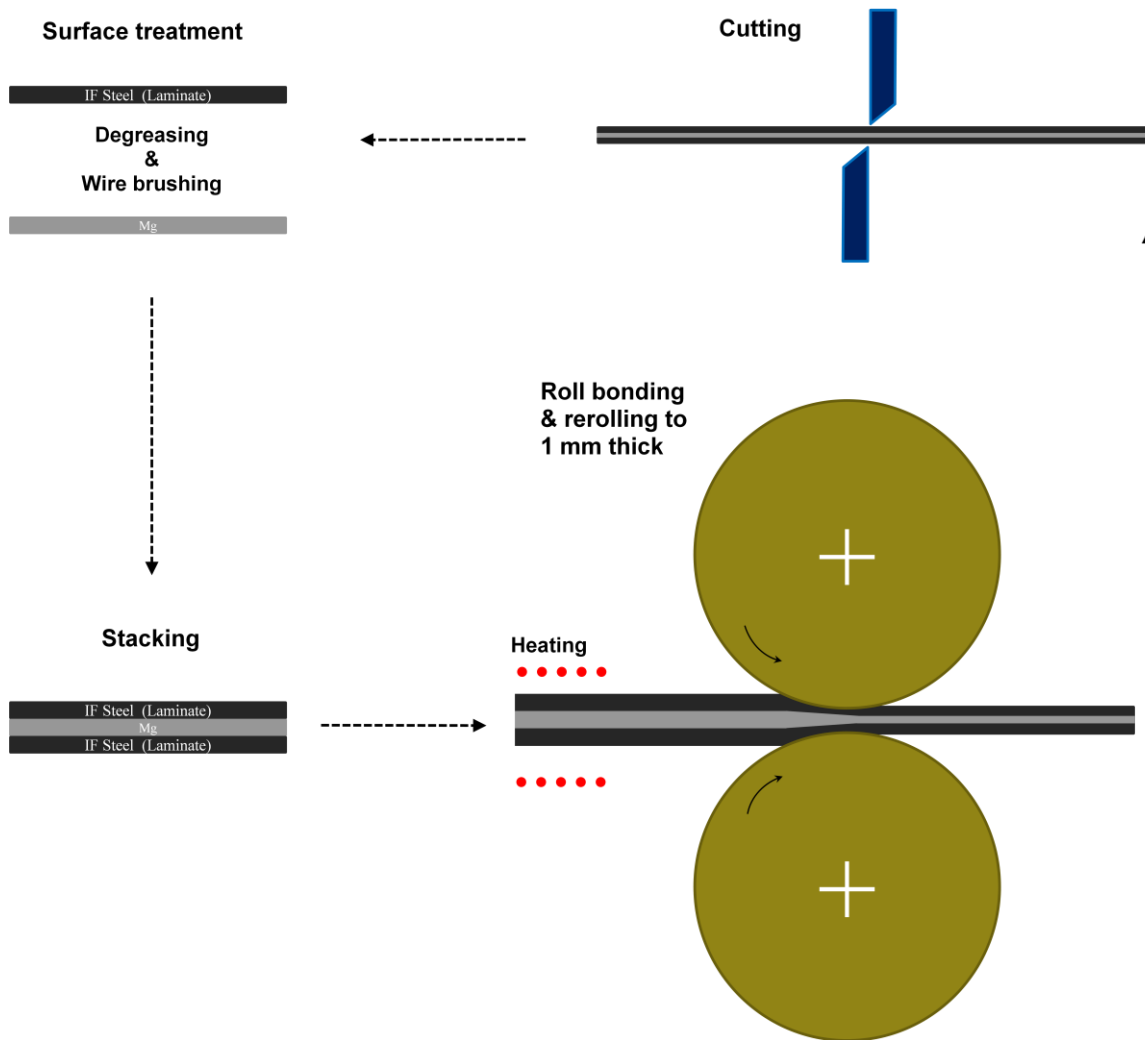


Fig. 4.4. Schematic of the ARB process.

4.3. Microstructural observation

Samples from the roll-bonded and accumulative rolled bonded laminated composite strips with different thicknesses were cut along both the rolling direction and transverse direction. The cut samples were then mounted in epoxy, with either the transverse direction or the rolling direction perpendicular to the observation plane, and prepared as metallographic samples. The mounted samples were first ground, at a low speed, with SiC sandpapers with water as lubricant and coolant, and then polished with 6 μm and 1 μm

diamond suspension on a polishing cloth. To avoid oxidation of magnesium, only diamond suspension and ethyl alcohol were used during the polishing. No etchant was used since the IF steel and magnesium system already had acceptable contrast when viewed in both secondary electron and back scattered channeling modes in the scanning electron microscope. For the case that magnesium layer is very thin (e.g. thinner than 80 μm at the cross-section), carbon particles from the diamond suspension might accumulate at the steel/magnesium interfaces and “conceal” magnesium at the cross-section during polishing, so those thin laminate samples were only ground to 1200 grid. After polishing, the metallographic samples were ultrasonically cleaned in ethyl alcohol for 15 min and were observed with a Hitachi S-3000N SEM.

4.4. Mechanical behavior tests

4.4.1. Room temperature tensile tests

Tensile test samples with different thicknesses (1 mm, 0.42 mm, 0.25 mm, corresponding to 80%, 92% and 95% reduction, respectively) were made from the roll-bonded laminates and the monolithic samples along the rolling direction. The dog-bone tensile specimens with a gauge length of 38.1 mm and a width of 6.35 mm were prepared by punching from the rolled sheets with a special die. For samples thicker than 1 mm, the tensile samples were prepared by machining. Tensile tests were carried out at room temperature using an Instron 8872 servo-hydraulic test machine with a crosshead speed of 0.1125 mm/second. For each case, at least three tests were carried out to confirm the reproducibility. After the tensile tests, the fracture surfaces of those samples were ultrasonically cleaned in acetone and examined in the secondary electron mode with a Hitachi S-3000N SEM. The

tested samples were also cut longitudinally, mounted in epoxy and prepared as metallographic samples to observe the fracture profiles.

4.4.2. Micro-hardness tests

The previously mentioned metallographic samples were also used for hardness measurements. The Vickers hardness was measured by using a Micromet 3 Micro Hardness Tester. The measurements were carried out on each layer in the cross-section of the laminate. The rolled monolithic materials were also cut and made into metallographic samples for the hardness measurement. It should be noted that the magnesium layer in the laminate sample may be very thin, and the surface of magnesium layer may be lower than that of IF steel layer at the observation plane because the soft magnesium could be removed more than IF steel during polishing. Thus, tapered samples were made, namely, the laminate strips was inclined by 45° from the observation plane to provide a larger projected area for the thin magnesium layer. The micro-hardness tests were done with a load of 500 g for the IF steel layer and 50 g for the magnesium layer. The indentations in the magnesium layer were carefully selected to ensure the deformation volume around the indentation did not reach the magnesium/steel interface. For each layer in each specimen, at least five tests were conducted and the average values were calculated.

4.4.3. Bending tests

For bending tests, specimens with dimensions of $100 \times 10 \times 1$ mm were sheared from the 1 mm thick roll-bonded laminated composites (i.e. 80% deformation), with the length direction parallel to the rolling direction. Three-point bending tests were conducted with the setup shown schematically in Fig. 4.5. A support span of 60 mm was adopted for these tests.

The three-point bending tests were run on an Instron 3369 test machine, and a crosshead speed of 5 mm/min was chosen. After the tests, the bent samples were mounted in epoxy and prepared as metallographic specimens, and then the cross-sections were observed with a Hitachi S-3000N SEM using secondary electron mode.

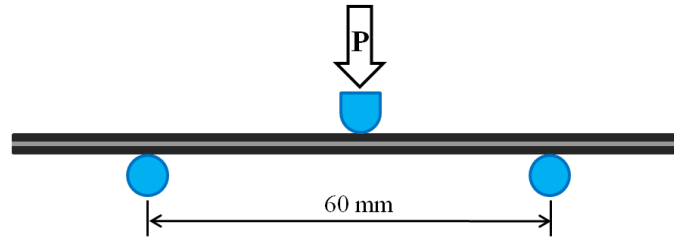


Fig. 4.5. Schematic of the setup for three-point bending tests.

The flexural modulus of the laminates was calculated from the three-point bending tests by using Eq. 4.1 [72].

$$E = \frac{L^3 m}{4bd^3} \quad (4.1)$$

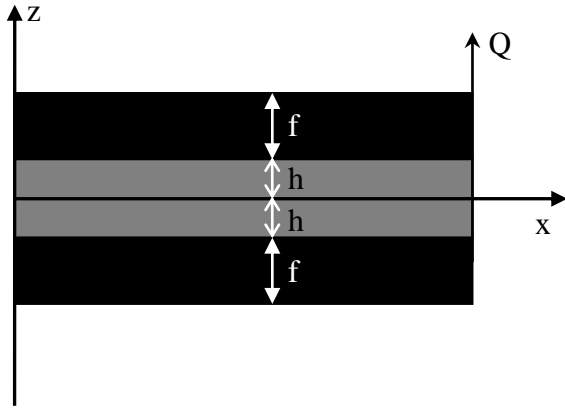
where E is the modulus of elasticity in bending (MPa), L the support span (mm), b the width of sample tested (mm), d the depth of sample tested (mm) and m the slope of the tangent to the initial straight-line portion of the load-deflection curve.

The flexural strain ε , which is the nominal fractional change in length of the outer surface of the sample at the middle point, can be calculated for any deflection by using Eq. 4.2 [72]:

$$\varepsilon = \frac{6Dd}{L^2} \quad (4.2)$$

where ε is the strain in the outer surface (mm/mm), D the maximum deflection of the center of the beam (mm), L the support span (mm) and d the depth of the sample.

The shear stress in the magnesium core that was induced during the three-point bending test can also be calculated based on the sandwich theory [73]. By assuming elastic deformation and the axial strain varies linearly over the cross-section of the beam, the shear stress in a sandwich deformed in the way as shown in Fig. 4.6 is given by Eqs. 4.3 through 4.5:



$$\tau^c = \frac{Q_x}{2D} [E^c(h^2 - z^2) + E^f f(f + 2h)] \quad (4.3)$$

$$D = \frac{2}{3} E^f f^3 + \frac{2}{3} E^c h^3 + 2E^f f h(f + h) \quad (4.4)$$

$$Q_x = \frac{dM}{dx} \quad (4.5)$$

Fig. 4.6. Schematic of bending of a sandwich beam.

where τ^c is the shear stress in the core, Q_x the shear force, D the flexural stiffness, M the bending moment, E^c the Young's modulus of core and E^f the Young's modulus of face, and h , z , f are defined in Fig. 4.6.

A U-shape bending test was also conducted to investigate the fracture behavior and crack propagation in the laminated composites during bending. Samples measuring $50 \times 10 \times 1$ mm were sheared from the 1 mm thick roll-bonded laminate samples (80% deformed), with the length direction parallel to the rolling direction. One sample was then placed in a laboratory vice and deformed slowly to bend the sample 180 degree (to a nominal interior

angle of 0 degree). The samples were bent perpendicular to the layers. After the test, the sample was cut longitudinally, mounted in epoxy and prepared as metallographic sample. Then the bend radius was examined with an optical microscope. In order to understand the crack initiation and propagation behavior, another three samples were deformed in the identical manner as mentioned above to three different interior angles, 50°, 35° and 12°, respectively, and then made as metallographic specimens and observed with an optical microscope.

Chapter 5: Experimental results and discussion

In this chapter, the experimental results and discussion on these results are presented. First, the microstructures of the roll-bonded and ARBed laminated composites will be shown and the rollability of the laminates as well as the deformation responses of laminates during rolling will be discussed. Second, the room temperature tensile behavior of the laminated composites will be assessed and compared with those of the monolithic materials under the same conditions. Third, the micro-hardness test results for the laminated composites and monolithic component materials will be presented. Last but not least, the bending behavior of the 80% deformed laminated composites, in both three-point bending tests and U-shape bending tests, will be evaluated, and the capacity of producing light yet stiff composite plate in bending will be discussed.

5.1. Microstructures of the steel-magnesium laminated composites

5.1.1. Microstructures of the roll-bonded laminated composites

The thickness measurements for both the overall laminated composites and the magnesium layer as a function of reduction after different passes of rolling are shown in Fig. 5.1. The microstructures of the cross-section along the rolling direction for samples rolled with different amounts of deformation are shown in Fig. 5.2. The images in Figs. 5.2a-f correspond to an overall reduction of 47%, 70%, 80%, 87%, 92%, and 95%, respectively. It can be seen from Figs. 5.1 and 5.2 that the thicknesses of both components, the IF steel and magnesium, decreased gradually as being rolled. It should be noted that the initial thickness ratio of magnesium to the whole laminate in the assembly prior to rolling was 20%, and it decreased to about 14% after the first rolling pass and then remained constant for subsequent

rolling passes. This suggests that a substantial amount of magnesium was extruded out in the first rolling pass, but thereafter the components deformed in an iso-strain manner.

Based on the volume fraction of magnesium determined from the cross section, it is possible to calculate the density of the laminated composites by:

$$D_{\text{laminated}} = V_f^{\text{IF}} \times D_{\text{IF}} + V_f^{\text{Mg}} \times D_{\text{Mg}} \quad (5.1)$$

where D is the density and V_f the volume fraction of each component. For a volume fraction of 14% for magnesium for this work, the density of the fabricated laminated composites calculated based on Eq. 5.1 is 7.00 g/cm^3 , which corresponds to an 11% density reduction compared to monolithic steel.

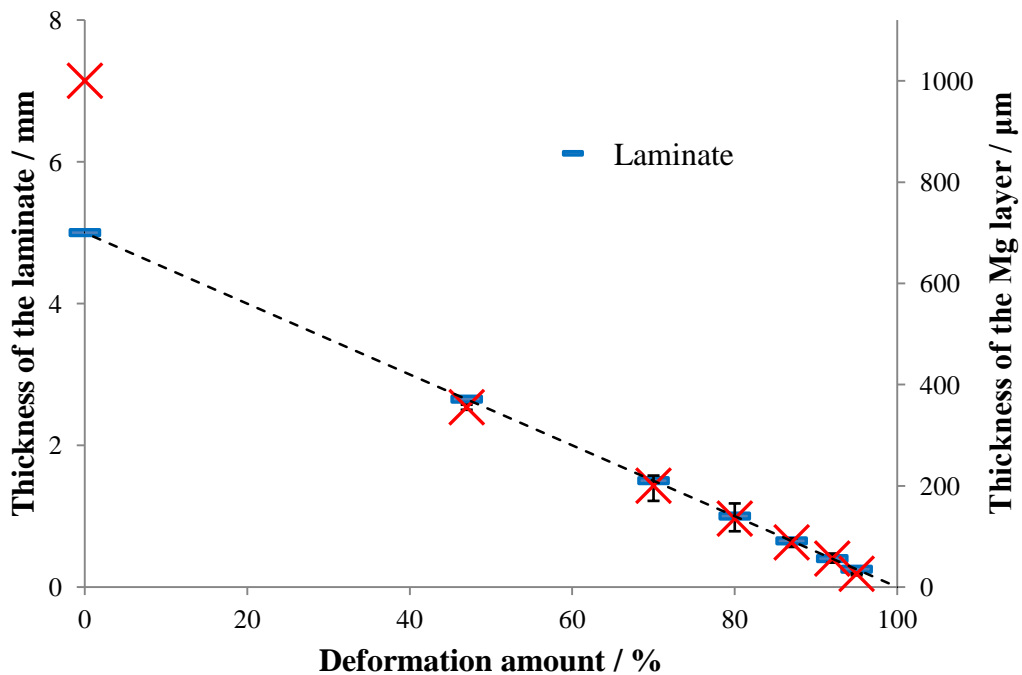


Fig. 5.1. Thickness measurements for the laminated composites and magnesium layer as function of reduction (the magnitude of right axis is set to be 14% of that at the corresponding point on the left axis).

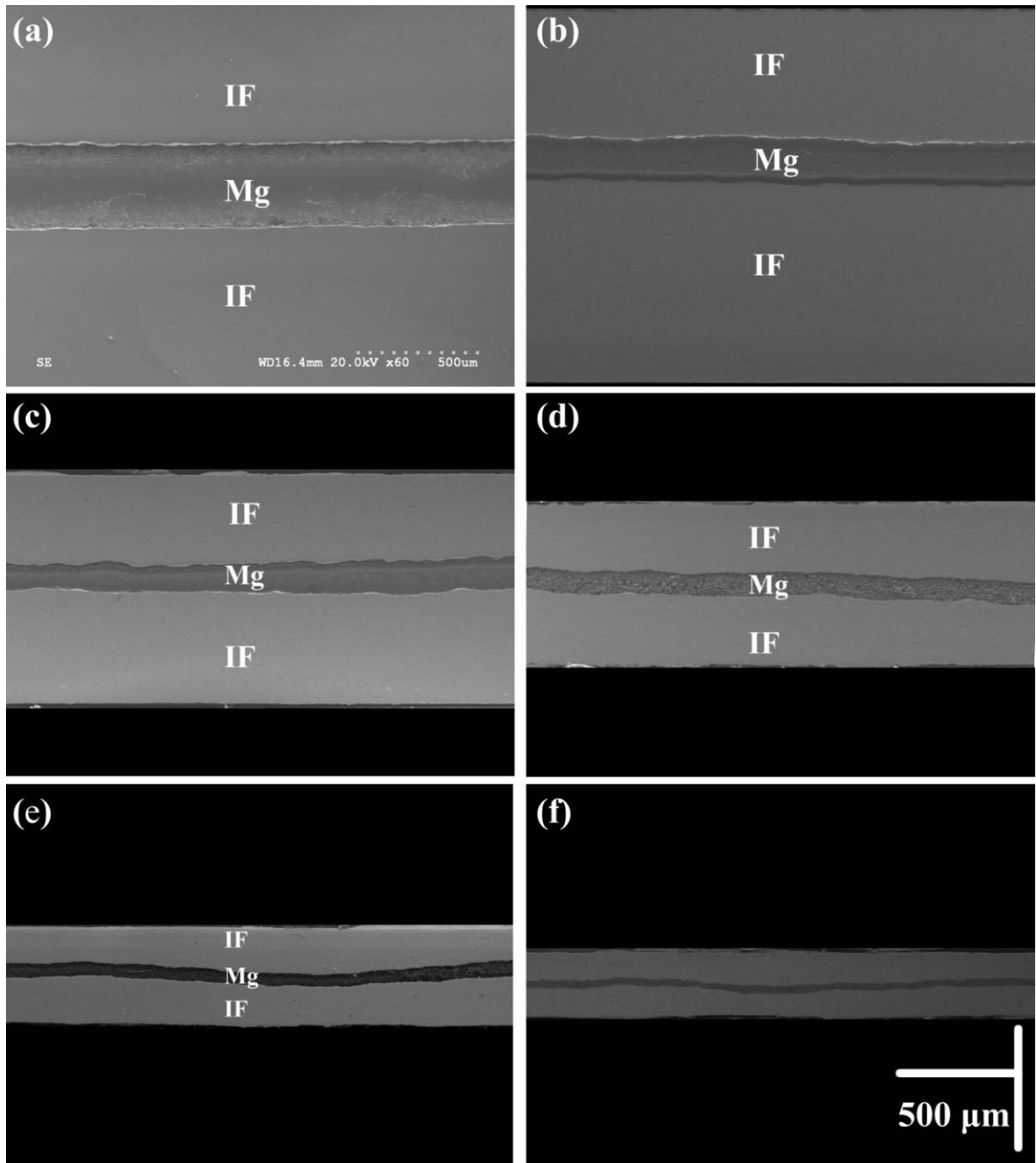


Fig. 5.2. SEM micrographs (in secondary electron mode) of the longitudinal cross-section of the roll-bonded steel-magnesium laminated composites after different passes.

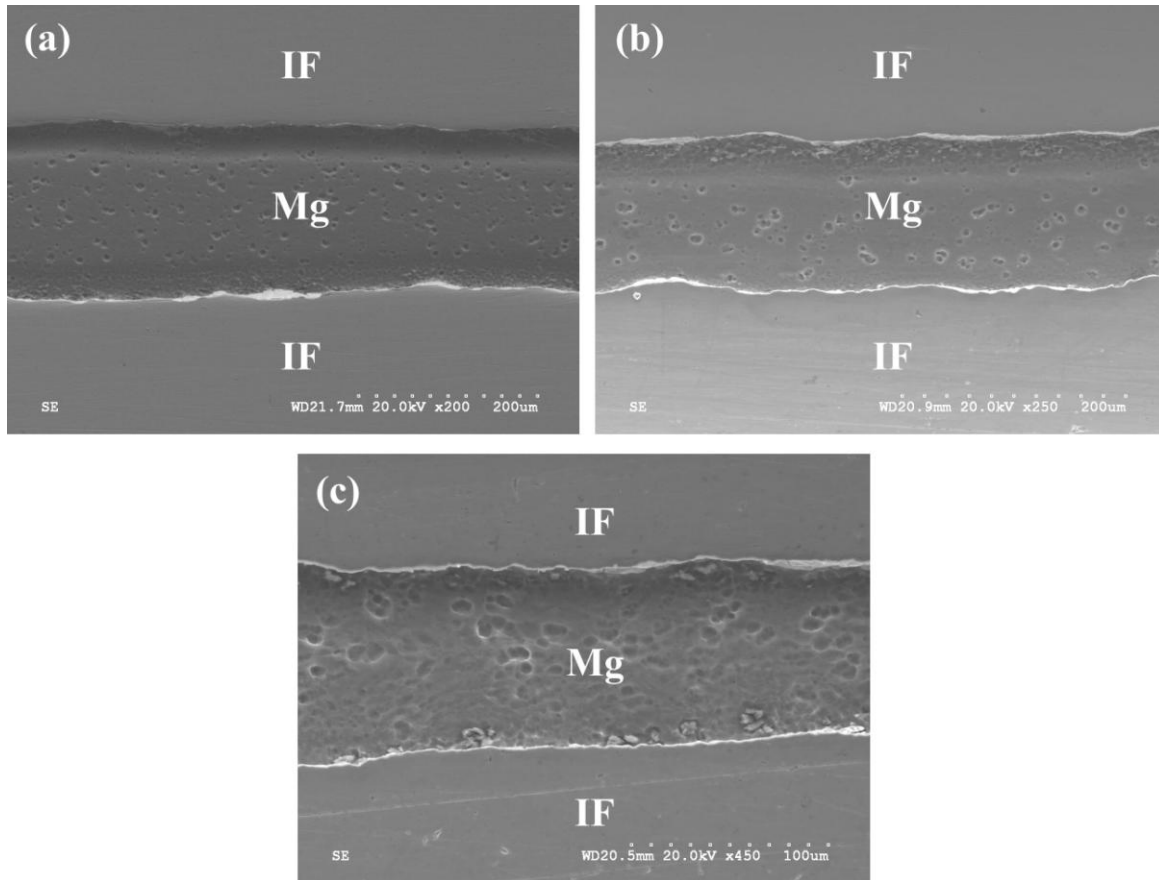


Fig. 5.3. SEM images showing details of the longitudinal interface (a) 70% reduction, (b) 80% reduction and (c) 87% reduction.

Fig. 5.3 shows the details of the longitudinal interfaces for samples with three different reductions. It can be seen from both Figs. 5.2 and 5.3 that for all cases, no voids or cracks could be detected at the interface between magnesium and steel, suggesting that a reasonable bonding could be produced between the steel and magnesium layers for reductions of 47% or greater. There was no obvious intermetallic layer or any other reaction layer at the interface. This is in agreement with the predictions from the equilibrium phase diagram. The absence of intermetallic compounds at the magnesium/steel interface was also confirmed by Cetin et al. [4] in their previous work on steel-magnesium composites made by infiltration. The transverse cross sections were also observed with SEM, and no voids, intermetallic layers or

delaminations were found. Although no obvious intermetallic layers were observed with SEM, further analysis of the interface with other high precision apparatus or techniques, such as transmission electron microscope, is needed to discover the atomic nature of the interface.

These SEM images also show that fracture did not occur in any of the layers during the roll bonding process and all the layers remained continuous till the highest strain examined in this work, i.e. 95%. However, it can be seen clearly from Figs. 5.2 and 5.3 that the steel/magnesium interfaces tended to develop some waviness as the overall level of reduction was increased.

5.1.2. Microstructures of the accumulative roll-bonded laminated composites

The schematic flow of the accumulative roll bonding process is shown in Fig. 5.4. After one cycle of the ARB process at 300°C, a seven-layer steel-magnesium laminated composite (four IF steel layers and three magnesium layers) was obtained, and the overall deformation accumulated in the laminate was 77 pct.

Although the overall deformation amount after the whole process was only 77 pct, the sample failed after the second step due to through-width cracks which developed in the surface IF steel layers. One may notice that no failure occurred during the rolling of monolithic IF steel and magnesium as well as the roll-bonded laminated composites up to a deformation amount of 95 pct, which is much larger than the 77 pct deformation in total during the ARB process.

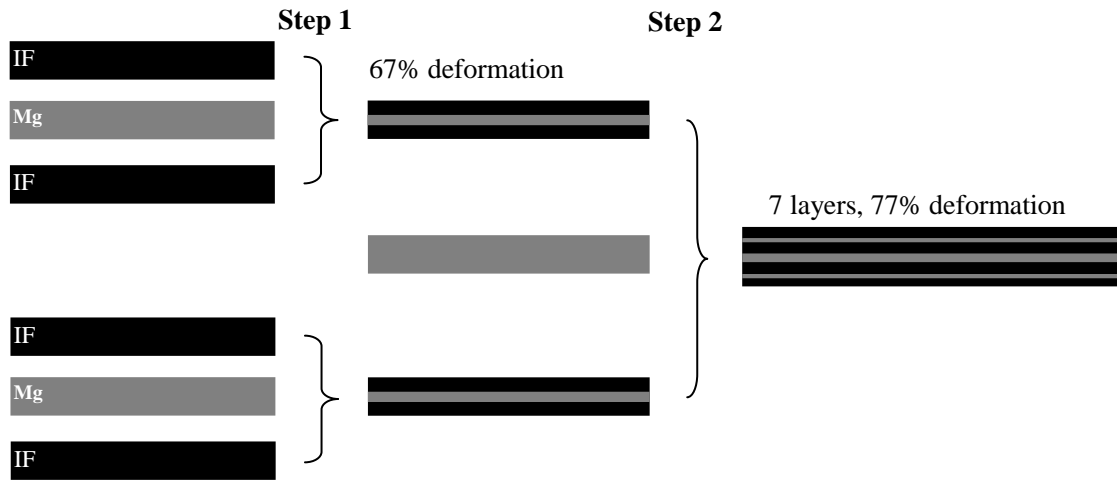


Fig. 5.4. The schematic flow of the two-step accumulative roll bonding process: step 1 with 67% deformation and an overall reduction of 77% after the two steps.

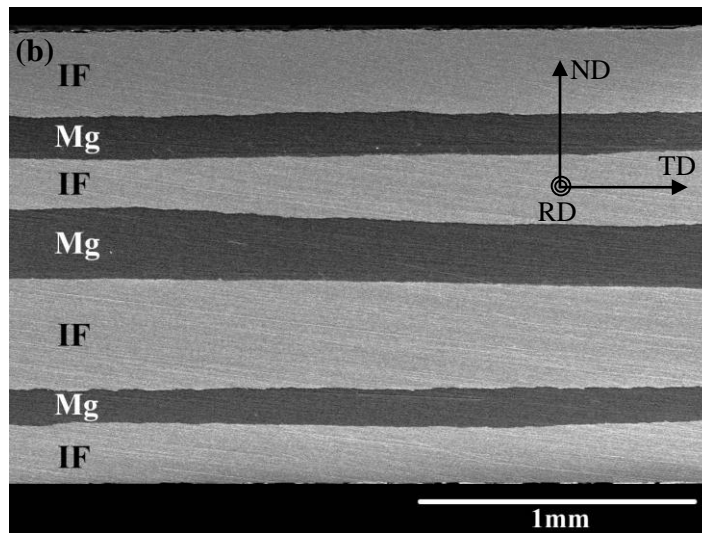
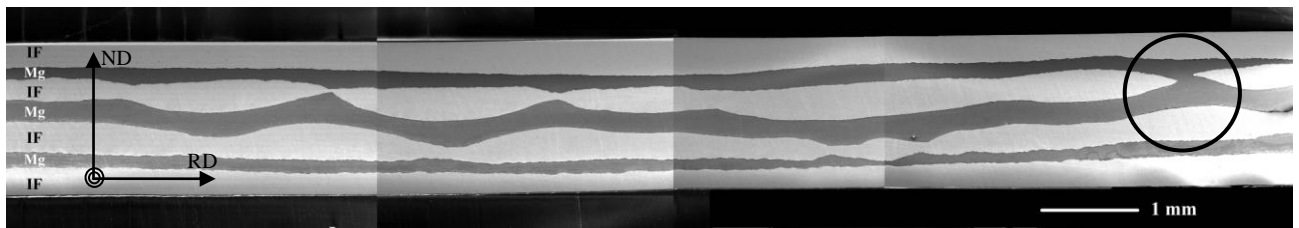


Fig. 5.5. SEM photographs (in secondary electron mode) showing the cross-sectional microstructure along (a) rolling direction (SEM images assembly) and (b) transverse direction of the ARBed laminated composites.

The SEM micrographs of the ND-RD section show some internal irregularities. Fig. 5.5a shows the assembly of the SEM micrographs showing the longitudinal cross-section of the areas without surface failure in the ARBed laminate. The localization and fracture of the hard steel layers were evident along the rolling direction. In contrast to the hard IF steel, the soft magnesium layers were continuous. This is in agreement with the previous observations by other authors [74] that the hard component may experience a load maximum in the longitudinal direction and an instable flow as well.

One of the most noticeable features of the cross-section along the rolling direction is the regular spacing of the localizations in the left part of Fig. 5.5a. It seems that the necks alternated between the upper steel layer (the third layer) and the bottom steel layer (the fifth layer), each on one side of the middle magnesium layer. And the localized thinning was very pronounced, since the thickness at the “neck” was only 20% of that of the unlocalized region. On the right side of Fig. 5.5a, the fracture occurred in the upper steel layer, and the magnesium layer in the previous laminate and the one added in after the first step contacted with each other. Such kind of fracture, along with the through-width macro cracks developed in the surface IF steel layers, have made further accumulative roll bonding cycles unfeasible.

The microstructure of the transverse cross section in the area without damage is shown in Fig. 5.5b. It can be seen that the seven layers were bonded well together with distinct interfaces. The middle magnesium layer is a bit thicker than the other two magnesium layers because it was added in after the first step. The microstructure is generally similar to those of the normal roll-bonded samples.

5.1.3. Rollability and deformation responses of the laminated composites

It was shown in Fig. 5.2 that the IF steel and commercial purity magnesium can be roll bonded together at 300°C with 47% deformation in a one pass roll bonding process, and the roll bonded laminated composites can withstand the subsequent rolling up to the highest strain examined in this work (95% reduction). It is interesting to compare the present results with those reported by Cetin et al. [4], who rolled the infiltration-processed steel-magnesium composite at 250°C. It is confirmed by both that rolling could lead to some waviness of the interface. However, although almost the same reduction per pass (15%) in the post-fabrication rolling (in this work the roll bonding process is considered as the fabrication process and the following rolling thereafter are defined as post-fabrication rolling) was used in both experiments, it was reported by Cetin et al. [4] that the maximum strains that could be reached in their warm rolling were on the order of 60%; at deformations higher than that, the LMCs tended to debond. This is in contrast to the results in this work, which show the composites can be rolled without any failure at least to 95% reduction (Figs 5.2 and 5.3). This difference may be attributed to the different rolling temperature, 250°C in [4] and 300°C in the present work. The higher rolling temperature is apparently beneficial to the recrystallization of magnesium which may reduce the residual shear stresses at the interface. Other possible reasons for the difference include different absolute reduction during rolling and the different natures of bonding in the two cases with different composite processing techniques.

During the roll bonding of dissimilar metal sheets (or simply the compression of dissimilar metal plates), there are normally two kinds of deformation behaviors, the iso-stress and iso-strain behaviors, as shown in Fig. 5.6. In this work, the unbonded metal assembly

deformed in an iso-stress manner in the first roll bonding pass (i.e. there was some squeezing of the magnesium out the sides of the sample), whereas the roll-bonded laminates deformed in an iso-strain state during the post-fabrication rolling (Fig. 5.6c). In practice, iso-strain behavior of laminate materials is approached when individual component layers are thin and frictional constraint or bonding between layers enforces uniform deformation [5]. After the first roll bonding pass in this work, bonding between layers was achieved and the layer thickness decreased as being further rolled, and these ensured the iso-strain deformation behavior that was observed. It should be noted that the iso-stress deformation of laminated composites can lead to the fact that the soft component would be preferentially extruded out from the laminate during rolling process. For instance, approximate 30 vol.% magnesium was extruded from the laminates during the first roll bonding pass. Future work is needed on the selection of rolling temperature and rolling speed (strain rate in nature) to limits the extent to which magnesium can be extruded out. On the other hand, once magnesium and IF steel layers are bonded, these rolling parameters are less important since the bond tends to enforce uniform deformation of all the component layers and a tendency to iso-strain deformation.

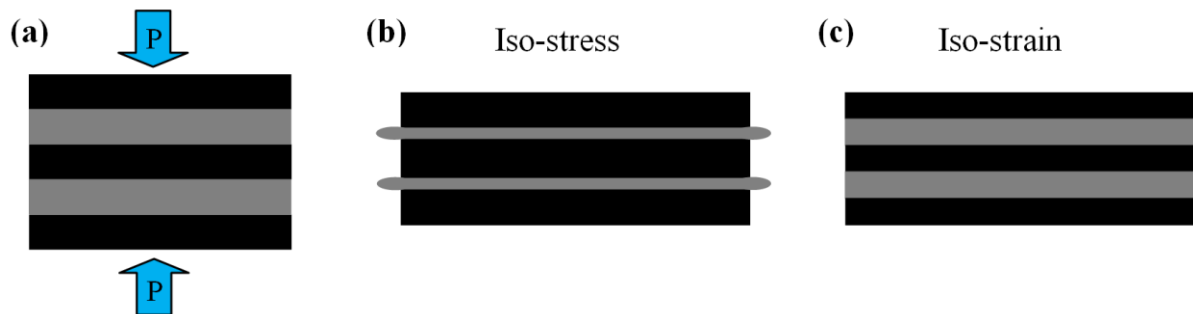


Fig. 5.6. Two different deformation responses of the laminates during rolling.

There have been some observations that during the co-deformation of dissimilar metals, the hard layers neck and fracture first because of the plastic instability caused by the different flow properties of constituent phases [54, 75]. In the present work, on one hand, the hard component layers, IF steel layers, were free of localization and fracture even to a reduction of 95% for the normal roll bonded laminated samples, and this is probably due to the fact that the samples were rolled at 300°C in each pass after the first roll bonding pass, i.e. annealing was conducted between passes. In contrast, for the accumulative roll bonding case, localization and even fracture of the steel layers occurred though rolled at the same temperature. Further work is needed to investigate the nature of this phenomenon as well as the stress state during the ARB process.

5.2. Room temperature tensile behavior

5.2.1. Tensile behavior of the monolithic materials

In order to compare the room temperature tensile properties of the steel-magnesium composites and those of the component materials, the tensile behavior of the monolithic IF steel and magnesium with different amounts of deformation were first assessed. Figs. 5.7 and 5.8 show the engineering stress-engineering strain curves for IF steel and commercial purity magnesium, respectively. These deformed materials were rolled at 300°C and cooled in air. For each deformation amount, at least three tensile tests were carried out, and the results were very reproducible.

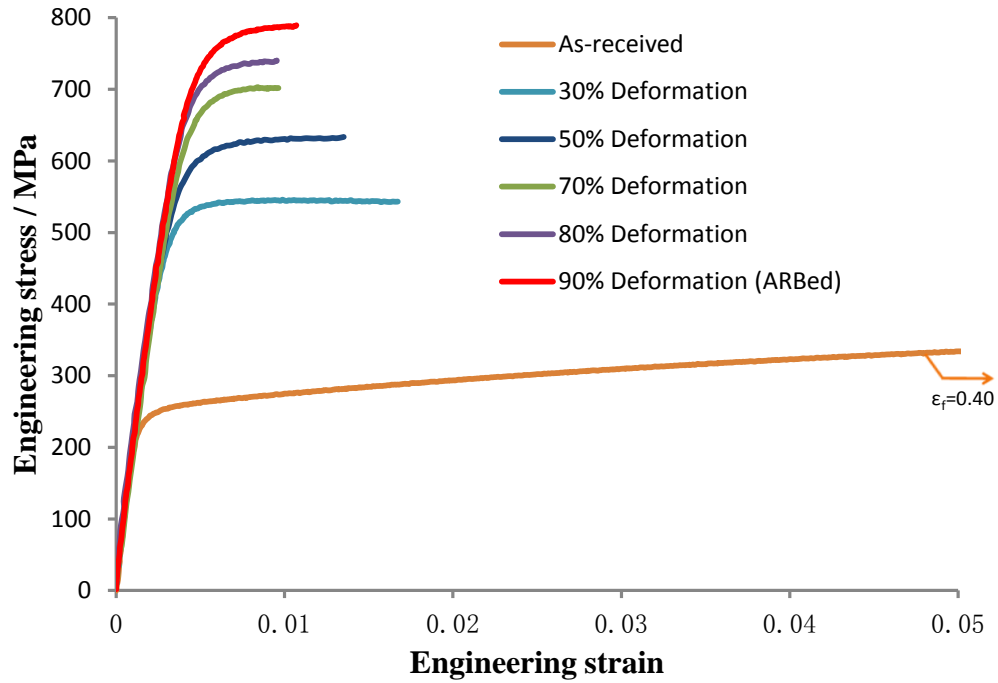


Fig. 5.7. Engineering stress vs. engineering strain curves for IF steel (curves are only plotted to the necking point for the deformed samples).

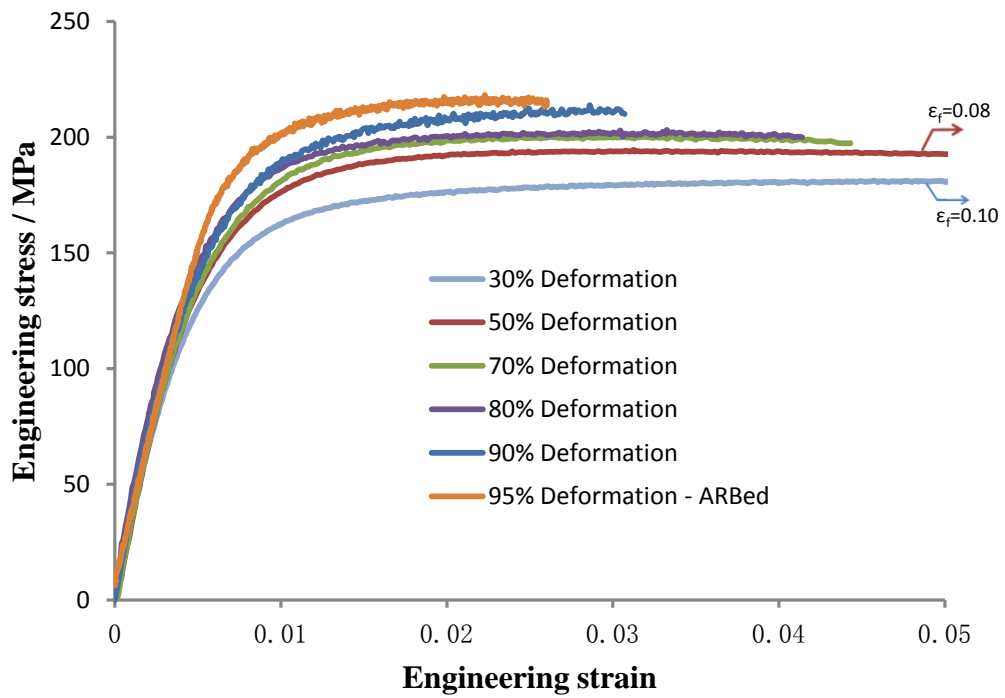


Fig. 5.8. Engineering stress vs. engineering strain curves for the deformed commercial purity magnesium.

It can be seen from Fig. 5.7 that the ultimate tensile strength (UTS) of IF steel increased with the amount of deformation, from 385 MPa of the as-received sample to 792 MPa in the case with the 90% deformation. This is mainly due to the work hardening effect, and also the low rolling temperature (nominally, 300 °C) which was not high enough for steel to recrystallize or recover significantly.

In contrast, the UTS of magnesium did not increase with the deformation amount, probably due to the dynamic recrystallization of magnesium at 300 °C during rolling [76, 77]. Although the dynamic recrystallization likely took place, Fig. 5.8 still shows a small increase in the UTS and decrease in the elongation to fracture with deformation amount. This may be caused by i) incomplete dynamic recrystallization, ii) grain refinement after recrystallization and iii) the actual temperature of the samples decrease during rolling with decreasing thickness, i.e. the sample might get chilled once it was taken out from the furnace and once it contacted with the cold rolls, especially when the sheet was thin (for instance, the thickness of the sample with 90% deformation was only 0.2 mm). It is hard to measure the actual temperature of the sample during rolling, and future effort should be paid to measure the exact temperature of the sheets during the rolling process.

One may also notice the serrations in the stress-strain curves for magnesium in Fig. 5.8. The amplitude of these serrations increased with the deformation amount, following the same trend as UTS. This phenomenon may be related to the interaction between dislocations and solute atoms (i.e. dynamic strain aging [78]), or it may be also related to twinning.

The fracture surfaces of IF steel with 80% deformation and magnesium with 90% deformation are shown in Fig. 5.9. It can be seen that the IF steel fractured in a ductile

manner, since one can see the evident localization, shear bands at the side surfaces and the evidence of void growth in steel. However, these voids are elongated along a direction parallel the fracture surface, rather than essentially equiaxed shaped in the case of normal dimple fracture of steel. Macro examination of the fractured sample reveals that a sharp localized necking, at an angle of 63° to the tensile axis, formed prior to the final fracture. Therefore, the formation of the elongated voids could result from the shear stress parallel to the localized neck. While for magnesium, it fractured in a less ductile manner, without obvious necking, and exhibited a full-slant fracture surface (about 45°). The true fracture strains calculated at the fracture surfaces are 1.16 for IF steel and 0.15 for magnesium.

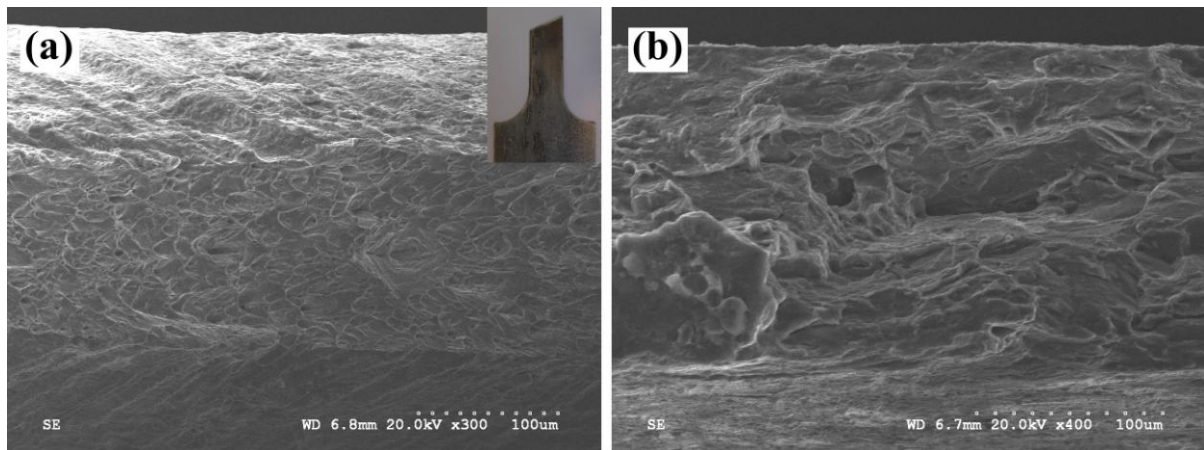


Fig. 5.9. Fracture surfaces of (a) IF steel (80% deformation, inset is the macro view of the fractured sample) and (b) magnesium (90% deformation).

5.2.2. Tensile behavior of the steel-magnesium composites

5.2.2.1. Tensile test results

In this section, the tensile behavior of the steel-magnesium laminated composites are shown and compared with those of the monolithic component materials. The experimental results are also compared with the predictions by the rule of mixtures. The rule of mixtures,

which suggests that the overall property of a composite is the arithmetic average of component properties weighted by their volume fractions, has been used in predicting the tensile properties of both continuous filamentary composites and laminated metal composites [5, 79, 80]. The application of ROM to predict the tensile behavior of composite materials is based upon the following assumptions [79]:

1) Each component of the composite deform together (iso-strain behavior), and there is no slipping of one component relative to the other at the interfaces. The strains within each component are uniform.

2) Different anisotropic properties (R values) between the components induce no transverse stresses.

In this work, the roll-bonded three layer laminated composites are symmetric in geometry, though minor waviness was introduced by the rolling, the bending stress can be ignored during the tensile tests. And each component in the laminates can be expected to deform together because of the bonding. As to the R values for components, it is assumed the transverse stresses due to the different anisotropies are negligible. Thus, it is reasonable to use the ROM to predict the tensile properties of the laminated composites in this work.

For the roll-bonded steel-magnesium laminated composites, the tensile test behaviors were assessed for samples with three different amounts of deformation, 80%, 92% and 95%, i.e. with a magnesium layer thickness of 140 μm , 56 μm and 28 μm , respectively. The engineering stress-engineering strain curves for these tests are shown in Fig. 5.10. The Young's modulus obtained from these curves varied from 163 GPa to 175 GPa, with an average value of 169 GPa. As mentioned in section 5.1, the volume fraction of magnesium in the laminated composites, measured by the thickness ratio at the cross-section, was 14%, and

then it is possible to calculate the Young's modulus of the laminated composites based on the rule of mixtures, which is described as,

$$E_{\text{laminated}} = V_f^{\text{IF}} \times E_{\text{IF}} + V_f^{\text{Mg}} \times E_{\text{Mg}} \quad (5.2)$$

where E is the Young's modulus and V_f the volume fraction of each component. By taking $V_f^{\text{Mg}} = 0.14$, $E_{\text{IF}} = 200$ GPa and $E_{\text{Mg}} = 45$ GPa [81] into Eq. 5.2, the Young's modulus predicted by ROM is 178 GPa. It can be seen that the measured Young's modulus, 169 GPa, is within 6% of the predicted value, validating the applicability of the ROM in predicting the Young's modulus of the roll-bonded laminated composites.

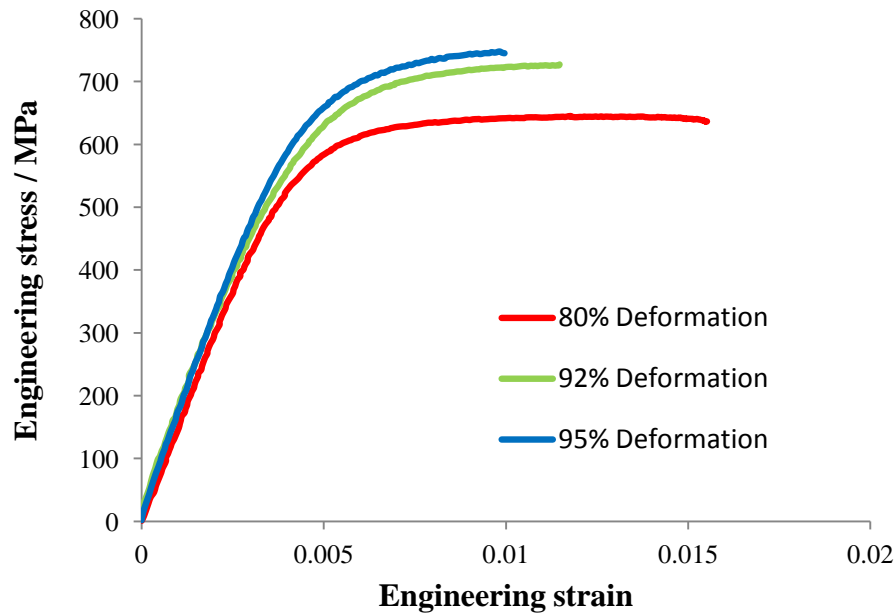


Fig. 5.10. Engineering stress vs. engineering strain curves for the roll-bonded laminated composites (curves are only plotted to the necking point).

It can be observed in Fig. 5.10 that the UTS of the laminated composites also increased with the deformation amount. For laminated composites with deformation amount from 80% to 95%, the UTS of these materials increased from 645 MPa to 763 MPa, while the ductility

deteriorated. These trends can mainly be attributed to the work hardening effect of the IF steel layers.

To compare the tensile behaviors of the laminated composites with those of the component materials, the UTS data of the laminates as well as the monolithic IF steel and magnesium, with respect to deformation amount, are summarized in Fig. 5.11.

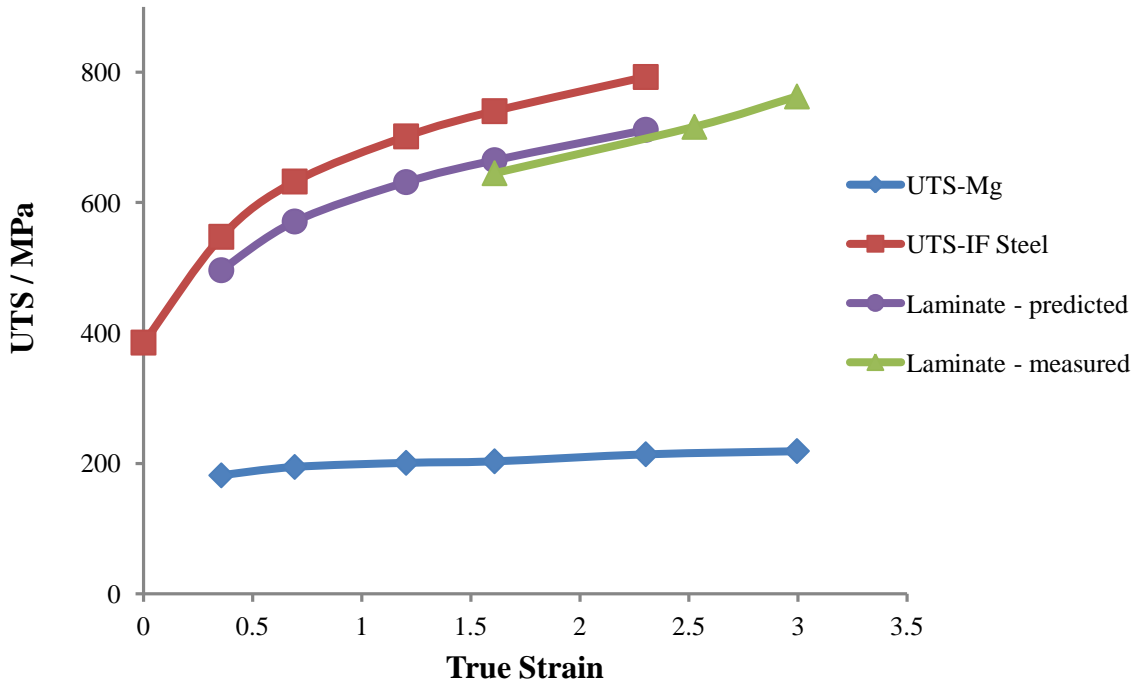


Fig. 5.11. UTS vs. deformation amount for steel-magnesium laminated composites and monolithic IF steel and magnesium.

The predicted UTS values in Fig. 5.11 were calculated according to ROM:

$$\sigma_{UTS}^{laminated} = V_f^{IF} \times \sigma_{UTS}^{IF} + V_f^{Mg} \times \sigma_{UTS}^{Mg} \quad (5.3)$$

where σ_{UTS} is the ultimate tensile strength and V_f the volume fraction of each component.

For $V_f^{Mg} = 0.14$ in this work, it can be seen that the experimental results and the predicted values are very close, with the experimental results a bit lower than the ROM predictions.

This is reasonable because the map was constructed based on the assumption that the IF steel and the magnesium layers deformed in an iso-strain manner during the rolling process.

Unlike the UTS, the ductility of these laminated composites did not show very good reproducibility. Fig 5.12 shows the engineering stress-engineering strain curves for three laminate samples with 80% deformation. It can be seen clearly that although all three tests exhibited nearly identical Young's modulus, work hardening rate and UTS, the ductility of these samples, including both elongation to localization and elongation to fracture, showed large differences among the three tests. This is because the tensile ductility of laminated composites is dependent on many variables, such as the susceptibility of the magnesium layer to early cracking, the contribution to cracking from the interlayer region, the ease of delamination, etc. The inapplicability of the ROM in predicting tensile ductility of composite materials was also confirmed by other authors [5, 79].

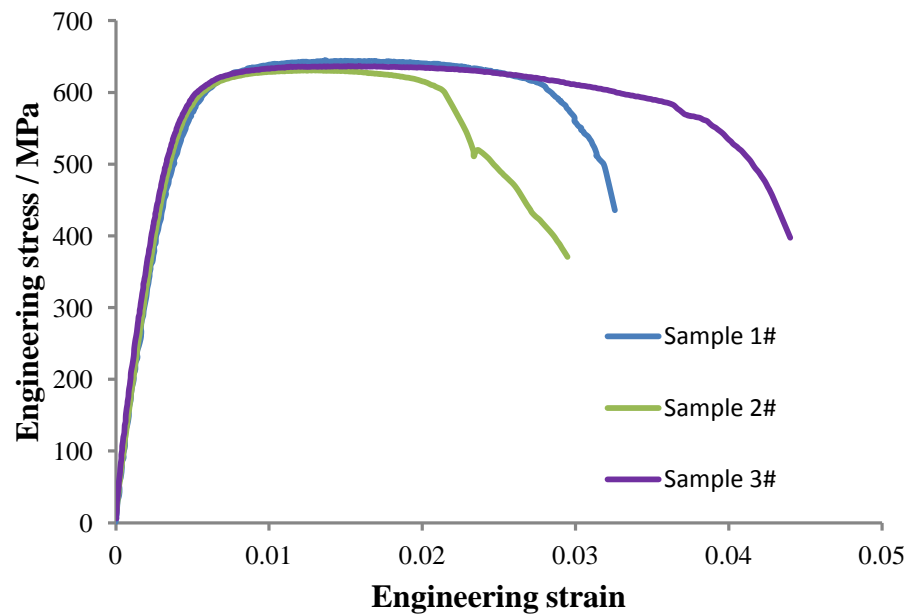


Fig. 5.12. Engineering stress vs. engineering strain curves for roll-bonded laminated composites with 80% deformation.

Another point that can be made from Fig. 5.12 is that substantial amount of localization in the laminated composites took place before fracture in the tensile tests. During the localization process, it was found that there was an obvious interruption in one of these curves (sample 2#). This is probably due to a sequential failure of the different material layers, i.e. most likely the failure of magnesium layer proceeded the IF steel layers.

The most important observation from the tensile tests related to the comparison of ductility between the laminated composites and the monolithic component materials. Fig. 5.13 shows the comparison between the engineering stress-engineering strain curve of the laminated composites with 80% deformation (sample 1# in Fig. 5.12) and those for the monolithic component materials with equivalent amount of deformation. It can be seen that the ductility of the composite exceeds that of the monolithic IF steel with 80% deformation, and even better than that of the one with 70% deformation. At first glance, it is surprising that magnesium has higher ductility than the IF steel, but it is reasonable given the large deformation amount, obvious working hardening effect and unrecrystallized state in the IF steel. We can, therefore, speculate from Fig. 5.13 that it was the magnesium layer in the composite that helped to delay the localization and final fracture of the IF steel, and to improve the ductility of the laminates as a whole. However, the ductility of the steel-magnesium composite materials still remains unexplored to a large extent, and further studies on the ductility, with particular attention to the influence of annealing, are needed.

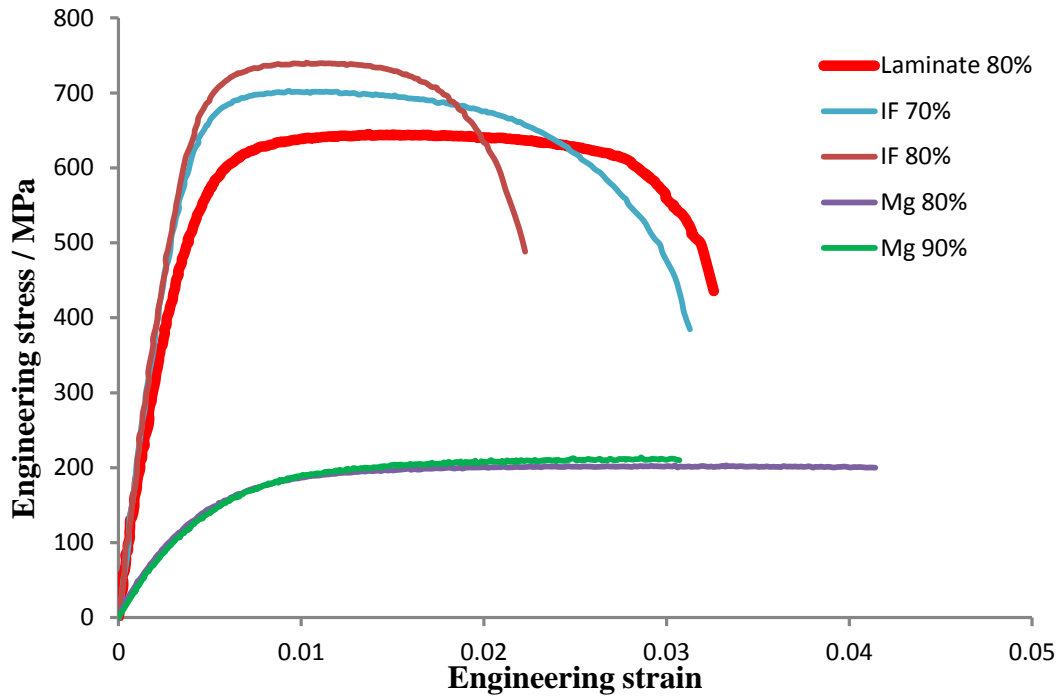


Fig. 5.13. Comparison of the engineering stress-engineering strain curves for laminated composites with 80% deformation and the corresponding component materials.

5.2.2.2. Fracture surfaces

The macro views of the fractured laminated composite samples are shown in comparison with that of the 80% deformed monolithic IF steel in Fig. 5.14. It can be seen that the fracture surfaces of the laminate samples are not at some characteristic angle θ to the tensile axis, and exhibit different levels of irregularity, which rises with the deformation amount. The steel layers, in most cases, were still likely to fracture in the identical manner as in the monolithic case (with a particular θ), but the tendency was interrupted by the lamination. The change of fracture surfaces can be attributed to the bonding between steel and magnesium layers.

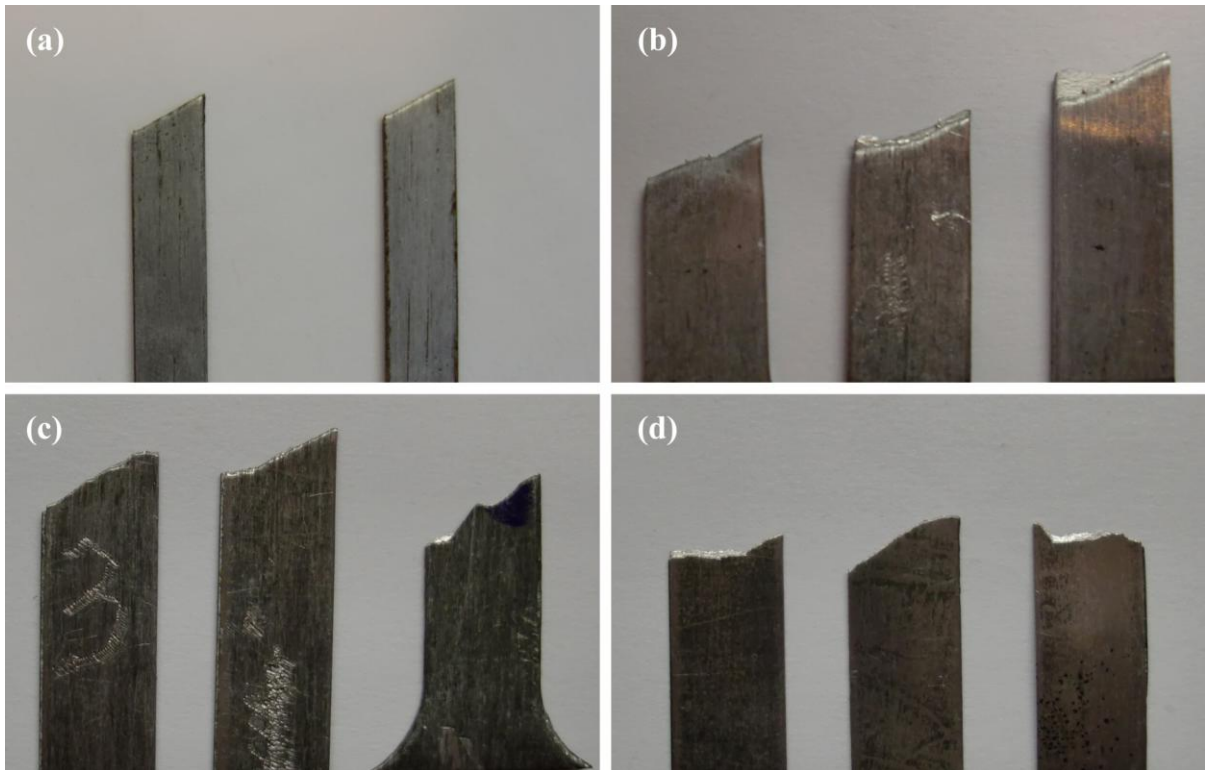


Fig. 5.14. Comparisons of the macro views of fractured samples of (a) monolithic IF steel with 80% deformation, (b) laminates with 80% deformation, (c) laminates with 92% deformation and (d) laminates with 95% deformation.

Fig. 5.15 shows the longitudinal views of the fracture profiles of the laminates for different amounts of deformation. In the cases of 80% and 92% deformation (Fig. 5.15a through c), the IF steel layers on both sides of magnesium necked before fracture. However, in the case of 95% deformation, as shown in Fig. 5.15d, the sample fractured by shear and no significant necking can be found in the steel layers. This may result from the improved bonding at the interface as the level of rolling strain was increased. For the magnesium layer, shear crack was found in the vicinity of fracture surface in the 80% deformed laminate. In the 92% deformed laminates, one sample (Fig. 5.15b) shows no interface delamination but the lateral tearing of magnesium accompanied by the necking of steel, while in another sample (Fig. 5.15c) where debonding occurred, the magnesium layer shows evidence of necking.

Because the monolithic magnesium did not neck, the “localization” of magnesium in the laminated composites may be related to the bonding and further studies on this are needed. It can also be seen from Fig. 5.15 that the debonding between magnesium and IF steel is caused by necking of the steel layers, and thus, it appears likely that the fracture mode of steel could be altered if debonding is inhibited.

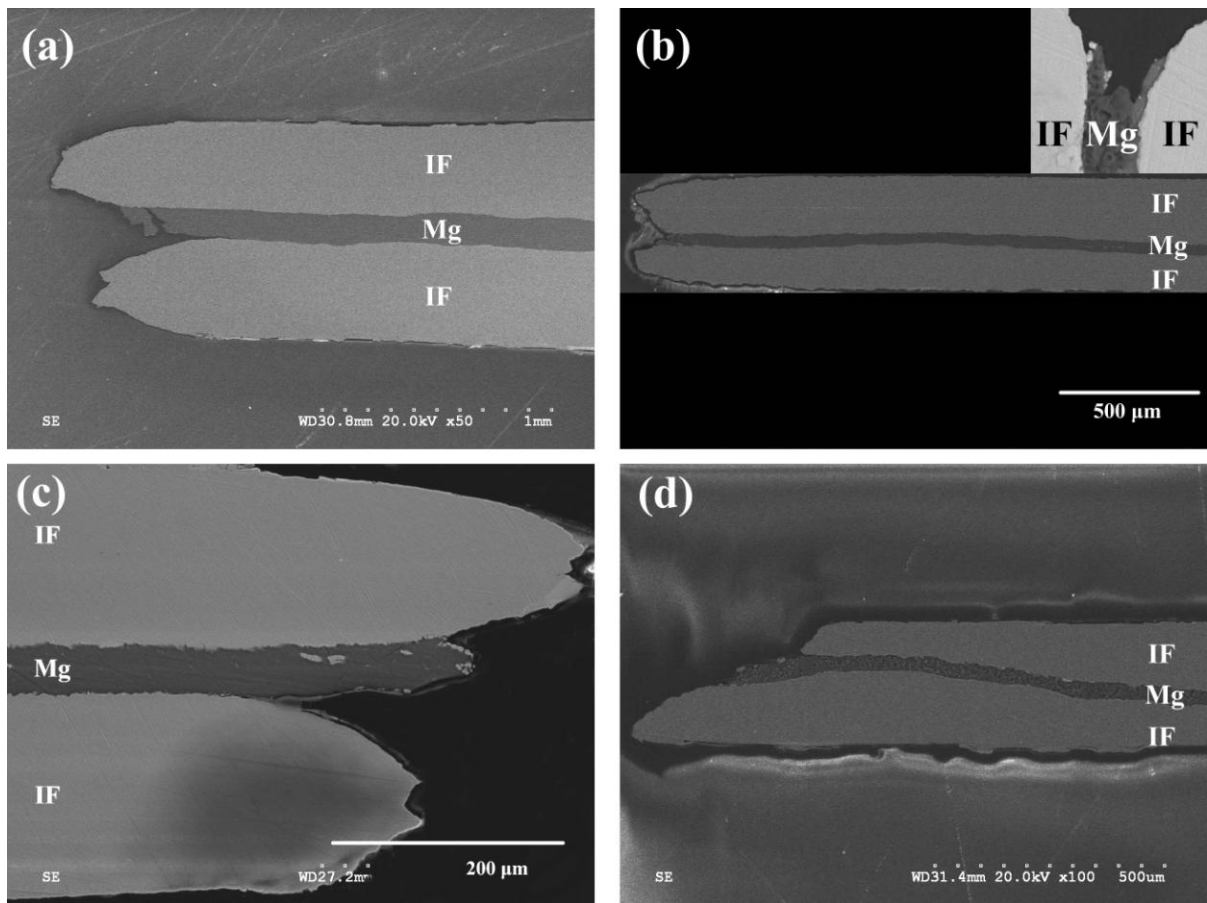


Fig. 5.15. Longitudinal view of the fracture samples for laminates with (a) 80% deformation, (b) 92% deformation (inset is the BSE image showing the detail of the fracture site), (c) 92% deformation (different sample) and (d) 95% deformation.

The fracture surfaces of the laminated composites with 80%, 92% and 95% deformation are shown in Figs. 5.16, 5.17, and 5.18, respectively. In all three cases, it can be seen that the

IF steel in the laminates fractured in a rather ductile manner, as evident from the dimples and the neck. The splitting at the center of the IF steel layer was found for some samples in the laminated composites (e.g. Fig. 5.16b and c, Fig 5.18b). Although the dimples can be observed in the IF steel layers for all cases, the orientations of those dimples differed amongst the three cases, and even altered within one single sample. The first type of the dimples are the essentially equiaxed dimples bounded by a lip, such as those in Figs. 5.16b and 5.18e, exhibiting a relatively deep, conical shape. This orientation and shape suggests a uniaxial tensile load in those areas [82]. Secondly, some dimples were elongated, with the length axis parallel to the width direction of the samples, such as those in Figs. 5.17c and 5.18b. These dimples oriented in a similar direction as those in the monolithic IF steel with 80% deformation (Fig. 5.9a). Last but not least, some dimples were elongated in the direction parallel to the thickness direction of the samples, such as these dimples in Figs. 5.17e and 5.18a. The elongated dimples suggest a tear (Mode I) or shear (Modes II and III) loading conditions in these areas [82]. It should be noted that all these different types of dimples may exist in one single steel layer, which suggests that the load condition and stress state are non-uniform through the samples during tensile tests. Further investigations on the stress state of the laminated composite as a whole and the stress states in each component layers during tension are needed.

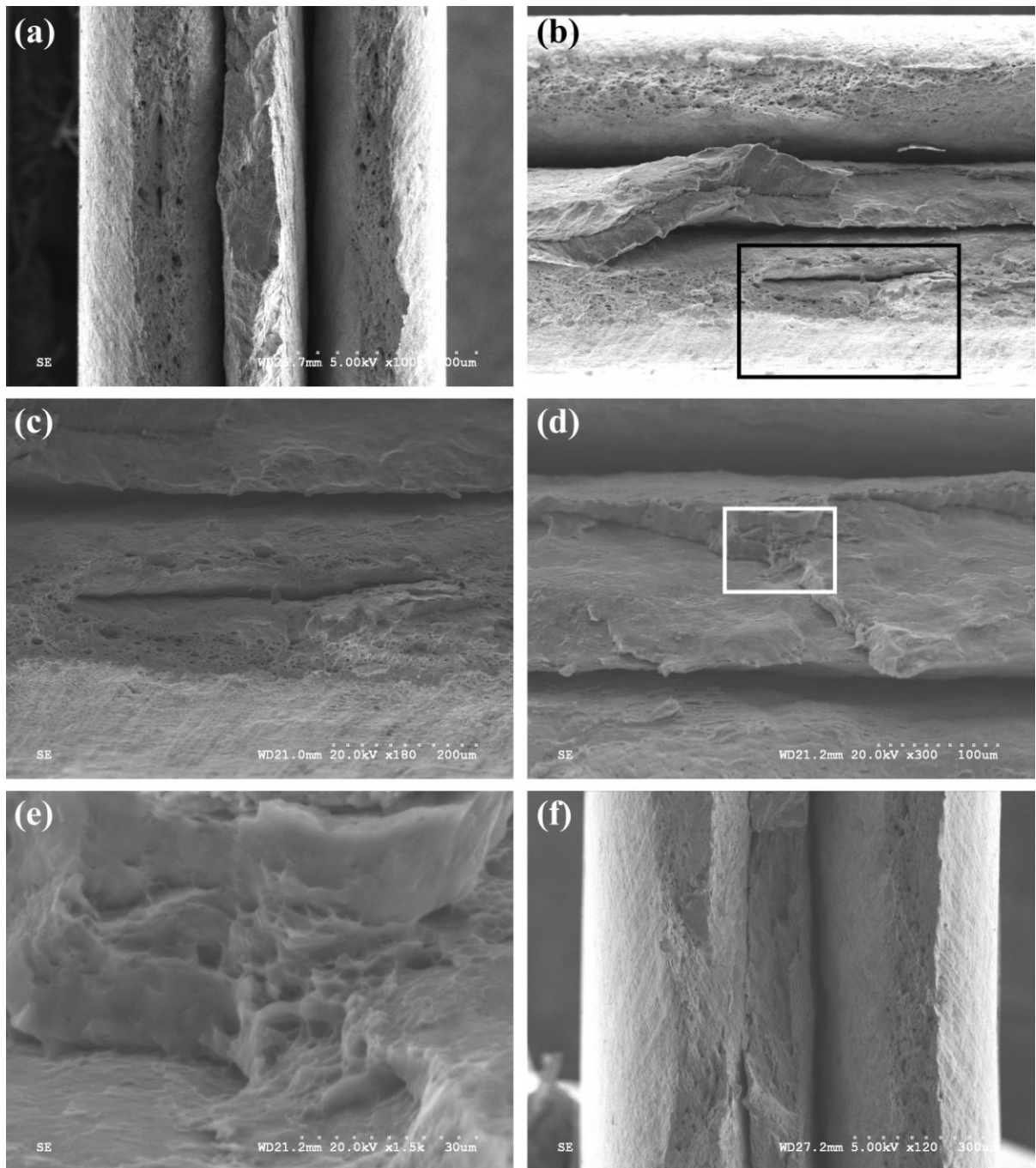


Fig. 5.16. SEM photographs showing the fracture surfaces of laminate samples with 80% deformation: (a) the macroscopic view of the fracture site; (b) debonding between layers and splitting in the IF steel layer; (c) details of the rectangle area in (b); (d) magnesium layer at the fracture site; (e) details of the rectangle area in (d); and (f) interaction between fractures in IF steel layer and magnesium layer.

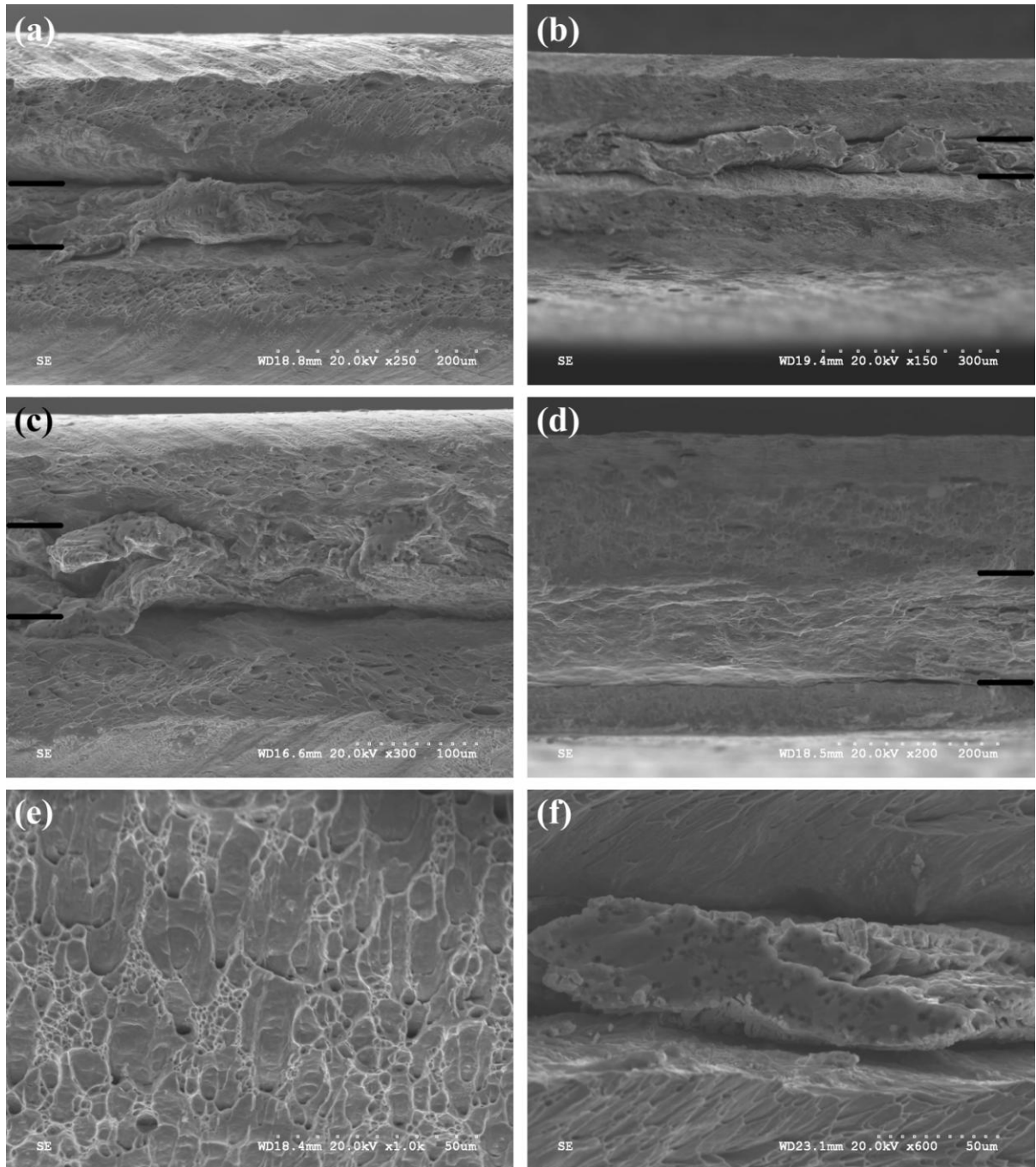


Fig. 5.17. SEM photographs showing the fracture surfaces of laminate samples with 92% deformation: (a) and (b) the macroscopic views of the fracture sites; (c) tearing of magnesium layer; (d) undebonded interface between IF steel and magnesium; (e) IF steel layer at the fracture site; and (f) magnesium layer at the fracture site.

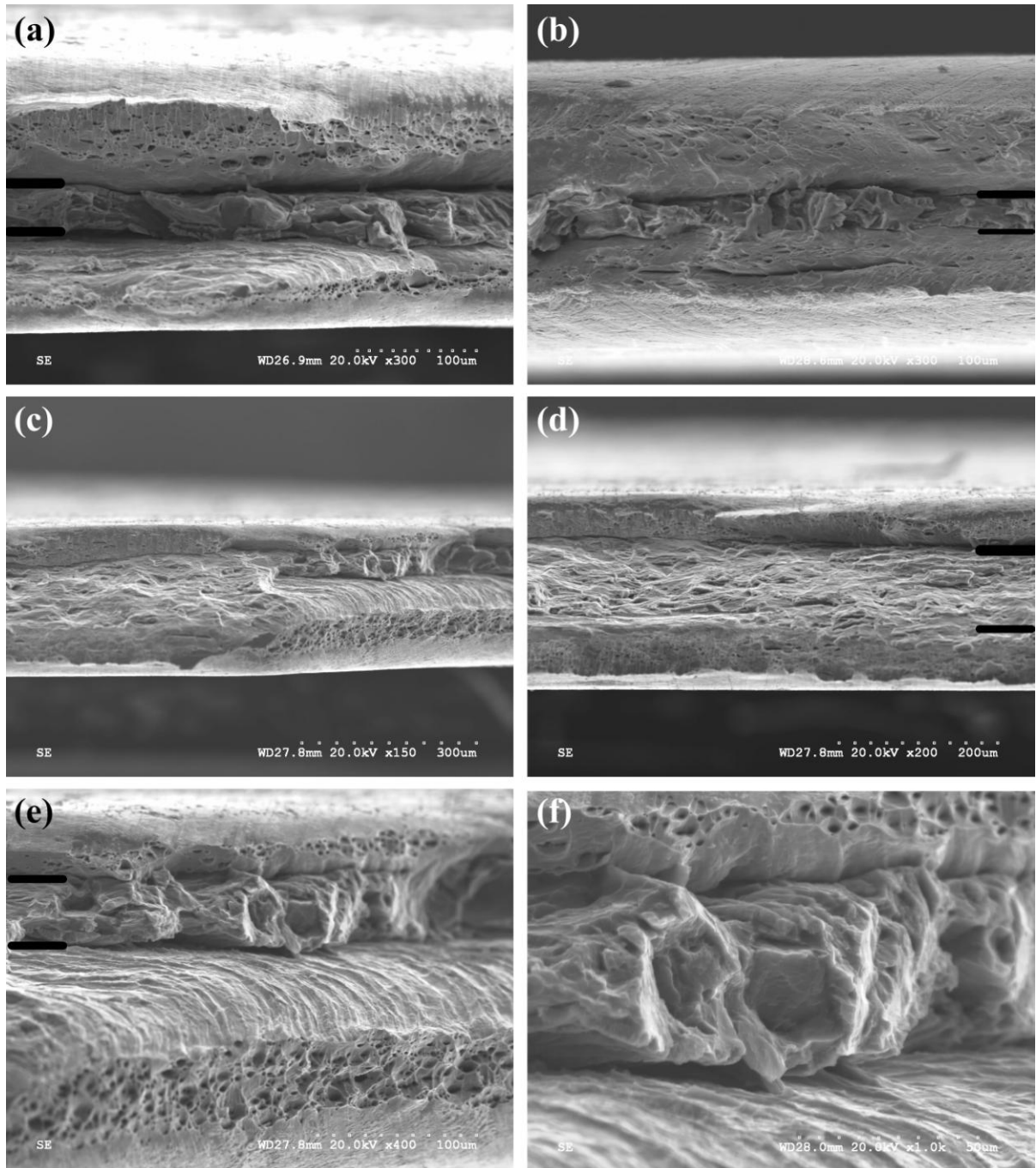


Fig. 5.18. SEM photographs showing the fracture surfaces of laminate samples with 95% deformation: (a) the macroscopic view of the fracture site; (b) splitting of the IF steel layer at the fracture site; (c) “transition” zone of the fracture site; (d) details of the left part in (c) showing undebonded interface; (e) details of the right part in (c) showing the debonding between layers; and (f) details of the magnesium layer in (e).

In regard to the magnesium layer in the laminates, the fracture mode changed significantly for the magnesium amongst the three cases. In the laminated composite with 80% deformation, as shown in Fig. 5.16, the magnesium layer, with a thickness of 140 μm , fractured in a relatively brittle way, exhibiting relatively flat and smooth surface. It is also shown in Fig. 5.16e that growth of voids was found in some points of magnesium layer. For laminate with 92% deformation, as shown in Fig. 5.17, the thickness of magnesium decreased to 56 μm , and substantial amount of void growth can be found in the magnesium layer, and the magnesium fractured in a more ductile way than that in Fig. 5.16. When the thickness of magnesium layer decreased to 28 μm in the laminates with 95% deformation, the magnesium layer fractured in a relatively ductile manner, as shown in Fig. 5.18f. A transition zone of the fracture mode was found in Fig. 5.18c, on the left of which the magnesium layer fractured by shear, whereas on the other side considerable void growth was evident. Such transition may be related to the bond since the magnesium and bottom IF steel layers on the left side of the transition zone were still bonded together, and it was likely that the localization of steel layer was absent. Thus, it is important to evaluate the bond strength evolution with increasing deformation amount.

The delamination can be found almost everywhere between steel and magnesium along the interfaces at the fracture site of the laminate with 80% deformation, as shown in Fig. 5.16. For the laminate with 92% deformation, local steel/magnesium interface without delamination could be observed, as shown in Fig. 5.17d. In particular, the bond may be also strong enough to cause the lateral failure of magnesium by tearing, as shown in Fig. 5.17c. With the decreasing thickness, in the laminate with 95% deformation, the unbonded interfaces can be easily found, and the fracture mode of the laminated composites was

changed, as shown in Fig. 5.18c. In the area without debonding, the localization of the steel layer could hardly be found, and the void growth was also inhibited to some extent. Therefore, it can be speculated that the bonding between the IF steel and the magnesium layers can be enhanced by further rolling.

5.3. Micro-hardness results

The micro-hardness results for the monolithic IF steel with different amounts of deformation are shown in Fig. 5.19a. It can be seen that the Vickers hardness increased with the true strain, resulting from the work hardening effect. It is shown in Fig. 5.19b the comparison between the measured UTS and the UTS calculated based on the hardness results ($UTS_{(in\ MPa)} \approx Hardness_{(in\ HV)} \times 3.3$ [83]) for samples with different amounts of deformation, and the two curves were found to match well with each other, indicating a good agreement between the tensile test results and the micro-hardness results.

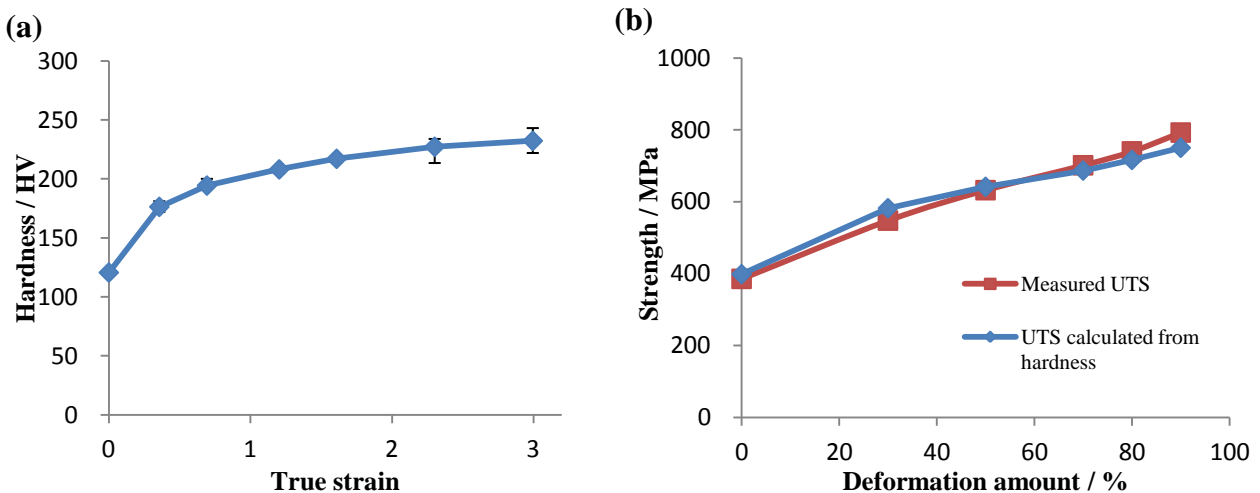


Fig. 5.19. Micro-hardness results: (a) the micro-hardness vs. true strain for monolithic IF steel and (b) comparison between the measured UTS and those calculated based on hardness.

The micro-hardness of the IF steel as one component in the laminated composites was also measured. For laminate with 80% deformation, the Vickers hardness was measured as 210 HV. This value corresponds to a deformation amount between 70% and 80% in Fig. 5.19a. For laminate with 92% deformation, the measured hardness for steel layer is 229 HV, which is similar to that of the monolithic IF steel with 90% deformation (227 HV).

Unlike the IF steel, the hardness of magnesium layer did not increase with the deformation amount, probably due to the occurrence of dynamic recrystallization at the rolling temperature. The hardness of magnesium, for laminates with either 80% or 92% deformation, was ~52 HV, corresponding to an approximate UTS of 172 MPa. It should be noted that this UTS value is apparently lower than those measured for the deformed monolithic magnesium, even lower than the UTS of 30% deformed monolithic magnesium (182 MPa). This could be related to the different actual rolling temperature in the layers. On the one hand, for the monolithic magnesium during rolling, the actual temperature of the sample may decrease by the heat emission into the ambient (radiation) and heat conduction between hot samples and cold rolls. On the other hand, for the magnesium inside the laminated composites, the magnesium layer was covered by two relatively thick IF steel layers, and those two faces may retard the heat loss of the magnesium core, so the actual temperature of the magnesium layer may be higher than that of the monolithic materials despite the same preheating temperature, then the recrystallization fraction in the magnesium layer in laminated composites may be higher than that in the monolithic magnesium.

5.4. Bending behavior of the laminated composites

5.4.1. Three-point bending test

The three-point bending test results for the $100 \times 10 \times 1$ mm samples (i.e. 80% deformed) were very similar for all three tests that were carried out, and a typical load-displacement curve is shown in Fig. 5.20. A maximum load of 132 N was achieved at a deflection of 9.15 mm (i.e. bottom surface strain 0.015), and no failure occurred throughout the test with a final deflection of 40 mm. The serration that was observed at the late stage of the test should be related to the friction between the bottom surface of the tested sample and the fixture. The shear stress generated during bending was calculated according to Eqs. 4.3 through 4.5, and the shear stress at the steel/magnesium interface was 15-18 MPa when the load reached 100-120 N. The microstructure of the bending tip is shown in Fig. 5.21, in which it can be seen that there is no crack, debonding or any other kind of failure after the bending test. These results indicate that reasonable bonding exists at the steel/magnesium interface (note some preliminary samples debonded at the interface for even moderate bending strains).

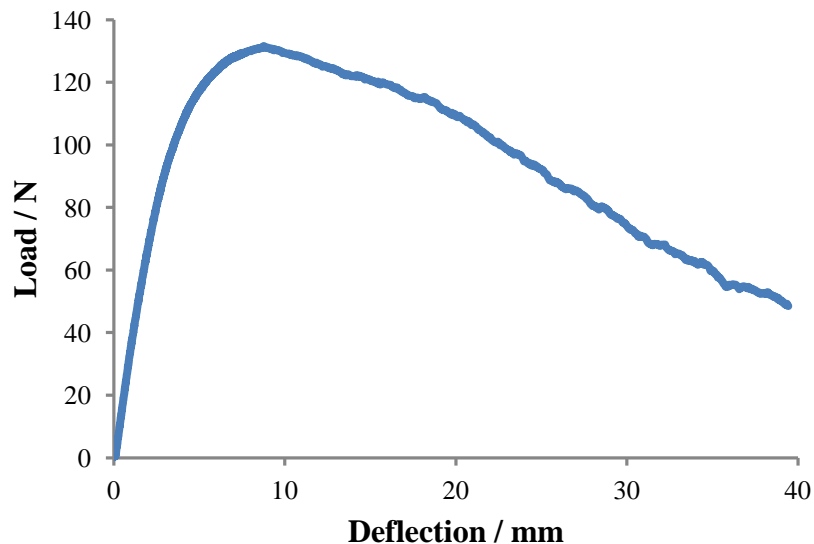


Fig. 5.20. The load-deflection curve of the three-point bending test of the 80% deformed laminate.

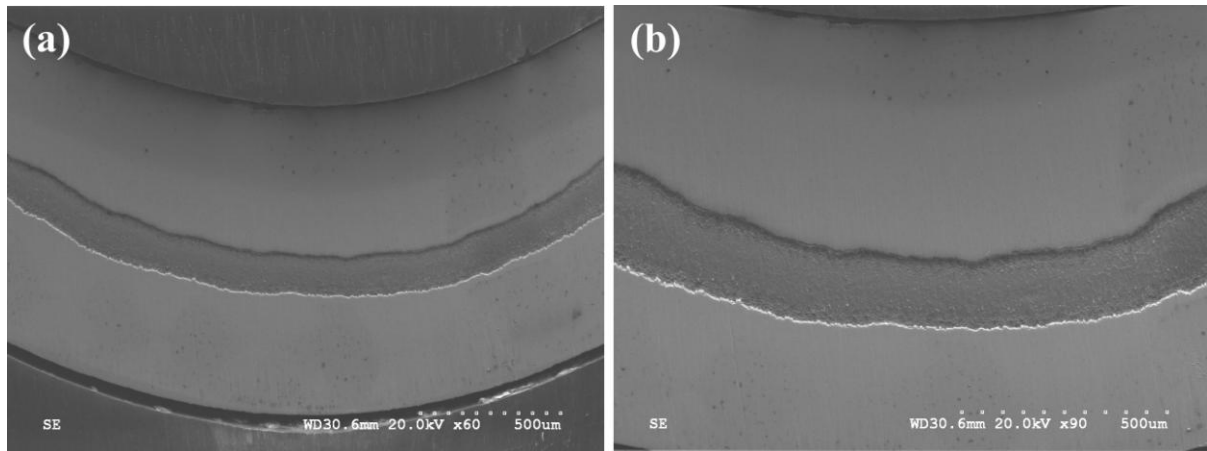


Fig. 5.21. The microstructure of the bending tip of the three-point bent sample (80% deformed laminate) under two magnifications.

It is also possible to calculate the flexural modulus from the bending test results. It is well known that a laminated structure has advantages in bending applications by giving a structure high bending stiffness at low weight, so the flexural modulus of the roll-bonded steel-magnesium composite is of interest. The flexural modulus was calculated from the three-point bending test results by using Eq. 4.1 and the average flexural modulus was 195 GPa.

5.4.2. U-shape bending

The U-shape bending experiments were conducted on the 1 mm thick laminate (80% deformation) to examine the fracture behavior of the laminated composites. The optical microscopic images of the bent sample are shown in Fig. 5.22. It can be seen from Fig. 5.22a that fracture occurred in the outer IF steel layer and also the magnesium core layer, while the inner IF steel layer remained intact. The fracture surfaces in both layers, although in different directions, appear to be a shear type since the cracks propagated at about 45 degree to the maximum tensile stress direction. Delaminations, at different levels, can be found at the each

of the steel/magnesium interfaces. Another obvious point can be found from Fig. 5.22 is the shear failure in the magnesium layer at some places adjacent to the bend tip.

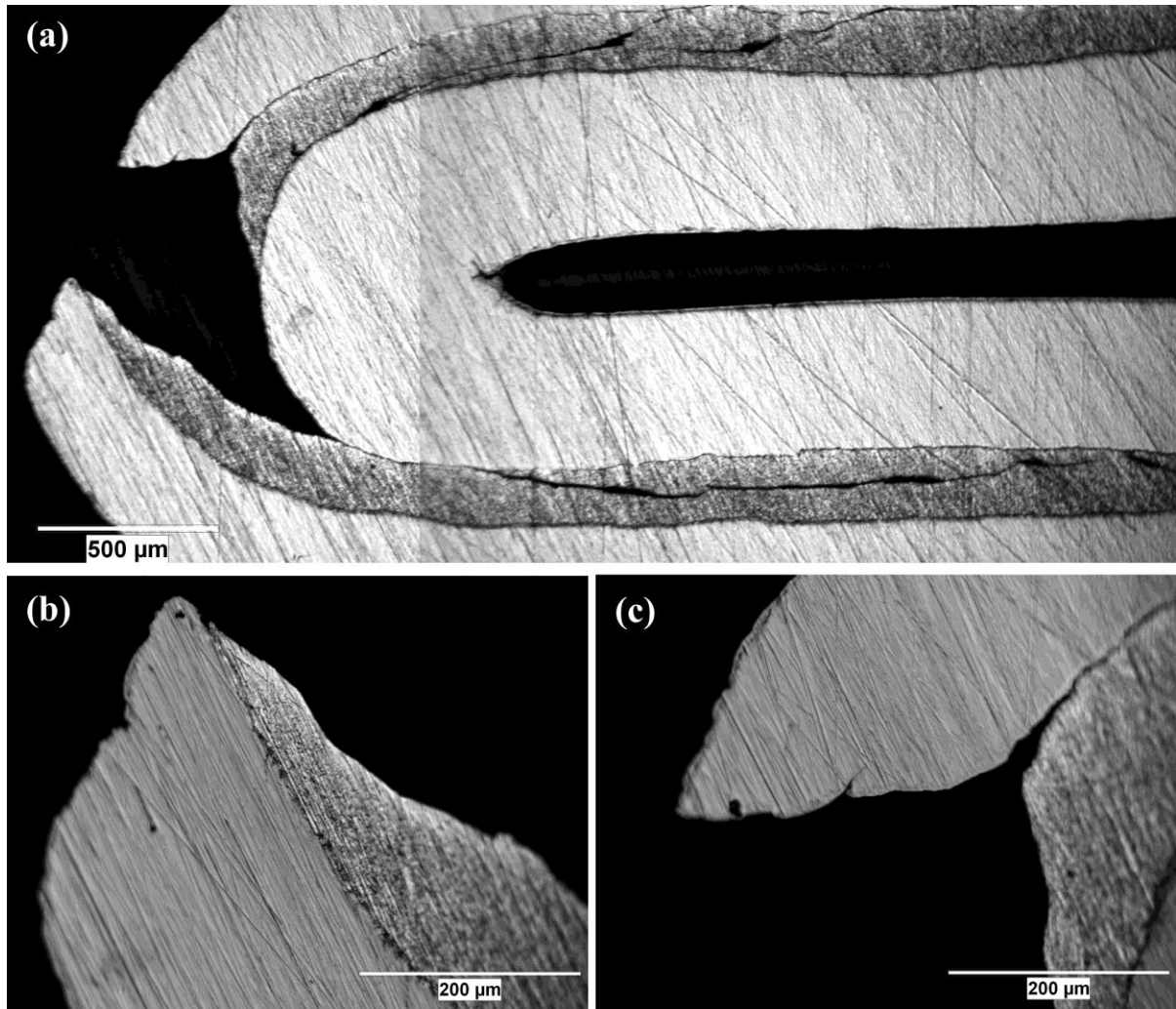


Fig. 5.22. Optical images of the bent sample (80% deformed laminates) after U-shape bending experiments: (a) macroscopic images assembly, (b) and (c) the microstructural details of the fracture profiles.

In order to trace the crack propagation and failure evolution during the U-shape bending experiments, three 1 mm thick laminate samples were bent to a nominal interior angle of 50°, 35° and 12°, respectively, and the optical microscopic images of the bent samples are shown in Fig. 5.23. It can be seen that what occurred first was the thinning and localization of the

outer steel layer due to shear deformation, as shown in Fig. 5.23a. In Fig. 5.23b, we can find the fracture of the outer steel layer and a crack in the magnesium layer. It was likely the fracture of steel layer directly penetrated into the magnesium later; however, it is unclear where the crack initiated and which direction (inward or outward) the crack propagated. For the third sample with a smaller interior angle, delamination between the outer steel layer and magnesium core occurred and shear cracks in the magnesium layer initiated besides the fracture of the outer steel layer. However, details of the interaction between the crack propagation and interface delamination are clearly complicated and further work is needed.

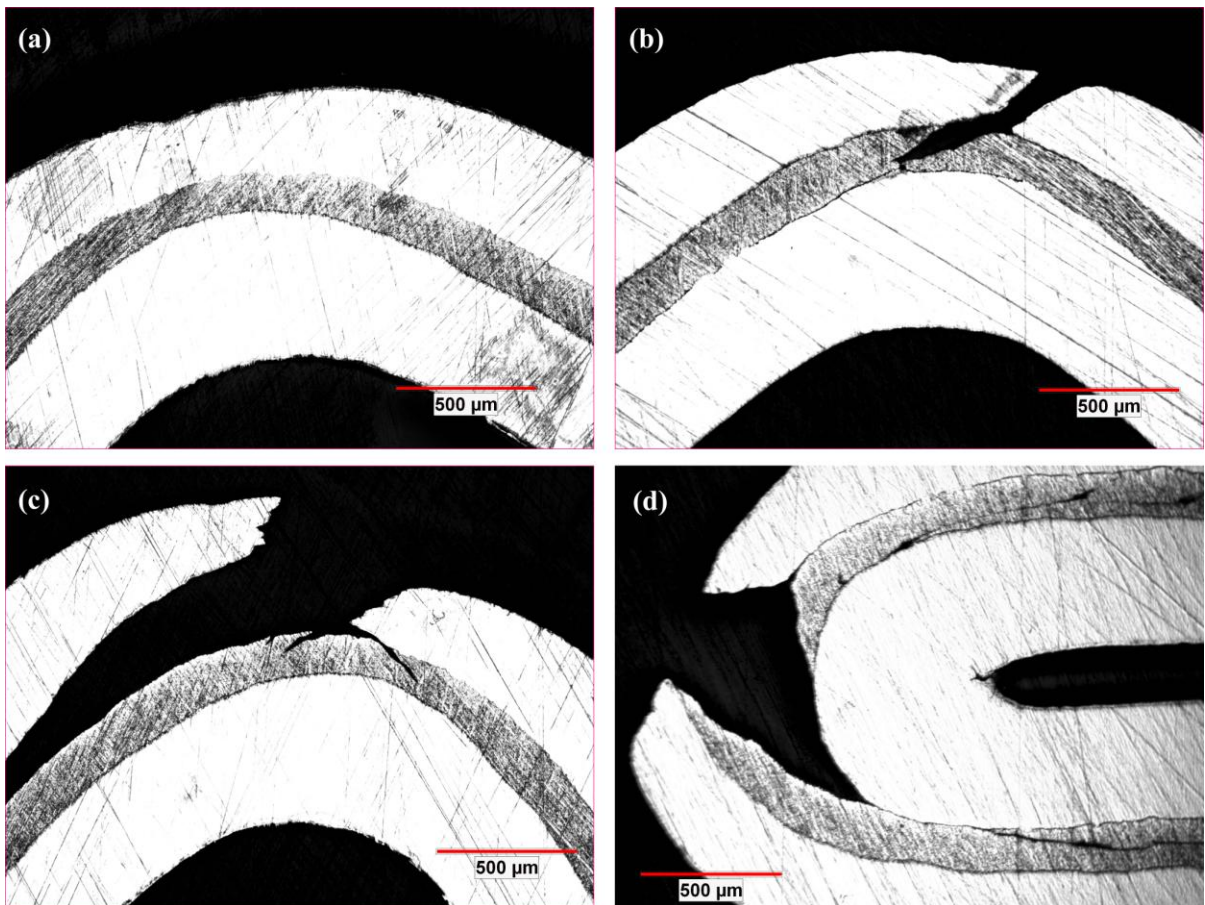


Fig. 5.23. Optical microscopic images of the bent samples (80% deformed laminates) to different nominal interior angles: (a) 50°, (b) 35°, (c) 12° and (d) 0°.

5.4.3. Evaluation of the bending behavior of the laminates

The sandwich materials have advantages in bending application by giving a structure high bending stiffness at low weight. The flexural properties of the laminated composites are quite different since there are two parts of the bending, one is the bending of the whole plate and the other is the shear of the core. The flexural properties of laminated composites can be estimated by defining an equivalent flexural modulus which is equal to the modulus of a monolithic material with the same bending stiffness [84]. The equivalent flexural modulus is given by [84]:

$$\frac{1}{E_{eq}} = \frac{1}{E_f \left\{ (1 - (1 - f)^3) + \frac{E_c}{E_f} (1 - f)^3 \right\}} + \frac{B_1}{B_2} \left(\frac{d}{L} \right)^2 \frac{(1 - f)}{G_c} \quad (5.4)$$

where E the Young's modulus, G the shear modulus, d the thickness of the plate, f the volume fraction occupied by the faces, L the load support span, and B_1 and B_2 are 48 and 4, respectively, for three-point bending with central load. The subscripts f and c refer to face and core, respectively. The calculated equivalent flexural moduli of the steel-magnesium laminates are plotted in Fig. 5.24a, and the specific flexural modulus, which is the flexural modulus divided by density, as function of the amount of magnesium in the laminate is shown in Fig. 5.24b.

The experimentally measured average flexural modulus of the laminated composites in this work was 195 GPa. This result is similar to the value calculated according to Eq. 5.4, 199 GPa, as shown in Fig. 5.25. It is also possible to compare the flexural property of the laminate with the monolithic steel by plotting one Ashby map [9], on which the flexural modulus vs. density is plotting in logarithmic scale, as shown in Fig. 5.25. The dashed line, which represents $E^{1/3}/\rho = \text{constant}$, is the guide line for selecting a light, stiff plate in bending,

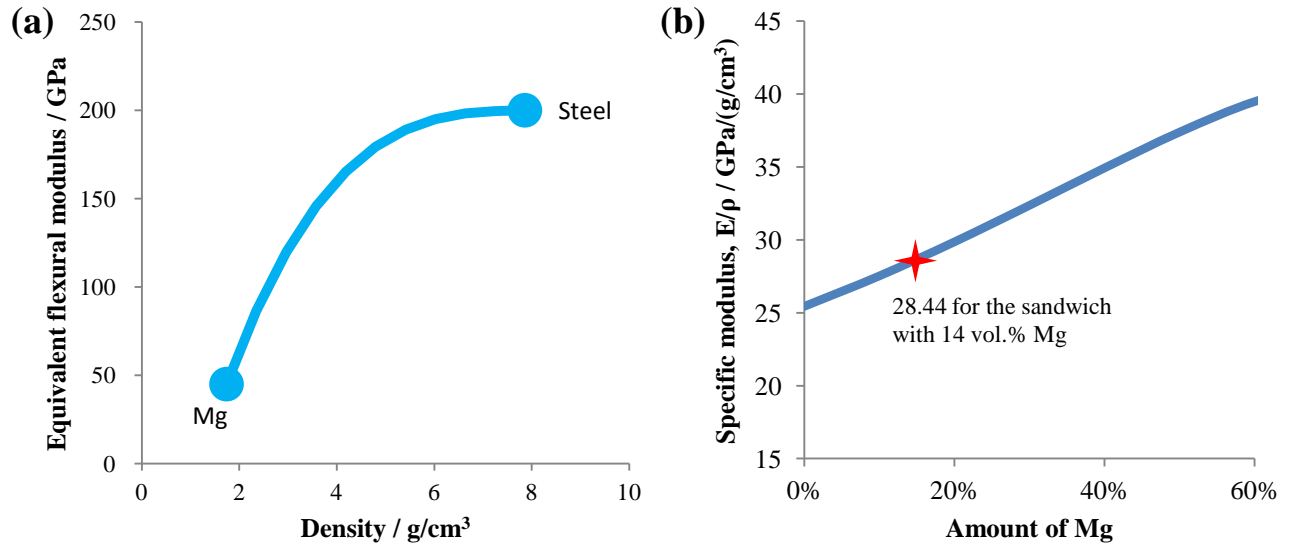


Fig. 5.24. (a) the equivalent flexural modulus of the laminated composites as function of density and (b) the specific flexural modulus as function of the amount of magnesium (calculations based on a support span of 0.1 m in Eq. 5.4).

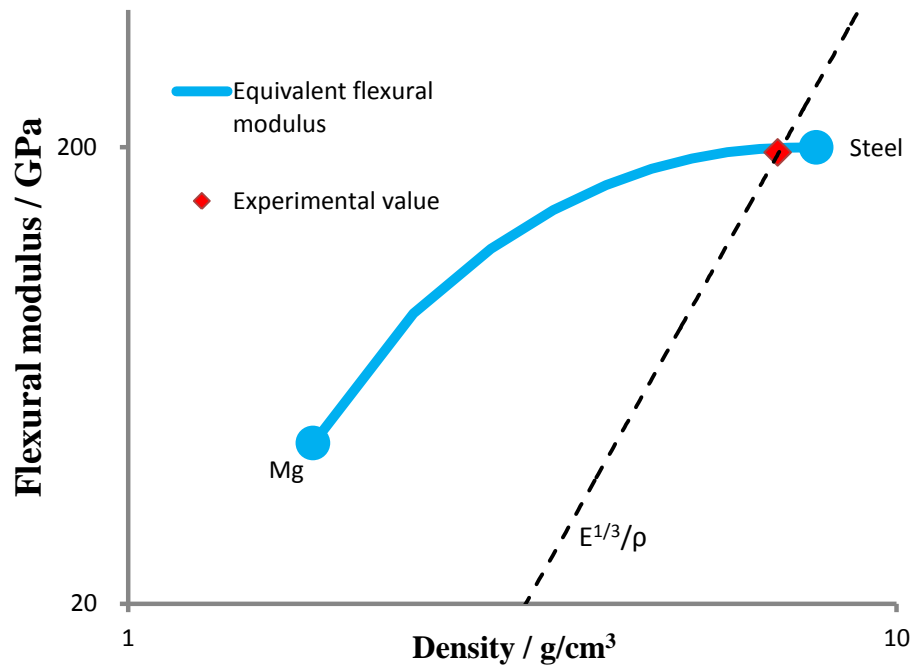


Fig. 5.25. The flexural moduli of the monolithic component materials as well as the laminated composites with different amounts of magnesium as function of density.

and the materials on the left and up of this line have superior performance while those on the right and bottom behave inferior. It can be seen clearly from the chart that the roll-bonded steel-magnesium laminated composites can behave better as a light, stiff plate than the monolithic IF steel. Such improvement is achieved without significant compromise of other mechanical properties of the laminates, such as the tensile property. Although it seems a laminate with more magnesium content is better in terms of bending application, some other properties may be deteriorated, so the magnesium fraction in the laminates should be chosen based on the overall requirements during the design process. Further studies are needed to explore the bending behavior as well as other mechanical properties of the laminates with higher magnesium content, e.g. 30%, and to determine the ideal magnesium content for application in transportation industry.

Chapter 6: Conclusions and future work

6.1. Summary and conclusions

In this work, steel-magnesium three-layer laminated composites were successfully fabricated using the roll bonding technique, during which two pieces of 2 mm thick IF steel with one piece of the 1 mm thick commercial purity magnesium were roll-bonded at 300°C with approximately 50% reduction in a single pass. This metal combination had reasonable bonding between the layers after the roll bonding process. As such these laminates could be further rolled to different thicknesses at 300°C using reductions of 15% per pass. These laminates were cut along both the rolling direction and the transverse direction so that the longitudinal microstructure as well as the cross-sectional microstructure were examined with SEM. It was found that no intermetallic layers or any kind of failure (cracks, voids, localization of component layers, fracture of layers, etc.) occurred during the roll bonding process and the subsequent rolling passes, up to the largest deformation amount examined in this work, i.e. 95%. The interfaces were found to tend to develop a small amount of waviness as the overall level of reduction was increased. The volume fraction of magnesium in the laminate calculated based on the thickness ratio of magnesium at the cross section was 14 percent, which means a density of 7.00 g/cm³ for the laminate. This density means an 11% reduction in density compared to steel.

Steel-magnesium laminate with seven layers was fabricated by means of the accumulative roll bonding. The sample failed after the one cycle ARB process since the through-width cracks were developed in the surface IF steel layers. The longitudinal microstructure indicated that localizations and even fracture took place in the steel layers that

contacted with the later added magnesium layer during the ARB process. Whereas the transverse microstructure at the places free of damages showed that these seven layers could be bonded well together.

The tensile properties of the three-layer laminated composites as well as the monolithic component materials rolled under the same conditions were assessed. The tensile tests were carried out for laminates with three different amounts of deformation, 80%, 92% and 95%, and the tensile curves indicate that the UTS of the laminated composites increased while the maximum uniform elongation decreased with the deformation amount. The average Young's modulus measured from tensile tests was 169 GPa, which is in well accordance with the elastic modulus predicted by ROM.

To compare the tensile properties of the laminates with those of the monolithic component materials, a property map, on which the UTS was plotted as function of true strain, was constructed for the laminated composites and monolithic component materials with equivalent deformation amount. The experimentally measured UTS data matched well with the ROM predictions. However, the ductility of the laminated composites showed poor reproducibility and, on the other hand, cannot be well predicted by the ROM.

The fracture surfaces of the tested laminated composites were observed with SEM. Steel layers in the laminated composites fractured in a rather ductile manner in all three cases, but a different manner from that of the monolithic steel. Dimples with three different orientations can be found, suggesting that the stress state in the steel layers during the tensile tests could be rather complicated. For the magnesium layer in the laminates, it fractured in a relatively brittle way in the 80% deformed laminate but in more ductile manners as the deformation amount increased. Delamination at the interface was found to be inhibited by the bonding as

the deformation amount was increased, probably because the bond quality was improved by rolling. Once the delamination was retarded, the fracture modes of the laminate as well as the steel layers were changed.

The flexural property of the laminated composites was evaluated by three-point bending tests with the 80% deformed laminate. The average flexural modulus measured was 195 GPa, which is in agreement with the theoretical result. The fracture behavior of the laminate in bending was investigated by the U-shape bending test series. Thinning and localization of the outer steel layer due to shear deformation first occurred, followed by the formation of a major crack , with 45 degree to the maximum tensile stress direction, throughout the outer steel layer and in the magnesium core. Then delaminations at the interfaces could be found along the pathway of the major crack and shear cracks in the magnesium layer initiated.

6.2. Future work

This work provides an attempt to fabricate the steel-magnesium laminated metal composites. The three layer steel-magnesium laminated composites can be successfully fabricated and some mechanical properties of the laminated composites were assessed. There are still many future studies on the steel-magnesium laminates are needed, the recommendations for future work are as follows:

(1) TEM analysis of the interface between steel and magnesium should be done to better understand the nature of the bond. Although no intermetallic phases or any other kinds of layer could be observed in this work, it is necessary to examine the interface at high resolution.

(2) The bond strength needs to be quantified. The strength of the bonding can be evaluated by other methods such as shear test, peeling test, etc.

(3) It is also useful to anneal the laminated composites that have already experienced large amounts of deformation. The fabricated laminated composites were with poor ductility in this work because of the cold deformation of steel. However, the heat treatment of the laminates would be challenging because of the large differences in the recrystallization temperatures and thermal expansion coefficients between magnesium and steel. The recrystallization temperature of steel is even higher than the melting point of magnesium, let alone the alloying elements in magnesium that may lower the melting point locally. And the thermal expansion coefficient of magnesium is 2.6 times larger than that of steel, and this may cause delamination during the heating and large residual stress during the cooling.

(4) More ARB experiments should be done to make laminates with more layers. The failure in the hard steel layer made further ARB unfeasible. It is suggested that the laminates and magnesium can be preliminarily bonded together by hot pressing so that the bonded metal combination can be rolled at a small amount of reduction in each pass, which may prevent the failure of steel layers.

(5) Other mechanical properties of the laminated composites should be assessed. These include the impact behavior, formability, fatigue behavior, high temperature behaviors such as creep, etc.

References

- [1] Massalski TB. In: Cahn RW, Haasen P, editors. *Physical Metallurgy Structure and Stability of Alloys* Vol. 1. 1996. p.134.
- [2] Kundu S, Chatterjee S, Olson D, Mishra B. Effects of intermetallic phases on the bond strength of diffusion-bonded joints between titanium and 304 stainless steel using nickel interlayer. *Metall Mater Trans A* 2007;38A:2053.
- [3] Bouaziz O, Sauvage X, Barcelo D. Steel-Magnesium Composite Wire Obtained by Repeated Co-Extrusion. *Materials Science Forum* 2010;654-656:1263.
- [4] Cetin A, Krebs J, Durussel A, Rossoll A, Inoue J, Koseki T, Nambu S, Mortensen A. Laminated Metal Composites by Infiltration. *Metallurgical and Materials Transactions A* 2011;42:3509.
- [5] Lesuer DR, Syn CK, Sherby OD, Wadsworth J, Lewandowski JJ, Hunt WH. Mechanical behaviour of laminated metal composites. *Int Mater Rev* 1996;41:169.
- [6] Saito Y, Utsunomiya H, Tsuji N, Sakai T. Novel ultra-high straining process for bulk materials - Development of the accumulative roll-bonding (ARB) process. *Acta Mater* 1999;47:579.
- [7] Tsuji N, Ito Y, Saito Y, Minamino Y. Strength and ductility of ultrafine grained aluminum and iron produced by ARB and annealing. *Scr. Mater.* 2002;47:893.
- [8] Tsuji N, Saito Y, Lee SH, Minamino Y. ARB (accumulative roll-bonding) and other new techniques to produce bulk ultrafine grained materials. *Adv Eng Mater* 2003;5:338.
- [9] Ashby MF. *Materials Selection in Mechanical Design* (3rd Edition): Elsevier, 2005.
- [10] Embury D, Bouaziz O. Steel-Based Composites: Driving Forces and Classifications. *Annu Rev Mater Res* 2010;40:213.
- [11] Bouaziz O, Brechet Y, Embury JD. Heterogeneous and architected materials: A possible strategy for design of structural materials. *Adv Eng Mater* 2008;10:24.
- [12] Chénab B, Zurob H, Embury D, Bouaziz O, Brechet Y. Compositionally Graded Steels: A Strategy for Materials Development. *Adv Eng Mater* 2009;11:992.
- [13] Ashby MF, Brechet YJM. Designing hybrid materials. *Acta Mater* 2003;51:5801.
- [14] Kromm FX, Quenisset JM, Harry R, Lorriot T. An example of multimaterials design. *Adv Eng Mater* 2002;4:371.
- [15] Ashby MF. Multi-objective optimization in material design and selection. *Acta Mater* 2000;48:359.
- [16] Ashby MF. Criteria for Selecting the Components of Composites. *Acta Metall Mater* 1993;41:1313.
- [17] Shanley FR. *Weight-strength analysis of aircraft structures: The Rand Corporation: McGraw-Hill, 1952.*

- [18] Schoutens JE, Zarate DA. Structural Indexes in Design Optimization with Metal-Matrix Composites. *Composites* 1986;17:188.
- [19] Ashby MF. On the Engineering Properties of Materials. *Acta Metallurgica* 1989;37:1273.
- [20] Gordon JE. Structures, or, Why things don't fall down: Penguin Books, 1991.
- [21] Wadsworth J, Lesuer DR. Ancient and modern laminated composites - from the Great Pyramid of Gizeh to Y2K. *Mater Charact* 2000;45:289.
- [22] Sherby OD, Wadsworth J. Damascus Steel and Superplasticity .2. Welded Damascus Steels. *Sampe J* 1995;31:32.
- [23] Alic JA, Danesh A. Fracture of Laminates Combining 2024-T3 and 7075-T6 Aluminum-Alloys. *Eng Fract Mech* 1978;10:177.
- [24] Embury JD, Petch NJ, Wraith AE, Wright ES. Fracture of Mild Steel Laminates. *T Metall Soc Aime* 1967;239:114.
- [25] Bose A. Micro-Infiltrated Macro-Laminated Composite (Mimlc) - Concepts for Fabrication of This Novel Composite. *Advances in Powder Metallurgy & Particulate Materials - 1992, Vol 9: Particulate Materials and Processes*. Princeton: Metal Powder Industries Fed, 1992. p.57.
- [26] Ellis LY. vol. MS. Cleveland, OH: Case Western Reserve University, 1992.
- [27] Alman DE, Hawk JA. Processing, structure and properties of aluminum-aluminide layered sheet composites. *Light Weight Alloys for Aerospace Applications*. Warrendale: Minerals, Metals & Materials Soc, 1995. p.531.
- [28] Jimenez JA, Ruano OA, Smirnov OM, Sherby OD. Microstructural Studies of a Roll-Bonded Laminated Ultrahigh Carbon-Steel Bar. *Mater Charact* 1991;27:141.
- [29] Wadsworth J, Kum DW, Sherby OD. Welded Damascus Steels and a New Breed of Laminated Composites. *Met Prog* 1986;129:61.
- [30] Menezes S, Anderson DP. Wavelength-Property Correlation in Electrodeposited Ultrastructured Cu-Ni Multilayers. *J. Electrochem. Soc.* 1990;137:440.
- [31] Tench D, White J. Enhanced Tensile-Strength for Electrodeposited Nickel-Copper Multilayer Composites. *Metallurgical Transactions a-Physical Metallurgy and Materials Science* 1984;15:2039.
- [32] Syn CK, Stoner S, Lesuer DR, Sherby OD. Influence of Volume Fraction of Component Materials and Interlayer Bond Strength on Fracture-Toughness of Multilayer Al-6090-25 Vol-Percent Sicp and Al-5182 Laminates. *High Performance Metal and Ceramic Matrix Composites*. Warrendale: Minerals, Metals & Materials Soc, 1994. p.125.
- [33] Syn CK, Lesuer DR, Sherby OD. Processing and Mechanical-Properties of Laminated Metal Composites of Al/Al-25 Vol-Percent Sic and Ultrahigh Carbon-Steel Brass. *International Conf on Advanced Synthesis of Engineered Structural Materials*. Materials Park: Asm International, 1993. p.149.

- [34] Sherby OD, Lee S, Koch R, Sumi T, Wolfenstine J. Multilayered composites based on ultrahigh carbon steel and brass. *Materials and Manufacturing Processes* 1990;5:363.
- [35] Lee S, Wolfenstine J, Sherby OD. Tensile Properties of Laminated Composites Based on Ultrahigh Carbon Steel. *Journal of Composite Materials* 1991;25:842.
- [36] Syn CK, Lesuer DR, Sherby OD. Enhancing tensile ductility of a particulate-reinforced aluminum metal matrix composite by lamination with Mg-9%Li alloy. *Mat Sci Eng a-Struct* 1996;206:201.
- [37] Syn CK, Lesuer DR, Wolfenstine J, Sherby OD. Layer Thickness Effect on Ductile Tensile Fracture of Ultrahigh Carbon Steel-Brass Laminates. *Metallurgical Transactions a-Physical Metallurgy and Materials Science* 1993;24:1647.
- [38] Ritchie RO. Mechanisms of Fatigue Crack-Propagation in Metals, Ceramics and Composites - Role of Crack Tip Shielding. *Mat Sci Eng a-Struct* 1988;103:15.
- [39] Ebert T, Mordike BL. Magnesium - Properties - applications - potential. *Mat Sci Eng a-Struct* 2001;302:37.
- [40] Roberts CS. Magnesium and its alloys. New York: Wiley, 1960.
- [41] Viala JC, Pierre D, Bosselet F, Peronnet M, Bouix J. Chemical interaction processes at the interface between mild steel and liquid magnesium of technical grade. *Scr. Mater.* 1999;40:1185.
- [42] Sacerdote-Peronnet M, Guiot E, Bosselet F, Dezellus O, Rouby D, Viala JC. Local reinforcement of magnesium base castings with mild steel inserts. *Mat Sci Eng a-Struct* 2007;445:296.
- [43] Levi FP. Permanent Magnets Obtained by Drawing Compacts of Parallel Iron Wires. *J. Appl. Phys.* 1960;31:1469.
- [44] Spencer K, Lecouturier F, Thilly L, Embury JD. Established and emerging materials for use as high-field magnet conductors. *Adv Eng Mater* 2004;6:290.
- [45] Thilly L, Renault PO, Van Petegem S, Brandstetter S, Schmitt B, Van Swygenhoven H, Vidal V, Lecouturier F. Evidence of internal Bauschinger test in nanocomposite wires during in situ macroscopic tensile cycling under synchrotron beam. *Appl. Phys. Lett.* 2007;90:241907.
- [46] Guillet A, Nzoma EY, Pareige P. A new processing technique for copper-graphite multifilamentary nanocomposite wire: Microstructures and electrical properties. *J Mater Process Tech* 2007;182:50.
- [47] Thomason PF. Ductile fracture of metals. Oxford: Pergamon Press, 1990.
- [48] Bay N. Cold Pressure Welding---The Mechanisms Governing Bonding. *Journal of Engineering for Industry* 1979;101:121.
- [49] Brick RM. Hot Roll Bonding of Steel. *Weld. J.* 1970;49:S440.
- [50] Li L, Nagai K, Yin FX. Progress in cold roll bonding of metals. *Sci. Technol. Adv. Mater.* 2008;9:023001.

- [51] Forster JA, Jha S, Amatruda A. The Processing and Evaluation of Clad Metals. *Jom-J Min Met Mat S* 1993;45:35.
- [52] Ohsaki S, Kato S, Tsuji N, Ohkubo T, Hono K. Bulk mechanical alloying of Cu-Ag and Cu/Zr two-phase microstructures by accumulative roll-bonding process. *Acta Mater* 2007;55:2885.
- [53] Sauvage X, Dinda GP, Wilde G. Non-equilibrium intermixing and phase transformation in severely deformed Al/Ni multilayers. *Scr. Mater.* 2007;56:181.
- [54] Min G, Lee J-M, Kang S-B, Kim H-W. Evolution of microstructure for multilayered Al/Ni composites by accumulative roll bonding process. *Materials Letters* 2006;60:3255.
- [55] Manesh HD, Taheri AK. Bond strength and formability of an aluminum-clad steel sheet. *J Alloy Compd* 2003;361:138.
- [56] Inoue H, Ishio M, Takasugi T. Texture of TiNi shape memory alloy sheets produced by roll-bonding and solid phase reaction from elementary metals. *Acta Mater* 2003;51:6373.
- [57] Ding HS, Lee JM, Lee BR, Kang SB, Nam TH. Processing and microstructure of TiNiSMA strips prepared by cold roll-bonding and annealing of multilayer. *Mat Sci Eng a-Struct* 2005;408:182.
- [58] Jha SC, Delagi RG, Forster JA, Krotz PD. High-Strength High-Conductivity Cu-Nb Microcomposite Sheet Fabricated Via Multiple Roll Bonding. *Metallurgical Transactions a-Physical Metallurgy and Materials Science* 1993;24:15.
- [59] Manesh HD, Taheri AK. Study of mechanisms of cold roll welding of aluminium alloy to steel strip. *Mater. Sci. Technol.* 2004;20:1064.
- [60] Zhang W, Bay N. Cold welding - Experimental investigation of the surface preparation methods. *Weld. J.* 1997;76:S326.
- [61] Yahiro A, Masui T, Yoshida T, Doi D. Development of Nonferrous Clad Plate and Sheet by Warm Rolling with Different Temperature of Materials. *Isij Int* 1991;31:647.
- [62] Lenard JG, Yan HZ. A study of warm and cold roll-bonding of an aluminium alloy. *Mat Sci Eng a-Struct* 2004;385:419.
- [63] Osman TM, Lewandowski JJ, Lesuer DR. The fracture resistance of layered DRA materials: influence of laminae thickness. *Mat Sci Eng a-Struct* 1997;229:1.
- [64] Cave JA, Williams JD. Mechanism of Cold Pressure Welding by Rolling. *J I Met* 1973;101:203.
- [65] Bay N. Cold welding, part 2: process variants and applications. *Metal Construction* 1986;8:486.
- [66] Vaidyanath LR, Nicholas MG, Milner DR. Pressure welding by rolling. *British Welding Journal* 1959;6:13.
- [67] McEwan KJB, Milner DR. Pressure welding of dissimilar metals. *British Welding Journal* 1962;9:406.

- [68] Vaidyanath LR, Milner DR. Significance of surface preparation in cold pressure welding. *British Welding Journal* 1960;7:1.
- [69] Sherwood WC, Milner DR. The effect of vacuum machining on the cold welding of some metals. *Journal of Institute of Metals* 1969;97:1.
- [70] Johnson KI, Keller DV. Effect of Contamination on Adhesion of Metallic Couples in Ultra-High Vacuum. *J. Appl. Phys.* 1967;38:1896.
- [71] Biggs T, Go J, Militzer M, Poole WJ. Microstructure evolution during annealing of a boron-containing IF steel. 44th Mechanical Working and Steel Processing Conference Proceedings., vol. XL. Warrendale, PA, 2002. p.631.
- [72] ASTM D790-10 Standard Test Methods for Flexural Properties of Unreinforced and Reinforced Plastics and Electrical Insulating Materials. West Conshohocken, PA: American Society for Testing and Materials, 2010.
- [73] Zenkert D. An introduction to sandwich construction. Sheffield: Engineering Materials Advisory Service, 1995.
- [74] Semiatin S, Piehler H. Formability of sandwich sheet materials in plane strain compression and rolling. *Metallurgical and Materials Transactions A* 1979;10:97.
- [75] Eizadjou M, Talachi AK, Manesh HD, Shahabi HS, Janghorban K. Investigation of structure and mechanical properties of multi-layered Al/Cu composite produced by accumulative roll bonding (ARB) process. *Compos Sci Technol* 2008;68:2003.
- [76] Tan JC, Tan MJ. Dynamic continuous recrystallization characteristics in two stage deformation of Mg-3Al-1Zn alloy sheet. *Materials Science and Engineering: A* 2003;339:124.
- [77] Al-Samman T, Gottstein G. Dynamic recrystallization during high temperature deformation of magnesium. *Mat Sci Eng a-Struct* 2008;490:411.
- [78] Vandenbeukel A. Theory of Effect of Dynamic Strain Aging on Mechanical-Properties. *Phys. Status Solidi A-Apl. Res.* 1975;30:197.
- [79] Semiatin S, Piehler H. Deformation of sandwich sheet materials in uniaxial tension. *Metallurgical and Materials Transactions A* 1979;10:85.
- [80] Hawkins R, Wright JC. Mechanical Properties and Press-Formability of Copper/Mild Steel Sandwich Sheet Materials. *J I Met* 1971;99:357.
- [81] ToolBox TE. Elastic Properties and Young Modulus for some Materials, http://www.engineeringtoolbox.com/young-modulus-d_417.html.
- [82] Mills K, Davis JR. *ASM Handbook, Volume 12 - Fractography*. ASM International, 1987.
- [83] Meyers MA, Chawla KK. *Mechanical Behavior of Materials (2nd Edition)*. Cambridge University Press, 2009.
- [84] Ashby MF. *Materials Selection in Mechanical Design (4th Edition)*. Elsevier, 2011.